Electronic Thesis and Dissertation Repository

8-21-2015 12:00 AM

Investigations in Hydrodynamics and Mixing Pattern in the Bubble Column Equipped with Internals

Keller J H George
The University of Western Ontario

Supervisor
Anand Prakash
The University of Western Ontario

Graduate Program in Chemical and Biochemical Engineering
A thesis submitted in partial fulfillment of the requirements for the degree in Master of Science
© Keller J H George 2015

Recommended Citation

INVESTIGATIONS IN HYDRODYNAMICS AND MIXING PATTERNS IN THE BUBBLE
COLUMN EQUIPPED WITH INTERNALS
(Thesis format: Monograph)

by

Keller <u>George</u>

Graduate Program in Chemical and Biochemical Engineering

A thesis submitted in partial fulfillment
of the requirements for the degree of
Master of Engineering Science

The School of Graduate and Postdoctoral Studies
The University of Western Ontario
London, Ontario, Canada

© Keller George 2015

THE UNIVERSITY OF WESTERN ONTARIO
SCHOOL OF GRADUATE AND POSTDOCTORAL STUDIES

Abstract

Bubble column reactors, with or without solid particles, have a number of applications in the chemical, petrochemical, biochemical and environmental industries. A number of these industrial applications require internals such as baffles, heat transfer surfaces and special distributors to meet demands. Proper selection and design of these internals can lead to the improved performance and efficiency of a bubble column reactor. Several experiments are carried out in a bubble column equipped with a concentric tube bundle (CT) and an internal combination consisting of a concentric tube bundle and concentric baffle (or static mixer) (CTB) respectively. Neutrally buoyant particles are used to determine the effect of the CT and CTB internals on the local flow structures in the equipped column respectively. More upward, near-linear particle movements are observed with the CTB internal over the CT internal. Several non-linear particle movements are also observed. Overall bulk liquid circulation flow patterns are proposed for the intermediate to high gas velocity range based on the observed local flow structures for both internals. Comparisons are made between the gas holdups obtained during internal equipment and that of a comparable hollow bubble column from the literature. Both internals increase the gas holdup of a hollow bubble column. However, the increases with the CT internal are higher by more than 25% of that obtained with the CTB internal on average. The effect of the internals on average bubble size is investigated for the small bubble class. Smaller average diameters are obtained when the CT internal is used. The interfacial area in the presence of the two internals is determined respectively. Higher interfacial areas are obtained with the CT internal. The average difference in interfacial area is 54.0 m^2/m^3. The effect of the internals on mixing time is determined through dye and aqueous salt tracer studies. In both instances, higher mixing times are obtained with the CTB internal. Liquid backmixing is quantified through the axial dispersion coefficients obtained from the salt tracer studies. The axial dispersion coefficients obtained with the CT internal are higher than that of the CTB internal by about 15% on average.

Keywords

Acknowledgement

I would like to thank my supervisor, Dr. Anand Prakash, for all of his guidance throughout my studies. This work would not have been possible without his advice and knowledge. I am also thankful to Anil Jhawar for his assistance during experimentation and for his support during this period.

A very special thanks to the administrative staff of the chemical and biochemical engineering department, Ashley Jokhu, Ingrid Timusk and Sarah Williams for their kind-hearted support in numerous aspects. I would also like to thank the staff of Engineering Store and the University Machine Shop for their assistance and patience.

This thesis is dedicated to my father Joshua, my mother Fidelis, my sister Londa, my aunts Beverlyann and Leana, my grandmother Esther and my deceased grandmother Theodora. Without their boundless support and unconditional love, both past and current, I would have been unable to complete this work.

<div align="center">

"I can do all things through Christ who strengthens me." Philippians 4:13

To Him I am most indebted to…

</div>

Table of Contents

List of Tables

List of Figures

Nomenclature

a	Interfacial area, m^2
A	Area, m^2
A_c	Cross-sectional area, m^2
c	Intercept of disengagement slope or 1.2 (constant)
C	Concentration or 0.61 (orifice constant)
D_a	Axial dispersion coefficient, m^2/s
d_b	Average bubble diameter, m
E	Exit age distribution function
f	Friction factor
F_g	Mass flow, kg/s
g	Acceleration due to gravity, m/s^2
H	Bed height, m
h_L	Headloss, m
K	Coefficient for energy loss due to geometry
K_b	$\max(14.7Mo^{-0.038}, 12)$
L	Length, m
m	Gradient of disengagement slope
Mo	Morton Number (Mo), $g\mu^4\Delta\rho/\rho_c^2\sigma^3$
MW	Molecular weight, g/mol
n	0.8 (constant)
N	Moles, mols or whole number
$\dot{n}$	Molar flow, mols/s
Pe_a	Peclet number, Lv/D_a
P	Pressure, Pa
Q	Volumetric flow, m^3/s
r_c	Critical Ratio
t	Time, s
T	Temperature, K
$\bar{t}$	Residence Time, s

U_b	Bubble rise velocity, m/s
v	Superficial liquid velocity, m/s
V	Volume, m^3
V_g	Superficial gas velocity, m/s
$\dot{V}$	Volumetric flow, m^3/s
Y	1 (expansion coefficient at low pressures)
z	Axial displacement, m

Greek Letters

β	Ration of diameters
Δ	Change in …
Δθ	Dimensionless constant
ε	Gas holdup
$ε_b$	Bubble fraction holdup
ρ	Density, kg/m3
θ	Dimensionless time, $t/\bar{t}$
σ	Surface tension, N/m
$σ^2$	Variance
π	Dimensionless constant, 3.1416 (5 significant figures)
γ	1.4 for air (constant)

Subscripts

0	Pertaining to steady state operation
1	Pertaining to the first disengagement period or arbitrary point 1
2	Pertaining to the second disengagement period or arbitrary point 2
b	Bubble
bed	Pertaining to the reactor's bed

dist	Distributor
dyn	Dynamic
E	Equilibrium
g	Gas
i	Tracer
l	Liquid
L/lg	Pertaining to the large bubble class
o	Orifice
p	Pipe
S/sm	Pertaining to the small bubble class
st	Static
T	Total

Superscripts

'	Dimensionless

1.0 Introduction

The bubble column is an extremely useful reactor type due to the numerous advantages associated with its operation and design. The high degree of mixing that takes place within a bubble column ensures desirable heat and mass transfer within the vessel, while the column's simple design and its lack of moving parts ensures low maintenance and little operating cost (Kantarci et al., 2005 Deckwer and Schumpe, 1993; Li and Prakash, 2002; Li et al., 2003,). Reduced plugging during operation, high catalyst durability as well as online catalyst addition and withdrawal (Degaleesan et al., 2001) are all benefits specifically associated with the use of slurry bubble columns within industry. Naturally, the numerous advantages associated with the bubble column makes it an attractive choice for many applications. Common industrial applications include hydrogenation, oxidation, chlorination, fermentation, biological waste water treatment, Fischer-Tropsch synthesis, methanol synthesis, dimethyl ether production (DME) and heavy oil upgrading (Shah et al., 1982, Duduković and Devanathan, 1992, Deckwer and Schumpe, 1993, Prakash et al., 1999, Duduković et al., 2002, Degaleesan et al., 2001, Miller, 1980, Shah et al., 1982, Merchuk et al., 1994).

Although especially advantageous, the bubble column is not devoid of limitations. Complex, scale-dependent hydrodynamic interactions make the scale-up of an existing bubble column reactor challenging, while the contained discontinuous phase typically travels very quickly within the reactor and thus, possesses a short residence time. Although the slurry bubble column allows for some degree of catalyst addition/withdrawal, the volumetric rate at which catalyst addition can take place is quite low. Lastly, the continuous phase of the reactor is subject to significant backmixing which can be particularly disadvantageous for reaction-containing systems (Shah et al., 1978). In order to obtain the desired performance for a given application, bubble columns often

need to be modified to overcome specific limitations. The addition of internals is one of the most promising means through which reductions to bubble column limitations, such as short gaseous phase residence time as well as liquid backmixing, can be achieved. These include internals such as baffles and heat transfer tubes. The configuration of the particular gas/liquid distributors can also affect the reactor's productivity.

1.1 Objective

The presence and arrangement of the internals in a bubble column affects its hydrodynamics and mixing patterns and thus, affects the reactor's performance and heat transfer characteristics. Only a limited number of literature studies have investigated the effects of internals on bubble column hydrodynamics (Jhawar and Prakash, 2014; Youssef and Al-Dahhan, 2009; Larachi et al., 2006; Chen et al., 1999; Schlüter et al., 1995; Saxena et al., 1992). To systematically determine the effects of internal type and arrangement on the limitations of a bubble column, quantification of the internals' effects on important design parameters such as gas holdup, interfacial area for mass transfer and liquid backmixing is mandatory. In this study, attempts have been made to gain insight into the local hydrodynamics and flow structure changes by tracking the motion of near-neutrally buoyant particles with a high speed camera. The effects of internals are also quantified through overall gas holdup, bubble population and liquid mixing measurements for selected configurations. Internals with little impact on the cross-sectional area of the reactor and offered low pressure drops were selected for the investigation.

1.2 Thesis Format

This thesis consists of 5 chapters and follows the "monograph" format as outlined by the Master's

Programs of GENERAL THESIS REGULATIONS by the School of Graduate and Postdoctoral

Studies (SGPS) in the University of Western Ontario. A summary of each chapter is listed below:

In Chapter 1, a general introduction to the bubble column reactor is provided. The motivation for

this work as well as its contributions are also clearly stated. Finally, the thesis structure is outlined.

In Chapter 2, a literature review summarizes some of the research available on gas holdup, liquid

mixing time and liquid backmixing. Measurement techniques to determine gas holdup, bubble

fractions, average small bubble size and liquid mixing time/axial dispersion are reviewed.

In Chapter 3, the experimental procedures used to determine gas holdup, bubble fractions, average

small bubble size and mixing time/axial dispersion are presented, along with the materials used. A

few of the equations used during data analysis are also shown.

In Chapter 4, the experimental results pertaining to the effect of the internals on gas holdup, bubble

fractions, bubble sizes, interfacial area, liquid circulation, mixing time and axial dispersion are

discussed.

In Chapter 5, the conclusions and recommendations for this study are summarized.

2.0 Literature Review

Bubble column reactors are types of multiphase reactors that facilitate substantial interactions between a continuous liquid/slurry phase and discontinuous gaseous phase by promoting distribution of the discontinuous phase within the continuous phase. In a typical bubble column, gas continuously enters a cylindrical vessel (Degaleesan et al., 2001) from its bottom where it is immediately distributed into the enclosed continuous phase through the use of a sparger. Naturally, the less dense of the two phases rises and in so doing, the continuous phase is circulated. When steady state is achieved, circulation of the continuous phase becomes structured and flow patterns are set up in the column. A schematic showing a typical bubble column reactor can be seen in Figure 2.1.

In general, there are two modes of operation for bubble columns. In the first mode, semibatch operation (Deckwer and Schumpe, 1993), the continuous phase stays within the bubble column while the gaseous phase enters at a particular superficial gas velocity, V_g. In continuous operation however, the continuous phase enters at a superficial "liquid" velocity V_1 (Deckwer and Schumpe, 1993) in which V_1 is less then V_g (Kantarci et al., 2005). The continuous phase portion of the effluent leaving the column is typically recycled (Kantarci et al., 2005) while the gaseous phase portion may be vented (Miller, 1980). It is important to note that continuous operation may be performed concurrently, in which the continuous and gaseous phases move in the same direction, or countercurrently, in which the continuous and gaseous phases move against each other (Deckwer and Schumpe, 1993). Although countercurrent operation is generally more advantageous than concurrent operation in many systems, neither mode offers any unique advantages in the case of bubble columns. Low superficial liquid velocities as well as substantial

inter-phase mixing make the outcomes of both the concurrent continuous and countercurrent continuous operations comparable (Deckwer and Schumpe, 1993).
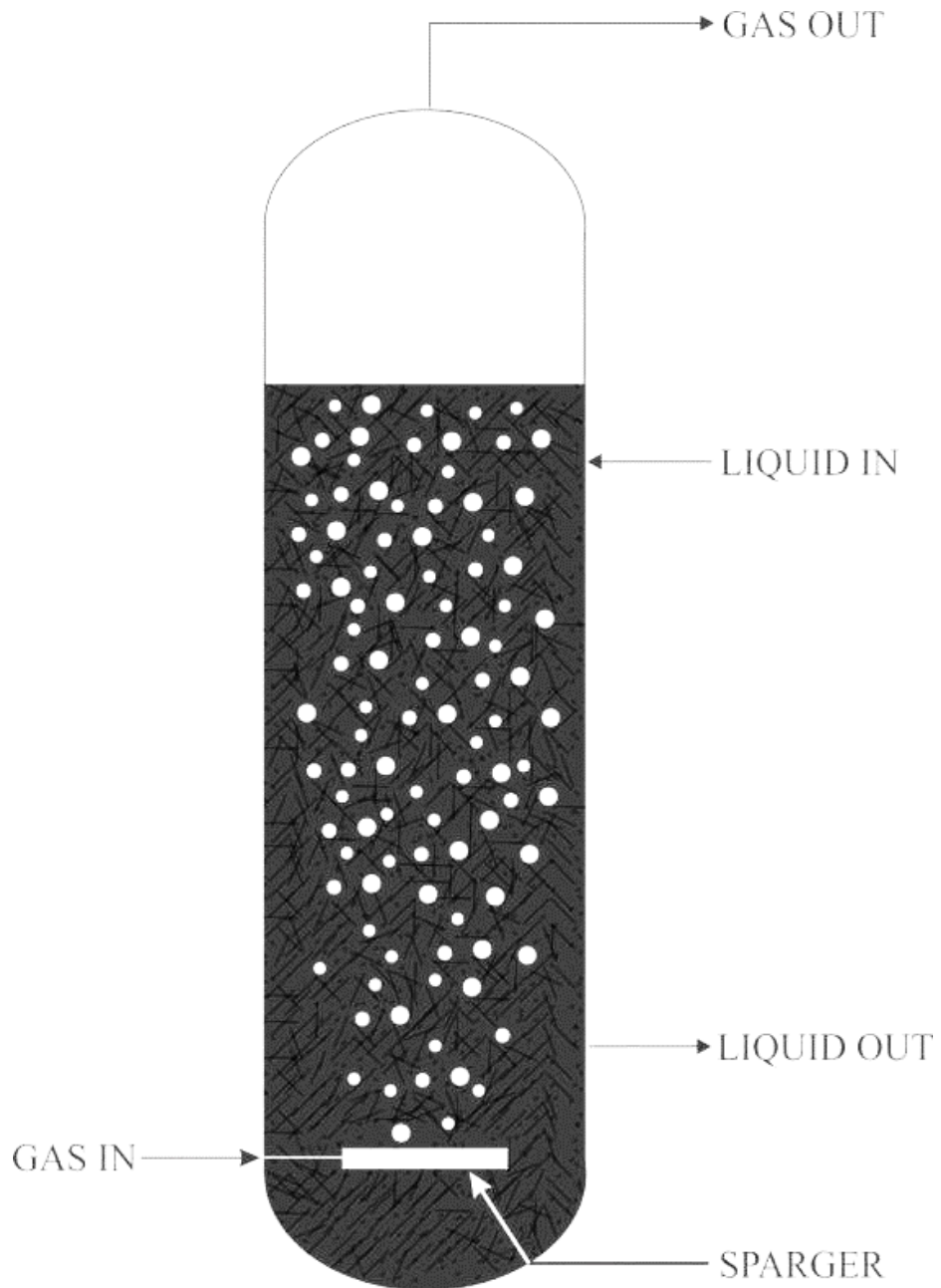
Figure 2.1: Schematic of a bubble column reactor

Although bubble columns are relatively simple to construct (Alvaré and Al-Dahhan, 2006), the interactions between the continuous and gaseous phases contained within are complex, intimate and difficult to predict or scale. For these reasons, characterization and quantification of the gaseous and liquid phase interactions is of great importance. There are two different methods that can be used to gain an understanding of bubble column systems (Deckwer and Schumpe, 1993). The first category refers to empirically-based methods in which rules and guidelines for bubble column design and scale-up are derived from trends in experimental data. The second category refers to model-based methods in which theoretical models are applied to the system of interest after flow regime analysis has been carried out. It is not uncommon to find a mix of both methods in an industrial setting. However, a greater dependence on model-base methods is encouraged (Deckwer and Schumpe, 1993) as they provide additional insight to a reactor's performance and a basis for reactor design.

2.1 Flow Regimes in Bubble Columns

The hydrodynamic behavior of a bubble column is strongly dependent on the flow regime in which it is operating within (Hyndman et al., 1997). There are three major flow regimes that can exist within a bubble column. These regimes are the bubbly, coalesced bubble and slug flow regimes (Kantarci et al., 2005) which can be seen in Figure 2.2. A transition period also exists between flow regimes.
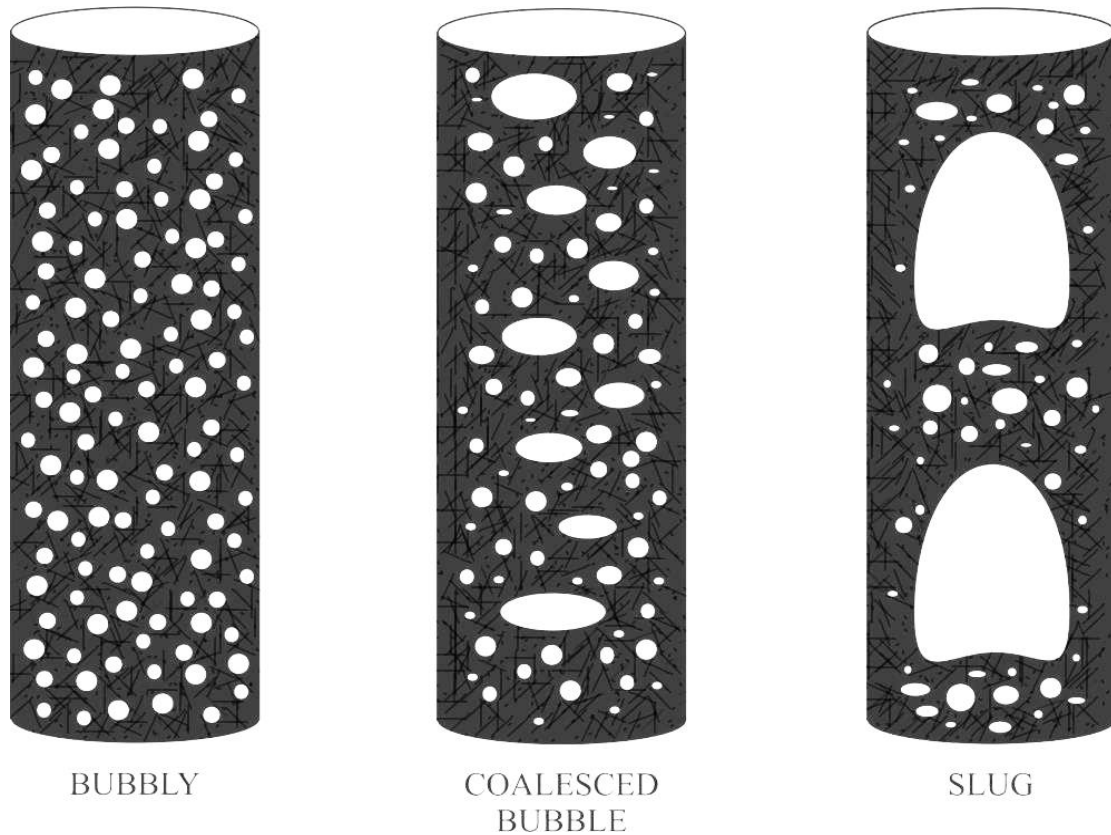
Figure 2.2: Schematic of flow regimes in bubble column

2.1.1 Bubbly Flow Regime

The bubbly flow regime (also called the homogeneous flow regime), is characterised by the presence of bubbles that are small and about uniformly sized (Schumpe and Grund, 1986). All bubbles have similar, small rise velocities due the dependence of bubble rise velocity on bubble size (Schumpe and Grund, 1986) and rise vertically with little transverse and axial oscillations (Throat and Joshi, 2004). The size distribution of this regime is also quite narrow since bubble coalescence and bubble break up are not common occurrences (Shaikh and Al-Dahhan, 2007). Bubble size is mainly dictated by the nature of the gas distributor and the physical properties of the continuous phase (Shaikh and Al-Dahhan, 2007). The bubbly flow regime is characterised by

"gentle mixing" or insignificant circulation within the continuous phase (Shaikh and Al-Dahhan, 2007). This "gentle mixing" is due to the radially uniform gas holdup profiles within the column (Shaikh and Al-Dahhan, 2007). Bubbly flow regimes have been found to occur at low superficial gas velocities, particularly at superficial gas velocities less than 0.05 m/s under semibatch operation (Fan, 1989, Hills, 1974).

2.1.2 Transition Flow Regime

Bubble columns shift from one flow regime to another when superficial gas velocity is manipulated adequately. However, these transitions do not occur as soon as a specific superficial gas velocity is exceeded. Instead, the column enters a "transition regime" before changing from the bubbly to the coalesced bubble or from the coalesced bubble to the slug flow regimes. Several observations have been made on the hydrodynamic behavior of a bubble column as it transitions from the bubbly to the coalesced bubble flow regime. In most cases, this regime is characterised by an increase in the presence of gaseous phase near the center of the column as well as bubble coalescence and an increase in liquid circulation (Kantarci et al., 2005, Olmos et al., 2003, Ohki and Inoue, 1970).

2.1.3 Coalesced Bubble Flow Regime

If superficial gas velocity sufficiently exceeds 0.05 m/s, the coalesced bubble flow regime (also called the heterogeneous or turbulent flow regime) is observed. The coalesced bubble flow regime is characterised by a wide range of bubble sizes (Schumpe and Grund, 1986), with each bubble having its own unique bubble rise velocity. In general, two classes of bubbles can be found within

the coalesced bubble flow regime – the large and small bubble classes. Typically, the small bubble class contains small bubbles with average diameters ranging from 3 mm to 6 mm (Daly et al., 1992, Schumpe and Grund, 1986). These bubbles are reliably spherical when average diameter is less than 5 mm (Deckwer, 1992). Bubbles with diameters greater than 5 mm are slightly deformed and ellipsoidal in shape. The bubbles of the large bubble class have a minimum diameter of 10 mm (Daly et al., 1992, Schumpe and Grund, 1986). When the diameter of a bubble is greater than 20 mm, the bubble's shape can be described as a 'spherical cap' (Krishna and Van Baten, 2001).

The wide range of bubble sizes found within the coalesced bubble flow regime is due to the continuous coalescence of small bubbles and the continued breakup of large bubbles (Kantarci et al., 2005). Average bubble size is dependent on the frequency with which bubble coalescence and bubble breakup occur within the system (Throat and Joshi, 2004). It is important to note that the breakup of larger bubbles occurs not long after the bubbles are formed. This phenomenon results in larger bubbles having short residence times (Kantarci et al., 2005). In addition to the variations in bubble sizes and bubble rise velocities, the coalesced bubble flow regime is characterised by increased turbulent motion of gaseous phase as well as increased liquid recirculation (Kantarci et al., 2005). Both phenomena result in the occurrence of unsteady flow patterns (Kantarci et al., 2005) and vigorous mixing (Hyndman et al., 1997). Liquid circulation is due to the radial, non-uniform gas holdup distributions within the column (Shaikh and Al-Dahhan, 2007).

2.1.4 Slug Flow Regime

When column diameter is small and gas throughput is high, a bubble column may shift from the coalesced bubble flow regime to the slug flow regime. The slug flow regime (also another type of

heterogeneous flow regime) is characterized by large, elongated bubbles called Taylor bubbles which have diameters slightly smaller than that of the bubble column (Shiea et al., 2013). Although Taylor bubbles are large, breakup of Taylor bubbles does not occur because the column walls have a stabilizing effect on the bubbles (Kantarci et al., 2005). Slug flow regimes have been observed in column diameters of up to 15 cm (Miller, 1980).

2.1.5 Characterization of Flow Regimes

One of the most efficient ways of presenting the possible regime boundaries of a bubble column system is through the use of flow regime maps. Figure 2.3 is one such map presented by Deckwer et al. (1980) for semibatch operated bubble and slurry bubble columns with low viscosity continuous phases. The chart shows the influence of both column diameter and superficial gas velocity on regime transition.

While helpful, flow regime maps are generally limited to two or three parameters. This makes it impossible to predict exactly the onset of transition for any system using a single map, a property that is extremely important in biotechnological systems which require operation within flow regimes with little shear (Merchuk et al., 1994). In addition, the superficial gas velocity at which a bubble column begins to transition depends on operating parameters such as temperature and pressure, which fluctuate greatly during non-steady state operation, particularly at reactor start-up and shut-down. Several parameters have been found to influence the superficial gas velocity at which the column enters the transition regime. These parameters may be classified generally as continuous phase properties, operating parameters and bubble column design parameters.

Unfortunately, little work has been carried out on the effects of internals on regime transition. As stated earlier, more systematic study is required in this area.
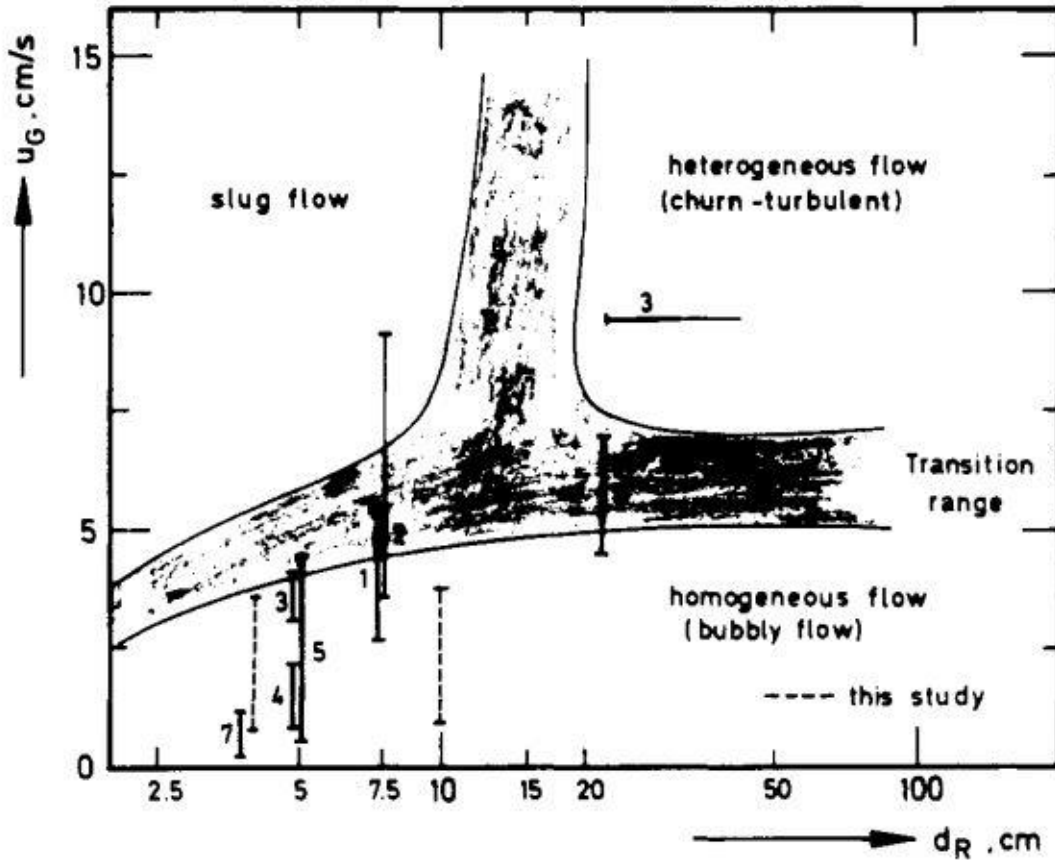
Figure 2.3: Flow regime map presented by Deckwer et al. (1980)

The effects of certain continuous phase properties such as viscosity, solids concentration and surface tension), have been studied in bubble columns transitioning from the bubbly to the coalesced bubble flow regime. Increases in continuous phase viscosity (Ruzicka et al., 2001, Wilkinson, 1991), solids concentration (for slurry bubble columns) (Shaikh and Al-Dahhan, 2006, Mena et al., 2005, Vandu et al., 2004) and surface tension (Urseanu, 2000) properties have been found to lower the superficial gas velocity at which transition is first observed (Shaikh and Al-

Dahhan, 2007). This occurs because increases in those continuous phase properties stabilizes the surfaces of the contained bubbles. The stabilized bubbles coalesce at rates greater than their unstabilized counterparts and are less likely to undergo breakup. Larger bubbles are experienced at lower superficial gas velocities (Shaikh and Al-Dahhan, 2007) and thus, an advance in regime transition is observed.

Operating parameters such as temperature, pressure and static height have significant effects on the onset of transition within bubble column systems. In general, increases in operating temperature (Lin et al., 1999, Bukur et al., 1987), operating pressure (Lin et al., 1999, Wilkinson et al., 1992, Krishna et al., 1991) and the continuous phase static height (Ruzicka et al., 2001, Sarrafi et al., 1999) increases the superficial gas velocity at which regime transition is observed and thus, delays transition. Higher operating temperatures tend to reduce the viscosity of the continuous phase. A reduction in viscosity destabilizes the larger bubbles in the system and as discussed earlier, delays transition. Increases in the operating pressure of a bubble column reactor increases the rate of bubble breakup within the system while simultaneously decreasing the rate of bubble coalescence, also delaying transition. Increases in the static height of the continuous phase generally results in transition delays since the probability of successful bubble coalescence increases along with it. However, static height was only observed to have an effect on transition below a certain critical reactor length (Sarrafi et al., 1999).

The aspect ratio and sparger design of a bubble column can affect the manner in which the gaseous and continuous phases interact with each other and by extension, the superficial gas velocity at which a bubble column begins to transition. Increases in aspect ratio generally lead to advances in

transition (Shaikh and Al-Dahhan, 2007, Throat and Joshi, 2004, Ruzicka et al., 2001) since the probability of successful coalescence increases. However, more research is required before a conclusive relationship can be established (Shaikh and Al-Dahhan, 2007). Decreases in sparger hole diameters and increases in perforation pitch have been found to delay regime transition below certain critical values (Jamialahmadi et al., 2000, Sarrafi et al., 1999). As mentioned earlier, the bubbles of the bubbly flow regime move vertically with little transverse or axial oscillations and do not coalesce. Thus, the size of these bubbles and their spatial arrangements are fully dependent on the sparger's design. As a result, bubble columns equipped with spargers which produce smaller, well-spaced bubbles require higher superficial gas velocities to experience coalescence and transition.

2.2 Gas Holdup in Bubble Columns

Gas holdup refers to the total volume fraction of gas found within a bubble column at any point during its operation. It is a dimensionless quantity and is used in bubble column design and analysis because it characterizes the transport phenomena of the system (Kantarci et al., 2005). Gas holdup can be used to characterize bubble column systems because it is dependent on the liquid phase properties of that system as well as certain operating and design parameters. These factors influence bubble size, which affects bubble rise velocity and ultimately the volume of gaseous phase (as gas bubbles) within the reactor. If the aforementioned properties favor the formation of small bubbles, the gas holdup of the particular system would be large because small bubbles have small bubble rise velocities and thus, longer residence times. However, if the formation of larger bubbles is supported, gas holdup will be smaller since larger bubbles have larger bubble rise velocities and thus, spend less time within the column.

Although gas holdup provides invaluable information with respect to reactor design, further analysis based on bubble sizes and spatial arrangements can yield useful information regarding a reactor's performance. Small bubble holdup, the fraction of total gas holdup due to small bubbles, has a great influence on the total interfacial mass transfer which occurs within the reactor (Deckwer, 1992) due to their high surface area- to-volume ratios. Their small bubble rise velocities also afford them enough time to engage in significant interfacial mass transfer with the liquid phase as they traverse the reactor. The gas holdup due to large bubbles (large bubble holdup) influences the occurrence of phenomena such as liquid entrainment, axial and radial liquid circulation and the presence of high energy eddies. In turn, these phenomena affect liquid mixing properties such as backmixing and mixing time (Deckwer, 1992). Such properties affect the productivity of a bubble column, the specific manner in which dependent on the reactor's application.

The gas holdup within a system can be affected by numerous factors. A summary of the effects of various liquid phase properties and operating and design parameters will be presented in following subsections. The effect of superficial gas velocity and various internals on gas holdup will be more thoroughly explored.

2.2.1 Effect of Continuous Phase Properties

Continuous phase properties, such as viscosity, solids concentration, solids diameter and surface tension, have considerable effects on the gas holdup of bubble column systems. Increasing the viscosity of the liquid phase generally results in the system experiencing a lowered gas holdup (Li et al., 1997). This occurs because viscous liquid phases are able to stabilize the larger bubbles that

are formed within the system and support bubble coalescence. Larger bubbles have shorter residence times and spend less time within the column, reducing gas holdup. Increases in the solids concentration of a slurry phase generally lead to decreases in gas holdup (Krishna et al., 1997) due to an increase in the system's 'pseudo-viscous' properties. The effect of particle size on gas holdup has also been investigated in slurry bubble columns. Although dependent on several system properties, Saxena et al. (1990) found that for a fixed superficial gas velocity and solids concentration, increasing the solids diameter decreased gas holdup within the system, particularly for lower slurry concentrations. Decreasing the surface tension properties of a continuous phase leads to increases in gas holdup (Urseanu, 2000). Decreased surface tension destabilizes the gas-liquid (or gas-slurry) interface of bubbles, which limits coalescence and increases bubble breakup.

2.2.2 Effect of Operating Parameters

The effect of operating parameters, such as temperature and pressure, on gas holdup has been the subject of several investigations. In general, increasing the operation pressure of bubble column reactors tends to increase gas holdup (Kantarci et al., 2005, Luo et al., 1999, Krishna et al., 1994) by increasing rate of bubble breakup within the system. The effect of temperature on bubble column systems is still undetermined, although it has been the subject of much research (Kantarci et al., 2005, Deckwer et al., 1980, Saxena et al., 1990). A significant number of studies concluded that gas holdup is independent of operation temperature (Kantarci et al., 2005). However, researchers such as Deckwer et al. (1980) and Saxena et al. (1990) made other observations. Deckwer et al. observed decreases in gas holdup up until a certain "critical" temperature was reached. However, when temperature was increased beyond this critical point, gas holdup remained unchanged. It is important to note that Deckwer et al. carried out this experiment in a

small diameter column which does not allow the influence of "wall effects" on their results to be ignored (Kantarci et al., 2005). Saxena et al. investigated the effects of temperature on both two– and three–phase bubble column reactors within temperatures ranging from 297 – 343 K. They found that gas holdup was dependent on temperature for the two–phased system. The three–phased system was found to be independent of operation temperature.

2.2.3 Effect of Design Parameters

The effects of several design parameters, such as aspect ratio, column diameter, column height, sparger design and sparger type, have been well documented in the literature. In general, gas holdup has been found to be a function of aspect ratio, column diameter and column height only when certain critical values are not exceeded. Luo et al. (1999) found gas holdup to be independent of column height when heights of 1 – 3 m were surpassed and aspect ratio was greater than 5. Shah et al. (1982) found that gas holdup was independent of column diameter when diameter was larger than 0.10 to 0.15 m. The type of sparger used and its respective properties have been found to influence the overall bubble sizes that are seen within an operating bubble column. Bouaifi et al. (2001) found that smaller orifice gas distributors yielded higher gas holdup values. They justified their findings by stating that the smaller the bubbles produced by a sparger, the higher the associated gas holdup values. Luo et al. (1999) and Schumpe and Grund (1986) have investigated the effects of several different spargers on gas holdup. Luo et al. found that gas holdup was strongly affected by sparger type at low superficial gas velocities (less than 0.06 m/s). Schumpe and Grund compared the gas holdups when two different types of spargers (ring type and perforated plate) were used. They found that the ringed type distributor yielded a lower total gas holdup than perforated plate distributors for the same 1 mm hole diameter.

2.2.4 Effect of Superficial Gas Velocity

Gas holdup is mostly dependent on the superficial gas velocity of an operating bubble column (Shah et al., 1982). In general, gas holdup has been found to increase with increases in superficial gas velocity (Krishna et al., 1997, Saxena et al., 1990, Schumpe and Grund, 1986, Deckwer et al., 1980), the extent to which dependent on the operating flow regime. In the bubbly flow regime, gas holdup increased proportionally with increases in superficial gas velocity (Kara et al., 1982, Lockett and Kirkpatrick, 1975). Gas holdup in the turbulent flow regime also increased with increases in superficial gas velocity, however the relationship with which was less defined (Koide et al., 1984, Kara et al., 1982). Hyndman et al. (1997) investigated the contributions of each of the two bubble classes to the total gas holdup for a hollow bubble column system throughout a variety of flow regimes. The group found that in the bubbly flow regime, the gas holdup for the small bubble class increased significantly until the transition regime was reached. However, in the turbulent flow regime, the contributions of the small bubble class experienced no further increases and remained equal to that experienced at transition. Thus, the increases in total gas holdup observed in the turbulent flow regime were due to increases in large bubble holdup only.

2.2.5 Effect of Internals

The gas holdup experienced in bubble column systems can be significantly altered by the presence of internals. As mentioned earlier, a wide variety of internal designs are under current investigation, though unsystematic. A summary of the effects of these internals on gas holdup will be presented in the following paragraph. However, more details on the particular internal will be given in a subsequent section.

In general, the addition of internals to a hollow bubble column reactor leads to increases in the gas holdup experienced. Internals such as partition plates (Van Baten and Krishna, 2003, Dreher and Krishna, 2001, Deckwer, 1992) and baffles of all types (Jhawar, 2011, Yamashita, 1987, Yamashita, 1985) increase gas holdup by filtering out and breaking up the larger bubbles found in the system. Internals such as packing ensure high gas holdup (Bhatia et al., 2004, Deckwer, 1992) by limiting the maximum stable size of the bubbles that pass through it. The packing internal can also increase gas holdup by increasing the residence time of the gaseous phase within the internal. The tube bundle internal has been found to have positive effects on gas holdup (Youssef, 2010) which are most likely due to a decrease in the average size of the small bubble class that occurs in its presence. Lastly, the presences of draft tubes within bubble column systems can be used to increase the system's interfacial area (and thus gas holdup) through the jet loop reactor configuration (Deckwer, 1992).

2.3 Gas Holdup Measurement Techniques

The overall gas holdup of a bubble column reactor can be estimated using three major techniques – techniques based on axial pressure profiles (Gandhi, 1997), techniques based on dynamic/static height (Gandhi, 1997, Deckwer, 1992) and techniques based on bed pressure drop (Gandhi, 1997). The specific contributions of the small and large bubble classes to gas holdup as well as other bubble class properties can be obtained through the dynamic gas disengagement technique (Li and Prakash, 2000).

2.3.1 Axial Pressure Profile Technique

An estimation of gas holdup through techniques based on the axial pressure profile require at least two static pressure measurements along the axial plane of the reactor for each gas velocity

investigated. It is important to note that although an estimate can be obtained using two static pressure measurements only, the accuracy of the obtained pressure gradient increases with an increase in the number of static pressure measurements taken. Pressure measurements are facilitated through the use of installed pressure taps and static pressure can be measured using a variety of pressure measuring devices, the simplest being a U-tube manometer. A plot of static pressure vs. axial displacement can be used to determine the pressure gradient while gas holdup can be estimated using the obtained gradient as well as Equation 2.1 and Equation 2.2 below.

$$\varepsilon_l + \varepsilon_g = 1 \tag{2.1}$$

$$\frac{\Delta P}{\Delta z} = g\left(\rho_l \varepsilon_l + \rho_g \varepsilon_g\right) \tag{2.2}$$

In these equations, ε_l is the fraction of liquid in the system, ε_g is the fraction of gas in the system or gas holdup, ρ_l is the liquid phase density, ρ_g is the gaseous phase density, g is acceleration due to gravity, ΔP is the change in pressure and Δz is the bed height. Although axial static pressure profiles yield reasonable results at low superficial gas velocities, use of this method at higher gas velocities is subject to substantial error due to the occurrence of large pressure fluctuations within the system. To increase the accuracy of this method at high gas velocities, a means through which fluctuations could be adequately dampened should be applied.

2.3.2 Dynamic/Static Height Technique

To estimate gas holdup using methods based on the dynamic/static height of a working bubble column reactor of constant cross-sectional area, knowledge of the bed's static height and an

estimate of the beds dynamic height is required. This method is based on the principle of conservation of mass since it assumes that the total volume of the reactor's bed is equal to the sum of the volume of all its contained phases. When the cross-sectional area of the reactor is constant, the relationship which exists between the volumes of the liquid and gaseous phases within the reactor also exists between the heights of each phase if completely segregated. As a result, the gas holdup for a constant cross-sectional area bubble column can be obtained via Equation 2.3.

$$\varepsilon_g = \frac{h_{dyn} - h_{st}}{h_{dyn}} \tag{2.3}$$

In this equation, ε_g is gas holdup, h_{dyn} is the dynamic height of the dispersion and h_{st} is the static height of the continuous phase. While relatively simple, methods based on the dynamic/static height of a system are not without their limitations, particularly for operation at high superficial gas velocities. At high gas velocities, the bed surface of a bubble column is subject to severe fluctuations due to the frequent occurrence of large bubble eruptions which reduce the accuracy of the dynamic height estimate. The bed also produces a foam layer which further reduces the accuracy of the dynamic height reading.

2.3.3 Bed Pressure Drop Technique

Gas holdup estimations based on bed pressure drop are obtained by first acquiring an estimate of the pressure drop experienced over a certain portion of the bed. This is achieved by measuring the pressure at two different axial positions in the bed and taking the difference between the values. The distance between which the pressure measurement points should also be noted. Using the fact that the bed density is equal the sum of the product of the individual phase densities and their

respective phase fractions as well as the relationship defined in Equation 2.1 above, an estimate of gas holdup from bed pressure drop can be obtained using Equation 2.4 below.

$$\varepsilon_g = \frac{-\Delta P - \rho_l H_{bed} g}{H_{bed} g (\rho_g - \rho_l)} \tag{2.4}$$

In this equation, ε_g is gas holdup, ΔP is the pressure drop across two points in the bed, H_{bed} is the distance between the two points, ρ_g is density of the gaseous phase, ρ_l is density of the liquid phase and g is acceleration due to gravity. Methods based on the overall bed pressure drop are quite advantageous as the errors associated with fluctuations and foam layer buildups are eliminated. However, the accuracy of the obtained estimations are fully dependent on the method used to determine the pressure drop across the given section of the bed.

2.3.4 Dynamic Gas Disengagement Technique

The dynamic gas disengagement technique is a unique technique which allows for further analysis of the overall gas holdup of a system based on its large and small bubble classes. For this technique, the pressure fluctuations which occur when gas flow to the column is suddenly stopped are recorded and analysed. Analysis of the fluctuations provides information on bubble class properties such as superficial gas velocity allocations, holdups and average bubble rise velocities (Li and Prakash, 2000; Schumpe and Grund, 1986).

2.4 Bubble Size Measurement Techniques

Although the dynamic gas disengagement technique provides important information about the bubble classes in gas-liquid dispersions, it provides no direct information about the size of the

bubbles in each class. As a result, several techniques have been developed for estimating the size of the small bubble class. Three major methods are used to determine the sizes of bubbles in a gas-liquid dispersion (Deckwer, 1992) – techniques based on visual observations/photography, techniques based on the insertion of probes/conductivity and techniques based on sample analysis/optics. These techniques can be found in the literature, a summary of which will be presented in following subsections.

2.4.1 Photography-based Techniques

Photography-based techniques provide bubble size measurements based on photographs of the phase mixture that have been recorded for further analysis with particle sizing software. This technique is facilitated by using clear material to construct the reactor's walls or through the addition of 'windows' which allow access to the reactor's innards. A light source may be added for additional clarity and all photographs should be taken against a standard of known dimension. Although simple to execute, the photographic method is subject to several limitations. The technique only allows for analysis of bubbles near the wall of the reactor while bubbles with diameters larger than 5 mm are not guaranteed to be spherical in shape and may be ellipsoidal or indented. These limitations make it difficult to determine the true average bubble diameter of the system since samples are limited to the wall region and the sizes measured are dependent on the bubble's orientation. In addition, analysis of the obtained photographs can be tedious for large samples. Wall curvature has been found to distort the shape of the bubbles within the reactor. However, the effects of wall curvature can be reduced through the use of plane parallel windows or by fitting the reactor with a transparent box that has been filled with the same liquid that makes up the continuous phase.

2.4.2 Conductivity-based Techniques

Bubble size measurement techniques based on conductivity can be used to measure the average size of a bubble class as well as its holdup and average bubble rise velocity provided that the continuous phase has good electrical conductivity. The technique is based on the principle in which reduced conductivity is associated with the presence of a poor conductor which is, in this case, the discontinuous gaseous phase, and that longer breaks in signal are associated with larger bubbles. There are two types of probes that are commonly used when carrying out this technique – the two-point and the four-point conductivity probes. Each probe consists of well-insulated detectors which are made out of noble metals (typically platinum and iridium) of different lengths. The two-point conductivity probe contains only two detectors of varying lengths. However, the four-point conductivity probe contains four detectors, the central detector being the shortest while the three remaining outer detectors being equal in length. To obtain accurate measurements, head-on contact between the probe and a bubble is a necessity and it is for this reason that probes are typically oriented vertically downward in the system of interest. However, head-on collisions with the probe, although more likely with the four point conductivity probe, are not guaranteed due to the random nature of a bubble's trajectory.

2.4.3 Optical Techniques

Techniques based on sampling and analysis through optical means are ideal for systems in which photography and conductivity are challenging due to visibility limitations and the absence of a good conducting continuous phase. In this technique, samples of the bed are taken and passed through a capillary tube of known dimensions as plugs of continuous and discontinuous phase. A beam of light is shone on the capillary tube and the absorbance, which depends on the phase being

analysed, is recorded with time. The length of a gaseous plug, and thus the volume and diameter of the respective bubble, can then be determined.

Like the other methods discussed earlier, this sampling technique is not without its limitations, the most pressing of which being the maintenance of isokinetic suction of the bed for analysis. Suction speed that are too high lead to dissociation of the large bubbles within the capillary tube while suction speeds that are too low can lead to the coalescence of the smaller bubbles at the inlet. This limitation makes the sampling technique unsuitable for systems in which the bubble size distribution is considerable. Thus, to obtain accurate results, this technique should be applied to systems in which the bubble size distribution is expected to be narrow.

2.5 Liquid Mixing

The phase interactions experienced in a bubble column reactor influence the properties of the bubble classes which in turn affect gas holdup, mass transfer and liquid circulation. Due to the great influence of phase interactions on those system parameters, a means through which the interactions could be accurately predicted and quantified is necessary. Several quantification means can be found in the current literature, the most popular of which being mixing time and the quantification of liquid backmixing through the axial dispersion coefficient. The topics are expounded upon in the following subsections.

2.5.1 Mixing Time

The amount of time required for a system to return to uniformity after perturbation can be referred to as the mixing time for that system. Like backmixing, the mixing time experienced within a

bubble column is dependent on its hydrodynamics – phenomena such as axial and radial liquid recirculation, turbulent eddies and liquid entertainment are all phase interactions found to influence mixing time (Camacho Rubio et al., 2004). The occurrence of such phenomena is attributed to the presence of a particular class of discontinuous, gaseous phase – the large bubble class (Deckwer, 1992). As they rise, the large bubbles entrain fluid elements from lower axial positions within the reactor. The initially entrained fluid becomes the wake of a large bubble and continues to grow as it is carried upwards. If the wake of the bubble gets too heavy for the bubble to carry before reaching the bed's surface, it is shed where it exist as a high energy eddy within the system for a period of time. If successfully carried however, the wake of the bubble is left at the bed's surface after bubble eruption. The law of conservation of mass is maintained within the system as a comparable volume of fluid is forced downward along the reactor's wall since large bubbles tend to travel along the bed's central axis. This continuous fluid displacement sets up liquid circulation within the axial plane of the reactor (Deckwer, 1992). Radial circulation, on the other hand, is achieved when large bubbles displace any fluid in their paths as they rise (Deckwer, 1992).

The extent of axial dispersion that occurs within a bubble column system is justifiably related to the amount of time required for the reactor to attain uniformity after perturbation (Muhsin and Abid, 2008). For completely statistical systems that are defined by larger axial dispersion coefficients, large amounts of backmixing occur within their continuous phases and thus, a smaller amount of time is required to regain uniformity after perturbation. Conversely, systems defined by small axial dispersion coefficients experience lesser amounts of backmixing and thus require more time to regain uniformity after perturbation.

2.5.2 Liquid Backmixing

The dynamics between the phases contained within a bubble column reactor greatly affects the performance of that reactor due to the influence of phase dynamics on various physical rate processes (Shah et al., 1978). Those physical rate processes (such as interphase and heat and mass transfer) along with the inherent kinetics of the contained reactants are the major factors influencing reactant conversion and product selectivity (Degaleesan, 1998, Shah et al., 1978). Bubble column reactors always contain a liquid continuous phase and a gaseous discontinuous phase who's mixing dynamics, in the simplest sense, may be modelled as completely mixed and plug flow respectively. Although the plug flow assumption for the discontinuous phase may be reasonable, the assumption of complete mixing for the continuous phase usually deviates significantly from reality, and often leads to considerable over sizing of reactors in cases of nearly-complete conversion (Degaleesan, 1998).

The mixing that a fluid experiences is due to two major phenomena – micromixing and macromixing. Micromixing can be simply defined as mixing on a molecular level. It is the mixing that occurs between the molecules or entities that make up a flow system. This class of mixing is independent of the residence time distribution of the fluid within a reactor. It is instead a function of the time association between the various molecules that make up the fluid. The extent of micromixing ranges from complete segregation to maximum mixedness. For the case of complete segregation, molecular mixing within the system is delayed to as late as possible while for the case of maximum mixedness, molecular mixing occurs almost instantly (Shah et al., 1978).

Macromixing, the second phenomenon, considers fluid mixing on a scale much greater than the molecular level. Instead, it considers the mixing that a fluid experiences as a complete, independent entity. This class of mixing is primarily the result of convective and diffusive transport and like micromixing, ranges from two extremes – plug flow to complete mixing. For the case of plug flow, mixing in the axial direction is non-existent, while fluid in the radial direction experiences complete mixing. As a result, all fluid elements have identical residence times and identical velocities. For the case of complete mixing, fluid elements experience complete axial and radial mixing, making the composition product stream identical to that in the reactor. The residence time distribution of the complete mixing case decays exponentially (Shah et al., 1978).

The degree of deviation from either of the extremes of macromixing is due to the degree of convective diffusion or 'dispersion' (Davis and Davis, 2003). Convective diffusion may result from non-uniform velocity profiles, short circuiting, bypassing and channeling, velocity fluctuations due to molecular and turbulent diffusion, reactor shape and internals, backflow of fluid due to velocity differences between phases, and recycling due to agitation (Shah et al., 1978). The deviation may also be due to another phenomenon – backmixing – which differs from channeling and recirculation in that it is a completely random case of axial mixing. Shah et al. (1978) presents the following definition of backmixing – "Backmixing is a specific case of axial mixing in which random movement of fluid is superimposed on and is in the direction of the main flow stream, and where the transverse mixing (that is, mixing in the direction perpendicular to the flow) is complete."

The degree of backmixing which occurs in a statistical system can be quantified through the use of models, with the model of choice depending heavily on that system's degree of deviation from either of the macromixing ideals. Systems in which plug flow is believed to occur may be adequately modelled by the plug flow model, while systems characterized by complete mixing may be modelled as continuous stirred tank reactors (CSTRs). Unfortunately, a real reactor is often neither fully plug flow or completely mixed in nature, and thus requires a model that is able to quantify its degree of mixing with respect to either of the mixing ideals. Dispersion models are plug flow models which justify the inherent non-ideality of the systems they describe through the superimposition of a diffusion-like spreading mechanism (Davis and Davis, 2003, Gupta et al., 2001, Levenspiel, 1998). This diffusion-like process accounts for the degree of backmixing found within individual plugs of fluid and is quantified through the model's axial dispersion coefficient. A large axial dispersion coefficient is indicative of rapid tracer spreading or large dispersion. This is indicated by a severely-altered outlet tracer signal when an ideal tracer pulse is injected at the reactor's inlet. A small axial dispersion coefficient indicates little dispersion and thus, a mildly altered outlet tracer signal. An axial dispersion coefficient equal to zero indicates the occurrence of no dispersion and hence, plug flow. As a result, the tracer signal obtained at the outlet is identical to that of the inlet.

2.5.3 Factors Influencing Mixing Time/Liquid Backmixing

Like all other hydrodynamic properties, liquid backmixing and liquid mixing time can be alter when certain continuous phase properties and operating and design parameters are altered. A summary of those effects will be presented below, with special emphasis being placed on the effect

of internals on the experienced mixing time. It is useful to keep the inverse relationship between liquid backmixing and liquid mixing time in mind when considering the following subsections.

2.5.3.1 Effect of Continuous Phase Properties

The effect of viscosity and surface tension have been studied in both hollow and modified bubble column reactors. Addition of surface acting agents and thus, decreases in the surface tension properties of the continuous phase lead to increases in the mixing time experienced in hollow bubble column reactors (Pandit and Joshi, 1982) as well as bubble column reactors that have been equipped with partition plates (Doshi and Pandit, 2005) and draft tubes (Bando et al., 1998). This occurrence could be accounted for using energy balances (Doshi and Pandit, 2005). Mixing time, like many other hydrodynamic properties, is dependent on the liquid circulation velocity of the continuous phase under given operating conditions. In the presence of electrolytes, gas holdup increases due to the bubble de-stabilization mentioned in a prior section. A corresponding increase in energy dissipation occurs due to the increase in gas-liquid interface and thus, less energy is available for liquid motion. The reduction in energy is reflected in the liquid velocities of the continuous phase and subsequent increases in mixing time occur.

Increases in viscosity have been found to increase the mixing time experienced in a hollow bubble column reactor (Pandit and Joshi, 1982) by increasing the internal friction of the continuous phase and thus, the amount of energy it dissipates. Less energy becomes available for liquid motion and a corresponding increase in mixing time is observed. It is interesting to note that decreases in mixing time with increases in viscosity have been reported for bubble column reactors that have been equipped with draft tube internals (Bando et al., 1998). For this case, increases in viscosity

lead to increases in the overall bed density of the downcomer since bubbles are less likely to be entrained due to an increase in the average bubble size of the system. As a result, circulation between the riser and downcomer increases and mixing time decreases (Bando et al., 1998).

Mixing time was also observed to increase in the presence of drag reducing agents for hollow bubble column systems, and increase with increases in the flow consistency index for various non-Newtonian continuous phases (Pandit and Joshi, 1982).

2.5.3.2 Effect of Operating Parameters

Mixing time was generally found to decrease with increases in superficial gas velocity for hollow bubble column systems (Pandit and Joshi, 1982) and bubble column systems that had been equipped with partition plates (Doshi and Pandit, 2005). However, an increase in mixing time was recorded for hollow bubble column systems after a critical superficial gas velocity was reached. The decreases in mixing time observed results from increases in the liquid circulation velocity that occurred as superficial gas velocity increased. However, the eventual decrease in mixing time experienced by the hollow bubble column system may be due to dominance of an opposing effect at higher superficial gas velocities, the most likely being bed dispersion height. Typically, increases in dispersion height lead to increases in mixing time since mixing takes place over a greater length (Pandit and Joshi, 1982).

2.5.3.3 Effect of Design Parameters

Mixing time was observed to increase with increases in aspect ratio for both the hollow bubble column system (Pandit and Joshi, 1982) and the bubble column system equipped with the draft

tube internal (Bando et al., 1998). The observation is justified by the fact that more time would be required for mixing since mixing takes place over greater lengths for higher aspect ratios. Mixing time was observed to increase with increases in column diameter for both systems. However, it is important to note that although total mixing time increases, the mixing time per unit volume of fluid experiences a decrease (Pandit and Joshi, 1983, Bando et al., 1998). The design of the sparger (in terms of open area) was found to have no effect on the mixing time experienced in the sectionalized bubble column reactor (Doshi and Pandit, 2005). However, decreases in the free area of the partition plate as well as decreases in hole size increased the mixing time experienced in the column (Doshi and Pandit, 2005).

2.5.3.4 Effect of Internals

Internals such as partition plates (Van Baten and Krishna, 2003, Dreher and Krishna, 2001, Deckwer, 1992), packing (Bhatia et al., 2004, Deckwer, 1992), tube bundles (Jhawar, 2011, Youssef, 2010), baffle plates (Jhawar, 2011, Yamashita, 1987, Yamashita, 1985) and the inserted loop/draft tube (Deckwer, 1992) have all been found to have effects on bulk liquid circulation as well as other hydrodynamic properties such as gas hold up. A schematic of these internals can be found in Figure 2.4.
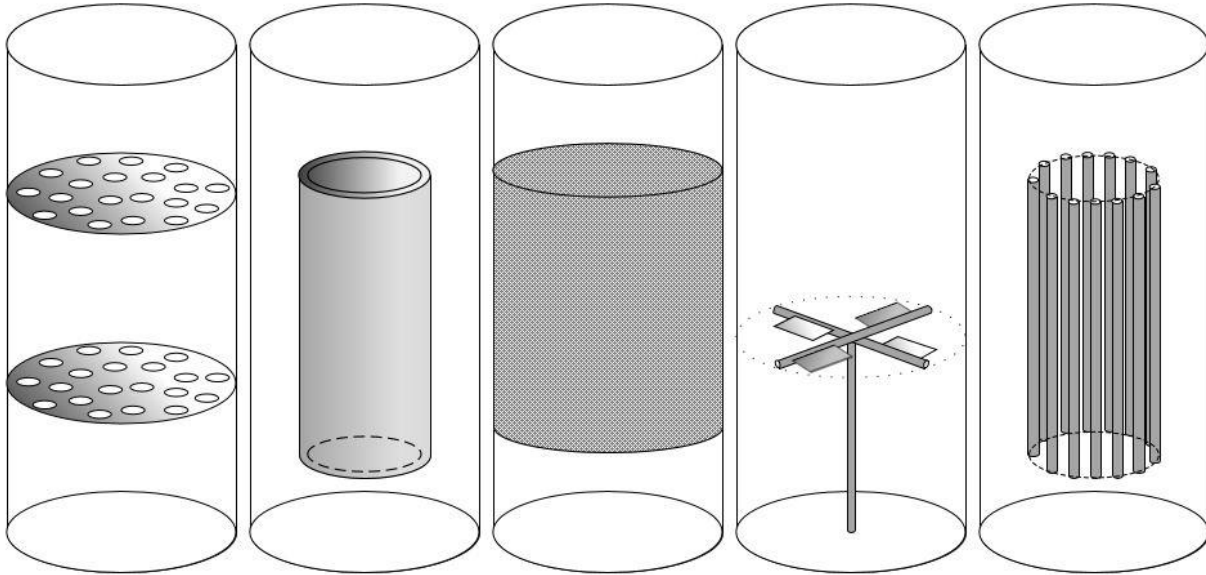
Figure 2.4: Schematic of bubble column reactor internals: (*from left to right*) partition plates, concentric draft tube internal loop, packing, concentric centrally mounted baffle and concentric tube bundle

The partitioned plate internal is a unique internal type as it is a means through which the continuous phase of a hollow bubble column reactor could be made to approach plug flow (Van Baten and Krishna, 2003, Deckwer, 1992) and thus, experience a reduced amount of backmixing and a corresponding increase in mixing time. The system also experiences an increase in gas holdup since coalesced bubbles are continuously filtered-out and broken at each plate. A feature of this internal type is that there exists an accumulation of gaseous material (called a gas cap) under each partition plate, with the degree of accumulation being dependant on the percentage of open plate area and the superficial gas velocity at which the column is operating under (Van Baten and Krishna, 2003). There are however, several disadvantages to the use of such internals in bubble column reactors. The formation of the gas cap beneath partition plates 'wastes' reactor space for bubble column systems operated in a semibatch manner (Dreher and Krishna, 2001) while

mechanical reinforcement of the plates may become challenging for very large reactors operating under extreme temperature and pressure conditions. Plugging, deposition and attrition are also disadvantages that are associated with the use of partition plates in slurry bubble column systems.

The addition of packing to a bubble column reactor has proven to be an effective means through which backmixing can be reduced within the system (Bhatia et al., 2004, Deckwer, 1992), despite the associated increase in mixing time. In addition, the presence of packing within bubble column reactors improves gas holdup and increases interfacial area by encouraging the formation of smaller bubbles within the column (Bhatia et al., 2004). However, like fixed beds, the packed bubble column reactor is unsuitable for heat generating/heat consuming reactions as the presence of the packing hinders effective temperature control. The packing internal may also be unsuitable for slurry bubble column reactors since particle deposition within the packing is likely to be unavoidable and undesirable.

Although the effect of the tube bundle internal on bubble column hydrodynamics has been investigated to some degree within the literature (due to the importance of heat exchanger tubes in the temperature control of reaction containing systems), more systematic studies are required to better understand its effects. Nonetheless, insertion of vertical heat exchanger tubes has been found to increase the gas holdup and interfacial area observed in equipped, working bubble columns (Jhawar, 2011, Youssef, 2010), with the increases most likely being due to a decrease in average bubble size. Although advantageous, the use of tube bundle internals has also been found to increase the degree of backmixing experienced in equipped columns to higher levels than that

occurring in their comparable, hollow counterparts (Youssef, 2010). However, a reduction in mixing time is expected given the inverse relationship between backmixing and mixing time.

Centrally positioned baffle plate internals are unique in that they allow for varying degrees of gas holdup to be achieved by manipulating the placement of the baffle plates along the axial plane for a given segment of reactor length, from the reactor's bottom (Jhawar, 2011, Yamashita, 1985). The degree of gas holdup achieved could also be controlled by increasing the area of the baffle plates or by increasing the number of baffle plates within the system (Yamashita, 1985). Although little work has been done on the effect of centrally located baffle plates on bubble column reactor backmixing, the presence of such is expected to reduce the occurrence of this hydrodynamic phenomenon (Yamashita, 1987) and increase mixing time. Side-mounted baffles, on the other hand, have been found to reduce the backmixing that occurs within bubble column systems (Albright, 2008) by disrupting the overall bulk liquid circulation that takes place in the reactor. However, the specific configuration of the side-mounted baffle can make it susceptible to dead zones which wastes reactor space. Both centrally positioned and side-mounted baffles face challenges with respect to mechanical reinforcement under extreme operating conditions.

The addition of an inserted loop/draft tube to a hollow bubble column reactor can be effectively used to control the direction of liquid recirculation within the reactor (Deckwer, 1992) as well as the intensity of the recirculation experienced through the manipulation of superficial gas velocity and the direction of gas flow. While several variations to this modified bubble column exist, a common operational principle is shared between the variants. For all cases, liquid circulation is controlled through the creation and maintenance of a density gradient within the bed (Deckwer,

1992). This is achieved through the restriction of gas to one specific region of the reactor, a regime maintained by the presence of the segregation-supporting inserted loop. The remaining region denied of gas flow contains continuous phase only and is thus the denser region of the bed. The resulting density imbalance sets up and sustains liquid circulation within the reactor in which downward flow occurs within the denser region and upward flow within the aerated, less dense region.

The addition of an inserted loop to a hollow bubble column greatly affects the operation of the reactor, the extent to which being dependent on the specific application. However, two major advantages of inserted loops have been observed and documented in the literature. The presence of the inserted loop has been found to heighten liquid circulation within the hollow bubble column system and thus, reduce the time required for liquid mixing (Deckwer, 1992). This property is quite advantageous in systems which require uniformity despite perturbations. The airlift reactor is also subject to reduced backmixing when compared to that experienced in a bubble column reactor, for certain operating conditions (Yang, 2007, Kadic and Heindel, 2014).

2.6 Tracer Techniques

Estimates of the axial dispersion coefficient can be obtained from the distorted tracer concentration curve that is recorded at a reactor's outlet after the injection of a particular tracer at its inlet. Throughout the literature, a large variety of tracers have been used to carry out these experiments. These tracers can be placed into five general categories – dyestuffs (Deckwer, 1992), acidic/basic solutions (Deckwer, 1992), salts (Deckwer, 1992), heat (Deckwer, 1992) and radioactive powders (Gupta et al., 2001) – and are summarized in the following subsections.

2.6.1 Dyestuff Tracers

The first tracer category, dyestuffs, refers to coloured, pigmented materials (Deckwer, 1992) that are typically suspended in a liquid carrier. If such a tracer is used, the outlet tracer concentration can be determined by taking absorption measurements using a device such as a spectrophotometer. The use of dyestuff tracers can be advantageous as it allows for both qualitative and quantitative assessments to be carried out on the system without affecting the system's properties. Dye pigments of various colours are also readily available and are relatively inexpensive. However, this method can be limited by the frequency with which samples can be collected and/or analysed.

2.6.2 Acidic and Basic Tracers

The second class of tracers, acidic or basic solutions (Deckwer, 1992), are advantageous tracers since the properties of a bubble column reactor have been shown to remain relatively unchanged with the addition of such solutions to its system. These solutions are also readily available and can be cheaply acquired. However, the acidity of a system is typically measured with pH meters which generally have long response times. A long response time can have an effect on the concentration/time curve acquired, a property which is extremely important for the estimation of the axial dispersion coeffecient. The use of acidic or basic solutions as tracers may also be unsuitable for certain reactor systems that are sensitive to pH, such as bubble column systems containing biological organisms.

2.6.3 Aqueous Salt Tracers

Aqueous salt tracers (Deckwer, 1992), the third tracer category, can be an advantageous tracer class as the instantaneous concentration of salt at the reactor outlet can be measured using conductivity probes which tend to have very short response times. Unfortunately, the addition of salts to a bubble column system can influence the hydrodynamics of the reactor (Kantarci et al., 2005) and can make it difficult to determine the dispersion occurring within the system unaffected by salt.

2.6.4 Heat Tracers

Heat (Deckwer, 1992), provided from a point source, is a unique and beneficial tracer class since bubble column hydrodynamics are only mildly affected by temperature (Kantarci et al., 2005). In addition, the continuous phase can also be easily regenerated through appropriate cooling means (Deckwer, 1992). On the other hand, use of heat as a tracer requires excellent temperature control through insulation as well as the means to provide a constant flux of heat at the heating source (Deckwer, 1992). Lack of control in both areas can increase the difficulty associated with acquiring measurements and can also lead to erroneous results. The instantaneous concentration of heat within the system can be determined by measuring the temperature of the continuous phase using devices such as thermocouples.

2.6.5 Radioactive Tracers

The last tracer class is the most recently developed of all of the methods implemented in current experimentation. Radioactive tracers (Gupta et al., 2001) refer to materials that have been enriched

with radioactive matter. These tracers can be injected into the continuous phase of a bubble column reactor through the use of a carrier medium. The concentration/time curve obtained using such tracers can be attained through the use of scintillation-base meters. These meters fluoresce according to the amount of radioactive matter that they are exposed to. Radioactive tracers can be an advantageous tracer class since they can be used for both continuous and discontinuous phase investigations when used with a carrier medium or as a powder respectively. Also, radioactive materials do not affect the properties of the systems that they are added to. Conversely, radioactive tracers are not easily accessible and are the most expensive of all the tracers outlined above. Several health risks can be associated with the use of such tracers and thus implementation of additional safety procedures and protocols may be necessary. Lastly, a radioactive tracer with an appropriate half-life needs to be properly selected since the tracer should be able to last the duration of the experiments without spending an excessively long time in the environment after experimentation has been completed.

2.7 Estimation of Mixing Time through Tracers

As mentioned earlier, the macromixing taking place within real reactor vessels falls somewhere between the extremes of plug flow and complete mixing. It is important to note that the fluid elements all spend different amounts of time within the reactor for varying shades of macromixing, with the exception of the plug flow ideal. The amount of time spent by a fluid element within the reactor is called the residence time of that element. This property is dependent on the specific path taken by the fluid element travelling from the reactor's entrance to its exit (Levenspiel, 1998). The distribution of those times is called the residence time distribution and it has units of time. The residence time distribution of fluid elements may be represented by the exit age distribution

function, 'E'. The 'E' distribution function is limited to closed vessel boundary conditions and as a result, fluid elements can only cross the entrance and exit boundaries of the system once. As a result, no manifestations of convective diffusion should take place at the vessel boundaries. The normalized form of this function is shown below:

$$\int_0^\infty E \, dt = 1 \qquad (2.5)$$

The fraction of fluid elements spending less than some arbitrary time "t_1" within the reactor may be found from the following expression:

$$\int_0^{t_1} E \, dt \qquad (2.6)$$

The fraction of fluid element ages equal to or greater than t_1 can be obtained by subtracting the above result from 1.

$$\int_{t_1}^\infty E \, dt = 1 - \int_0^{t_1} E \, dt \qquad (2.7)$$

The E-curve is one of the most helpful properties with respect to a reactor's deviation from ideality. A system's E-curve may be determined from tracer experiments using physical or non-reactive liquid tracers. Tracers may be injected in four different manners – pulse input, step input, periodic

input and random input – with each having its own unique means of interpretation. The following paragraphs explore the analysis of one of the most simple tracer input methods, the pulse input.

The pulse input approach involves the instantaneous injection of a known amount of tracer at the entrance of reactor, along with the entering fluid. This method also requires the continuous recording of the tracer concentration with time at the reactor's outlet. For explanatory purposes, consider Figure 2.5.
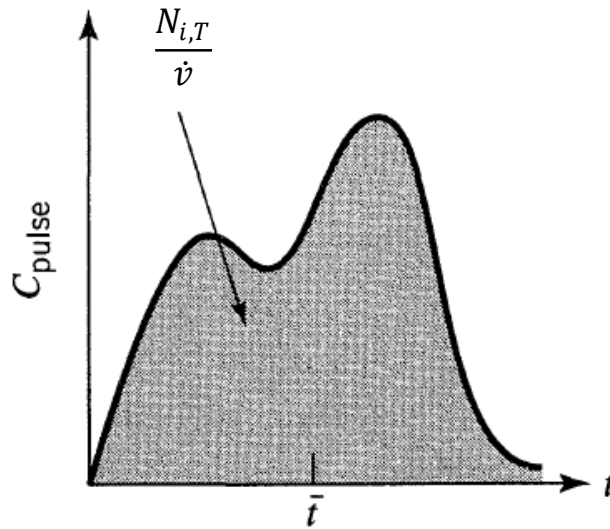
Figure 2.5: Sample C-curve (Levenspiel: 1988), adapted

The area under the graph could be found through simple integration (Levenspiel, 1988),

$$A = \int_0^\infty C_{pulse} \, dt \cong \sum C_i \Delta t_i = \frac{N_{i,T}}{\dot{v}} \tag{2.8}$$

where A is the area under the graph, C_{pulse} is the instantaneous tracer concentration, $N_{i,T}$ is the total number of moles of tracer introduced to the system and $\dot{v}$ is the volumetric flow of the liquid

through the system. Δt_i is a discrete, specified time interval and C_i is the corresponding instantaneous tracer concentration. The average time spent by the tracer and hence, the mean of the C-curve ($\bar{t}$), may be found from the following (Levenspiel, 1988):

$$\bar{t} = \frac{\int_0^\infty t C_{pulse} \, dt}{\int_0^\infty C_{pulse} \, dt} \cong \frac{\sum t_i C_i \Delta t_i}{\sum C_i \Delta t_i} = \frac{V}{\dot{v}} \qquad (2.9)$$

where $\bar{t}$ is the mean residence time of the tracer and V is the volume of the reactor. The C-curve may be converted into the E-curve by altering the tracer concentration scale in a manner that makes the area under the C-curve unity. This is achieved through the following expression (Levenspiel, 1988):

$$E = \frac{C_{pulse}}{N_{i,T}/\dot{v}} \qquad (2.10)$$

A second type of curve in which time is measured as multiples of mean residence time, E_θ, can be generated using the following substitution:

$$\qquad (2.11)$$

$$\theta = {t}/{\bar{t}}$$

Thus,

$$E_\theta = \bar{t}E = \frac{V}{\dot{v}} \frac{C_{pulse}}{N_{i,T}/\dot{v}} = \frac{V}{N_{i,T}} C_{pulse} \tag{2.12}$$

The extent of spreading or the variance of the tracer as it passes through a particular system, σ^2, can be obtained from the following equation (Levenspiel, 1988):

$$\sigma^2 = \frac{\int_0^\infty (t - \bar{t})^2 C_{pulse}\, dt}{\int_0^\infty C_{pules}\, dt} = \frac{\int_0^\infty t^2 C_{pules}\, dt}{\int_0^\infty C_{pulse} dt} - \bar{t}^2 \tag{2.13}$$

Or,

$$\sigma^2 = \frac{\sum (t_i - \bar{t}_i)^2 C_i \Delta t_i}{\sum C_i\, \Delta t_i} = \frac{t_i^2 C_i \Delta t_i}{C_i \Delta t_i} - \bar{t}^2 \tag{2.14}$$

$\bar{t}$ and σ^2 have been theoretically linked to the dispersion properties of a reactor that has been modelled using the axial dispersion model. The following subsection further expands on this relationship.

2.8 Estimation of Liquid Backmixing through Tracers

The model chosen to represent a particular flow system is primarily based on that system's degree of deviation from either of the macromixing ideals. Dispersion models are plug flow models which justify the inherent non-ideality of the systems they describe through the superimposition of a diffusion-like spreading mechanism (Degaleesan, 1998, Shah et al., 1978, Fogler, 2006, Davis and Davis, 2003). This diffusion-like process accounts for the degree of backmixing found within individual plugs of fluid. Backmixing is due to random disturbances within flow systems, such as eddies. This leads to the redistribution of material within individual plugs and thus, implies the

non-existence of stagnant zones or gross fluid recirculation through short-circuiting and bypassing (Shah et al., 1978).
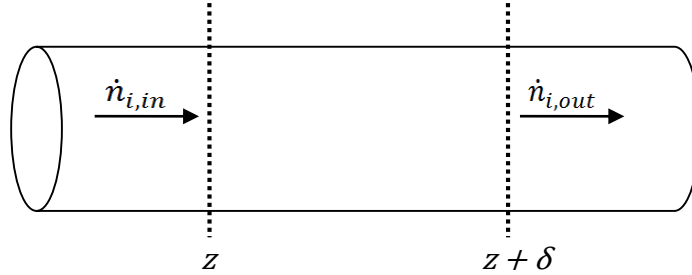
Figure 2.6: Schematic of Plug Flow Reactor

Based on Figure 2.6, the equation of conservation of mass for the pulse injection of a tracer, i, into any reactor system may be written as follows,

$$\frac{\delta N_i}{\delta t} = \dot{n}_{i,in} - \dot{n}_{i,out}$$

(2.15)

Where t is time, N_i is the number of moles of tracer and $\dot{n}_i$ the molar flow of tracer into and out of the system. When a system is completely plug flow in nature, molar flow is only due to convective molar flow and can be defined as follows,

$$\dot{n}_\iota = A_c v C_i$$

(2.16)

where A_c is the cross-sectional area of the reactor, v the velocity of the liquid within the reactor and C_i the concentration of tracer within the reactor. However, for real systems with imperfect plug flow properties, molar flow within the system may be described as convective molar flow superimposed with dispersion in the axial direction (Degaleesan, 1998, Shah et al., 1978, Fogler,

43

2006, Davis and Davis, 2003). Thus, the molar flow within real systems can be defined as follows (Fogler, 2006, Davis and Davis, 2003),

$$\dot{n}_\iota = A_c v C_i - A_c D_a \frac{\delta C_i}{\delta z} \tag{2.17}$$

where the latter term represents the degree of backmixing or axial dispersion occurring within the system. From prior studies, the dispersion occurring within real flow systems has been found to occur frequently enough to be considered statistical in nature. This property allows dispersion to be treated in a manner similar to that of the molecular diffusion in Fickian systems. As a result, the dispersion term contains a dispersion coefficient, D_a, and tracer concentration, C_i, is described as a function of the axial direction, z.

Substituting the expression for molar flow in real reactors into the equation of conservation of mass yields the following expression,

$$\frac{\delta N_i}{\delta t} = \left(A_c v C_i - A_c D_a \frac{\delta C_i}{\delta z} \right) - \left(A_c v C_i - A_c D_a \frac{\delta C_i}{\delta z} + \partial \left(A_c v C_i - A_c D_a \frac{\delta C_i}{\delta z} \right) \right) \tag{2.18}$$

Simplifying this expression yields,

$$\frac{\delta N_i}{\delta t} = -\partial \left(A_c v C_i - A_c D_a \frac{\delta C_i}{\delta z} \right) \tag{2.19}$$

If N_i is rewritten in terms of concentration and cross-sectional area, and v and D_a are assumed to be constant variables, the above equation can be further simplified to,

$$A_c \partial z \frac{\delta C_i}{\delta t} = -A_c v \partial C_i + A_c D_a \frac{\delta^2 C_i}{\delta z} \qquad (2.20)$$

$$\frac{\delta C_i}{\delta t} = -v \frac{\partial C_i}{\delta z} + D_a \frac{\delta^2 C_i}{\delta z^2} \qquad (2.21)$$

The dimensionless form of the above equation can be obtained through the following substitutions,

$$Z = {}^{z}/_{L} \qquad (2.22)$$

$$\theta = {}^{t}/_{\bar{t}} \qquad (2.23)$$

$$Pe_a = {}^{Lv}/_{D_a} \qquad (2.24)$$

in which Z is dimensionless length, L is the length of the reactor, θ is dimensionless time, $\bar{t}$ is mean residence time and Pe_a is Peclet number. Substituting and rearranging yields,

$$\frac{1}{Pe_a} \frac{\delta^2 C_i}{\delta Z^2} = \frac{\delta C_i}{\delta \theta} + \frac{\partial C_i}{\delta Z} \qquad (2.25)$$

The magnitude of the axial dispersion coefficient offers valuable information on the extent of dispersion within the system as well as the nature of the C-curve obtained. As Peclet number tends to infinity, dispersion within a particular flow system becomes negligible and that system approaches plug flow. When Peclet number tends to zero, dispersion is large and the system approaches complete mixing.

3.0 Experimental

3.1 Gas Holdup from Bed Pressure Drop Technique

All experiments were carried out in a 0.15 m diameter Plexiglas bubble column reactor. The height of the reactor was 2.50 m. To minimize mechanical vibrations, the column was supported by a rigid metal structure, which also kept it vertically oriented. A schematic of the experimental setup is shown in Figure 3.1. Gas was added to the reactor using a coarse sparger with four arms. Each arm had five, downward facing holes that were 1.90 mm in diameter. The specific sparger design has been outlined in previous work (Gandhi, 1997). Experiments were carried out in the presence of two different internals. A top view of the first internal, the centrally-mounted concentric baffle (a static mixer), can be found in Figure 3.2 while the top view of the second internal, the concentric tube bundle, can be found in Figure 3.3. Experiments were carried out with the tube bundle internal (CT) and a combination of the tube bundle and baffle internals (CTB). Specifications concerning the internals' design and orientation can be found in Table 3.1. Oil free, compressed dry air was used as the discontinuous phase for all experiments. Its flow rate was controlled using three calibrated sonic nozzles of varying diameters (0.60 mm, 1.50 mm and 2.50 mm). Experiments were carried out at superficial gas velocities ranging from 0.01 m/s to 0.30 m/s. The continuous phase used in all experiments was tap water which was maintained at a static height of about 1.40 m.

Gas holdup was estimated from pressure fluctuations recorded within the column. Two pressure transducers (OMEGA Type PX541-7.5GI and Type PX541- 45 15GI) were used to measure the pressure fluctuations. The response time of the transducers was 2 ms. The transducers were located in distributor and disengagement sections of the column at elevations of $z = 0.027$ m and $z = 1.318$

m respectively. This can be seen in Figure 3.1. Pressure was measured in voltage since the transducers were connected to a DC power supply that generated a voltage proportional to measured pressure. The readings were later converted to pressure units using the calibration found in Appendix B. Pressure fluctuations were measured at a rate of 60 Hz for 180 s. All readings were obtained through the use of LabVIEW 8. The Pressure difference was calculated by averaging the difference between the two transducer readings. The average gas holdup was obtained using Equation 3.1.

$$\varepsilon_g = \frac{-\Delta P + \rho_l H_{bed} g}{H_{bed} g (\rho_g - \rho_l)} \tag{3.1}$$

In this equation, ε_g is gas holdup, ΔP is the pressure drop across the pressure transducers, H_{bed} is the distance between the pressure transducers, ρ_g is density of the gaseous phase, ρ_l is density of the liquid phase and g is acceleration due to gravity. The experiment was repeated three times for each internal at all the superficial gas velocities investigated. The gas holdup results presented in the following section are averages of the data obtained over multiple days.
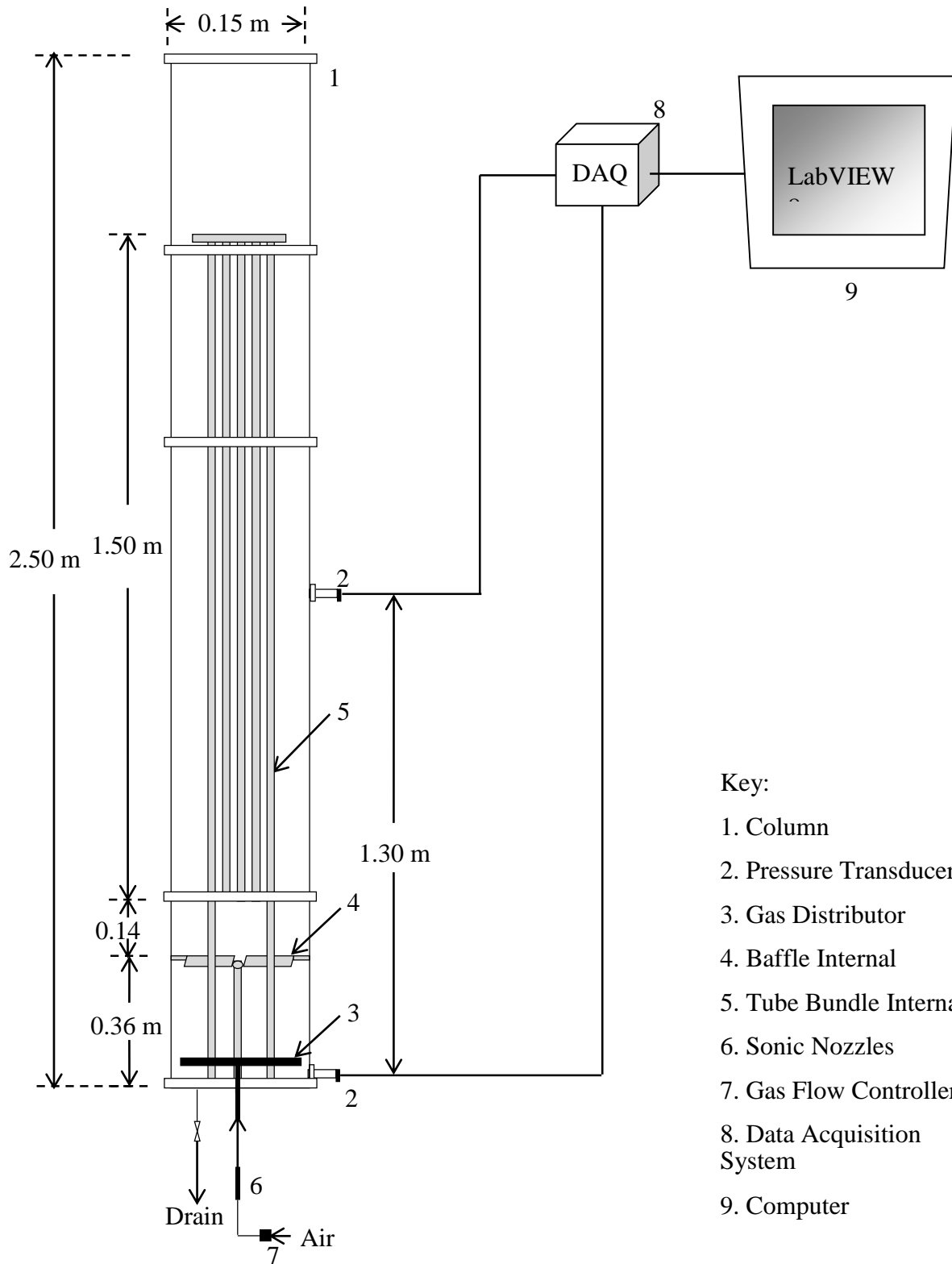
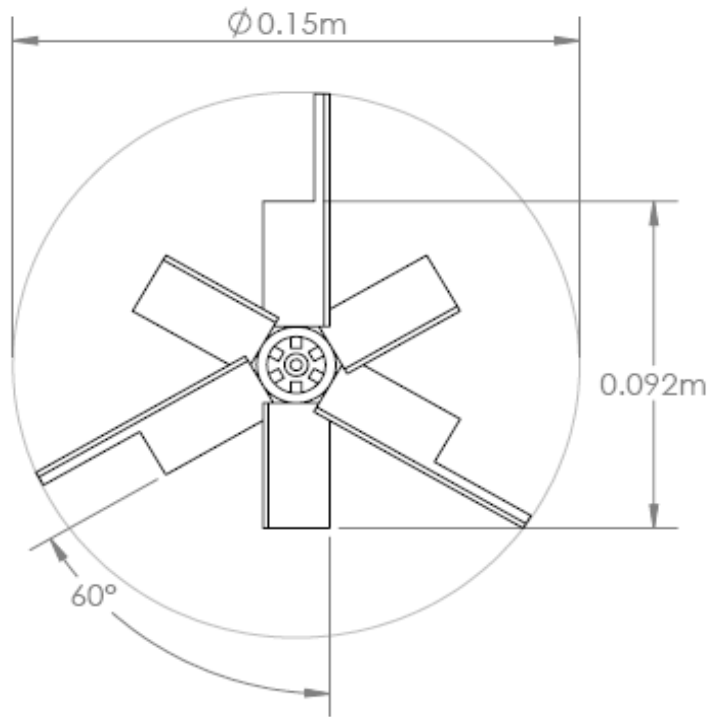Figure 3.1: Schematic Showing Experimental Setup 1

Figure 3.2: Top View of Baffle Internal
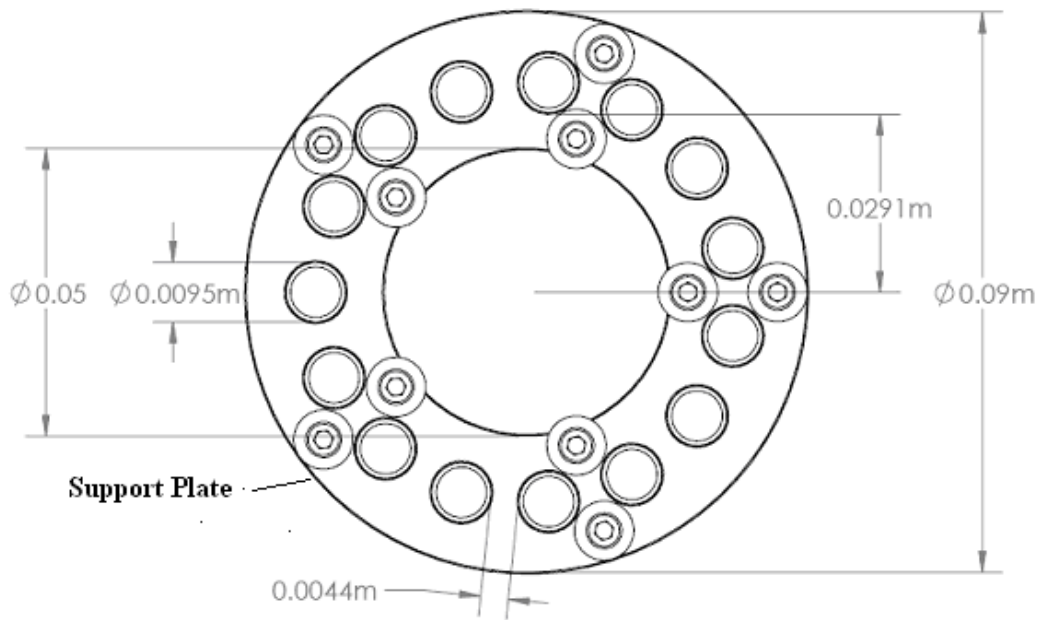
Figure 3.3: Top View of Tube Bundle Internal

50

Table 3.1: Summary of internal properties

Internal Combination Type	Details
Circular Tube Bundle (CT)	Tube Bundle: No. of tubes: 15 Tube diameter: 0.95 cm Tube length: 150 cm Wall to wall spacing between tubes: 4.4 mm z = 0.5 m (from bottom)
Circular Tube Bundle + Concentric Baffle (CTB)	Tube Bundle: Same as above Concentric Baffle: No. of blades: 6 Length of blade: 3.5 cm Width of blade: 1.9 cm Blade angle: 60º from axis z = 0.36 m (from bottom)

3.2 Bubble Fractions from Dynamic Gas Disengagement Technique

All experiments were carried out in a 0.15 m diameter Plexiglas bubble column reactor. The height

of the reactor was 2.50 m. To minimize mechanical vibrations, the column was supported by a

rigid metal structure, which also kept it vertically oriented. A schematic of the experimental setup

is shown in Figure 3.1. Gas was added to the reactor using a coarse sparger with four arms. Each

arm had five, downward facing holes that were 1.90 mm in diameter. The specific sparger design

has been outlined in previous work (Gandhi, 1997). Experiments were carried out in the presence

of two different internals. A top view of the first internal, the centrally-mounted concentric baffle

(a static mixer), can be found in Figure 3.2 while the top view of the second internal, the concentric

tube bundle, can be found in Figure 3.3. Experiments were carried out with the tube bundle internal

(CT) and a combination of the tube bundle and baffle internals (CTB). Specifications concerning

the internals' design and orientation can be found in Table 3.1. Oil free, compressed dry air was used as the discontinuous phase for all experiments. Its flow rate was controlled using three calibrated sonic nozzles of varying diameters (0.60 mm, 1.50 mm and 2.50 mm). Experiments were carried out at superficial gas velocities ranging from 0.01 m/s to 0.30 m/s. The continuous phase used in all experiments was tap water which was maintained at a static height of about 1.40 m.

To carry out the dynamic gas disengagement technique, gas flow to the column was suddenly shut and the resulting pressure fluctuations were recorded. The distributor section pressure transducer (OMEGA Type PX541- 45 15GI) was used to measure the pressure fluctuations. The response time of the transducer was 2 ms. The transducer was located at an elevation of $z = 0.027$ m. Pressure was measured in voltage since the transducers were connected to a DC power supply that generated a voltage proportional to measured pressure. The readings were later converted to pressure units using the calibration found in Appendix B. Pressure fluctuations were measured at a rate of 60 Hz for 180 s. All readings were obtained through the use of LabVIEW 8. The dynamic gas disengagement curve for each case was obtained from the readings of the axially lower pressure transducer. The equations used to analyse the data can be found in the following chapter. The experiment was repeated three times for each internal at all of the superficial gas velocities investigated. The bubble fraction results presented in the following section are the results obtained from the second repeat for each of the investigated internals. A single day's result is compared since the difference between the results from the two internals is expected to be significant. This assumption is reasonable since statistical differences were obtained for the results from the related, overall gas holdup experiments.

3.3 Small Bubble Sizes from Photography-based Technique

All experiments were carried out in a 0.15 m diameter Plexiglas bubble column reactor. The height of the reactor was 2.50 m. To minimize mechanical vibrations, the column was supported by a rigid metal structure, which also kept it vertically oriented. A schematic of the experimental setup is shown in Figure 3.1. The pressure transducers and data acquisition system were not used in this experiment. Gas was added to the reactor using a coarse sparger with four arms. Each arm had five, downward facing holes that were 1.90 mm in diameter. The specific sparger design has been outlined in previous work (Gandhi, 1997). Experiments were carried out in the presence of two different internals. A top view of the first internal, the centrally-mounted concentric baffle (a static mixer), can be found in Figure 3.2 while the top view of the second internal, the concentric tube bundle, can be found in Figure 3.3. Experiments were carried out with the tube bundle internal (CT) and a combination of the tube bundle and baffle internals (CTB). Specifications concerning the internals' design and orientation can be found in Table 3.1. Oil free, compressed dry air was used as the discontinuous phase for all experiments. Its flow rate was controlled using three calibrated sonic nozzles of varying diameters (0.60 mm, 1.50 mm and 2.50 mm). Experiments were carried out at superficial gas velocities ranging from 0.01 m/s to 0.30 m/s. The continuous phase used in all experiments was tap water which was maintained at a static height of about 1.40 m.

To obtain estimates for the average bubble sizes of the small bubble class, short video clips of the previously explained dynamic gas disengagement process were taken using a Canon PowerShot SX50 HS Camera. From these videos, five frames in which the bubbles could be clearly identified were saved for further analysis with Image-Pro Premiere 9.1.All frames were obtained using

CyberlinkPowerDirector 12. As a precaution, a reference clip containing a particle of known size was captured at the same camera orientation and zoom settings that would be used to capture the disengagement process. The sizes of the bubbles and reference particle were determined (in pixels) using Image-Pro Premier 9.1. These bubble sizes were later scaled to length dimensions based on that of the reference particle. A sample of 55 bubbles size measurements were obtained for analysis. An average small bubble size will be presented in the following sections. No repeats were taken for this experiment. However, the experiment was carried out for each of the investigated internals.

3.4 Liquid Circulation from Neutrally Buoyant Particle Technique

All experiments were carried out in a 0.15 m diameter Plexiglas bubble column reactor. The height of the reactor was 2.50 m. To minimize mechanical vibrations, the column was supported by a rigid metal structure, which also kept it vertically oriented. A schematic of the experimental setup is shown in Figure 3.1. The pressure transducers and data acquisition system were not used in this experiment. Gas was added to the reactor using a coarse sparger with four arms. Each arm had five, downward facing holes that were 1.90 mm in diameter. The specific sparger design has been outlined in previous work (Gandhi, 1997). Experiments were carried out in the presence of two different internals. A top view of the first internal, the centrally-mounted concentric baffle (a static mixer), can be found in Figure 3.2 while the top view of the second internal, the concentric tube bundle, can be found in Figure 3.3. Experiments were carried out with the tube bundle internal (CT) and a combination of the tube bundle and baffle internals (CTB). Specifications concerning the internals' design and orientation can be found in Table 3.1. Oil free, compressed dry air was used as the discontinuous phase for all experiments. Its flow rate was controlled using three

calibrated sonic nozzles of varying diameters (0.60 mm, 1.50 mm and 2.50 mm). Experiments were carried out at superficial gas velocities ranging from 0.01 m/s to 0.30 m/s. The continuous phase used in all experiments was tap water which was maintained at a dynamic height of about 2.18 m.

To obtain a visual on the hydrodynamics occurring within a working bubble column, several near-neutrally buoyant particles of different colours and sizes were added to the system. The properties of the two major beads used in all experiments can be found in Table 3.2. However, details of the near-neutrally buoyant particle design could be found in Appendix C. For each case, videos were taken with the Canon PowerShot SX50 HS Camera and observations were noted. The most frequent particle motions have been reported in the results section. The particles were observed at the various gas velocities on at least five separate occasions for both of the investigated internals.

Estimates of the local liquid velocity were also obtained from the videos of the near-neutrally buoyant particles. Clips in which the particles moved upward or downward in a relatively straight manner were selected for the analysis. The vertical displacement of the particle was determined from the initial and final particle positions in the clips. This was obtained from the tape measure that had been attached to the column and captured in the videos. The time taken for the displacement to occur was determined from the frame rate and the number of frames within which the displacement had occurred.

Table 3.2: Summary of selected near-neutrally buoyant particle properties

Particle	Diameter, mm	Mass, kg	Density, kg/m^3	Sphericity	Settling Velocity, m/s
Particle 1	9.64	0.467	996.4	0.999	− 0.69
Particle 2	5.52	0.083	1046.2	0.850	0.89

3.5 Mixing Time from Dye Tracer Technique

All experiments were carried out in a 0.15 m diameter Plexiglas bubble column reactor. The height of the reactor was 2.50 m. To minimize mechanical vibrations, the column was supported by a rigid metal structure, which also kept it vertically oriented. A schematic of the experimental setup is shown in Figure 3.5. The probe and data acquisition system were not used in this experiment. Gas was added to the reactor using a coarse sparger with four arms. Each arm had five, downward facing holes that were 1.90 mm in diameter. The specific sparger design has been outlined in previous work (Gandhi, 1997). Experiments were carried out in the presence of two different internals. A top view of the first internal, the centrally-mounted concentric baffle (a static mixer), can be found in Figure 3.2 while the top view of the second internal, the concentric tube bundle, can be found in Figure 3.3. Experiments were carried out with the tube bundle internal (CT) and a combination of the tube bundle and baffle internals (CTB). Specifications concerning the internals' design and orientation can be found in Table 3.1. Oil free, compressed dry air was used as the discontinuous phase for all experiments. Its flow rate was controlled using three calibrated sonic nozzles of varying diameters (0.60 mm, 1.50 mm and 2.50 mm). Experiments were carried out at superficial gas velocities ranging from 0.01 m/s to 0.30 m/s. The continuous phase used in all experiments was tap water which was maintained at a static height of about 2.18 m.

Blue dye tracer solution was made by adding 500 drops of food colouring to 0.0005 m^3 of water. The solution was later added to the injection system, a schematic of which is shown in Figure 3.5. The tracer injection system consists of an open loop and a closed loop. Before injection, the dye was circulated within the closed loop labelled *a* to *d* in Figure 3.5 for at least 5 minutes. This step was added to ensure steady tracer circulation within the injection system. After steady tracer circulation had been reached, the dye solution was directed to the column and thus, entered the open loop labelled *a* to *f* in Figure 3.5. The dye was added to the top of the column using a ring-type sparger containing four, 1.3 mm diameter holes. The sparger was positioned 0.38 m from the top of the column. A schematic of the tracer injection sparger can be seen in Figure 3.4. Further details on the design of the injection system can be found in Appendix E. About 0.0075 mm^3 of the dye solution was injected into the working column within a 10 second time span. As mixing occurred, videos of the system's distributor region were taken using the Canon PowerShot SX50 HS Camera. For clarity, a white background was placed behind the part of the column being videotaped. Complete mixing was defined as the time within which the column first appeared to be uniformed in colour from the onset of dye tracer injection. The time required for complete mixing was obtained by determining the point in which the column's colour first seemed to remain unchanged in the respective video clips. This was determined using CyberlinkPowerDirector 12. This experiment was repeated at least three times for each superficial gas velocity investigated, for each internal. The mixing times presented in the results section are an average of the mixing times obtained during each repeat.
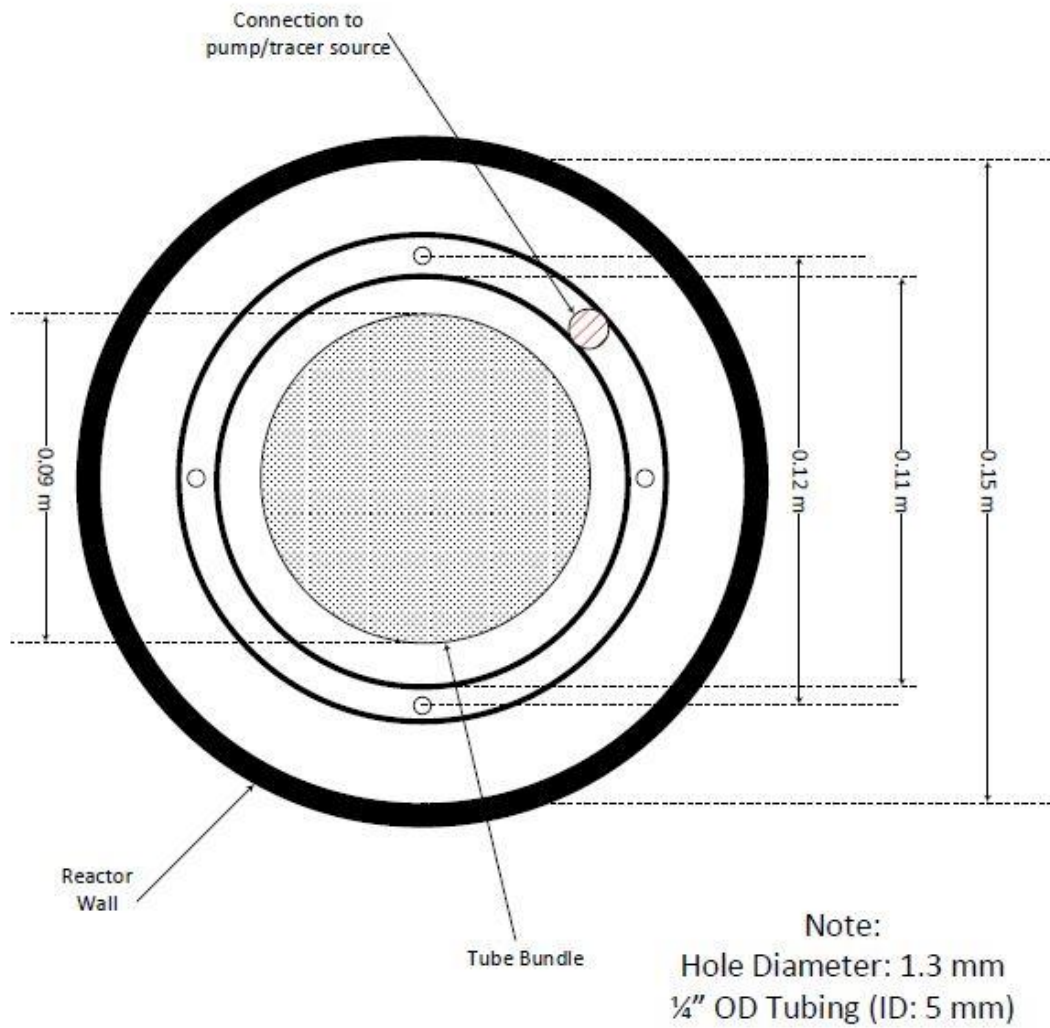
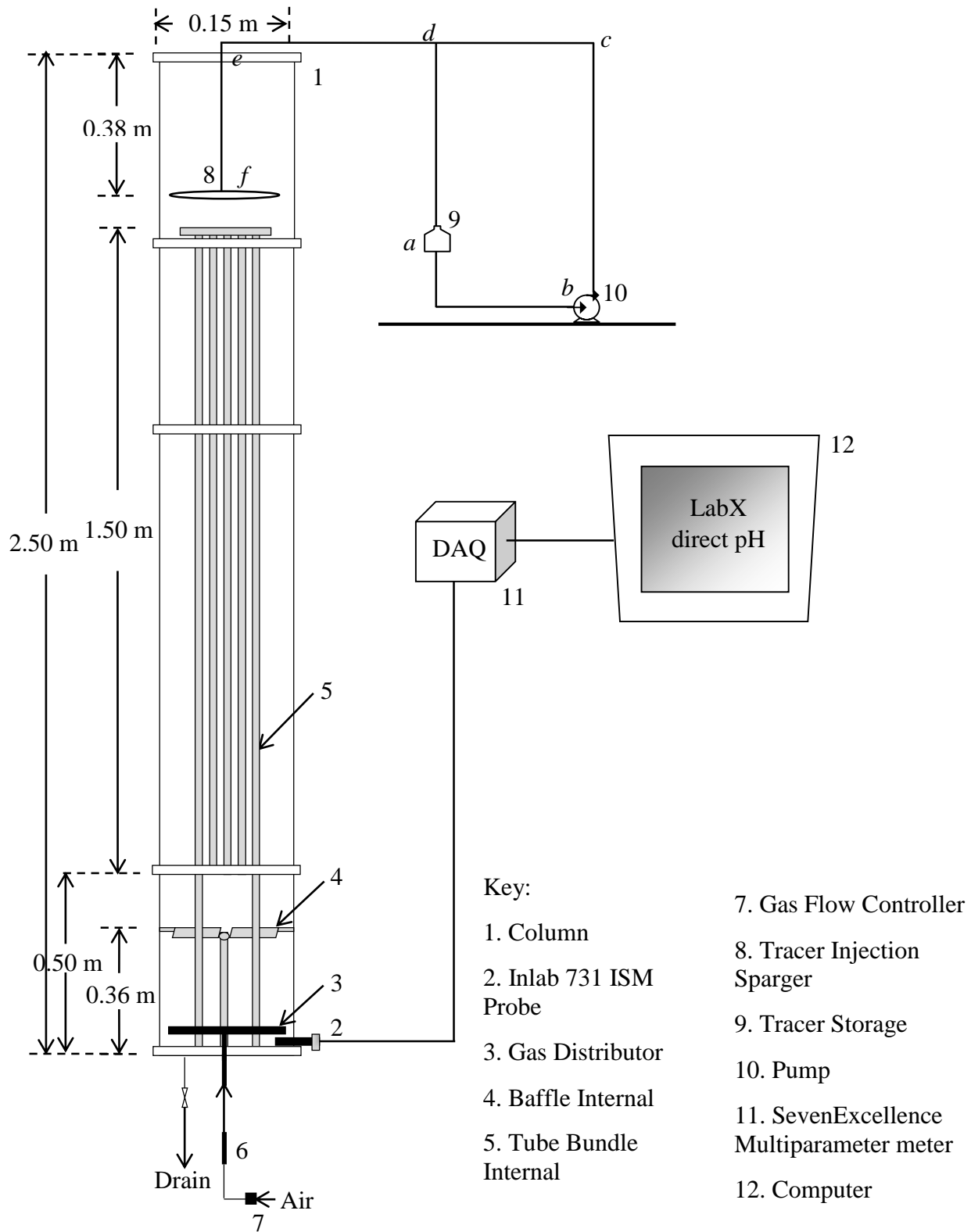Figure 3.4: Schematic of sparger used in tracer injection

Figure 3.5: Schematic Showing Experimental Setup 2

3.6 Mixing Time and Axial Dispersion Coefficient from Salt Tracer Technique

All experiments were carried out in a 0.15 m diameter Plexiglas bubble column reactor. The height of the reactor was 2.50 m. To minimize mechanical vibrations, the column was supported by a rigid metal structure, which also kept it vertically oriented. A schematic of the experimental setup is shown in Figure 3.5. Gas was added to the reactor using a coarse sparger with four arms. Each arm had five, downward facing holes that were 1.90 mm in diameter. The specific sparger design has been outlined in previous work (Gandhi, 1997). Experiments were carried out in the presence of two different internals. A top view of the first internal, the centrally-mounted concentric baffle (a static mixer), can be found in Figure 3.2 while the top view of the second internal, the concentric tube bundle, can be found in Figure 3.3. Experiments were carried out with the tube bundle internal (CT) and a combination of the tube bundle and baffle internals (CTB). Specifications concerning the internals' design and orientation can be found in Table 3.1. Oil free, compressed dry air was used as the discontinuous phase for all experiments. Its flow rate was controlled using three calibrated sonic nozzles of varying diameters (0.60 mm, 1.50 mm and 2.50 mm). Experiments were carried out at superficial gas velocities ranging from 0.01 m/s to 0.30 m/s. The continuous phase used in all experiments was tap water which was maintained at a static height of about 2.18 m.

A solution of 100 Kg/m^3 aqueous sodium chloride solution was made by adding 0.05 Kg of table salt to 0.0005 m^3 of distilled water. The solution was later added to the injection system, a schematic of which is shown in Figure 3.5. The tracer injection system consists of an open loop and a closed loop. Before injection, the salt solution was circulated within the closed loop labelled *a* to *d* in Figure 3.5 for at least 5 minutes. This step was added to ensure steady tracer circulation

60

within the injection system. After steady tracer circulation had been reached, the salt solution was directed to the column and thus, entered the open loop labelled *a* to *f* in Figure 3.5. The salt solution was added to the top of the column using a ring-type sparger containing four, 1.3 mm diameter holes. The sparger was positioned 0.38 m from the top of the column. A schematic of the tracer injection sparger can be seen in Figure 3.4. Further details on the design of the injection system can be found in Appendix E. About 0.0075 mm^3 of the salt solution was injected into the working column within a 10 second time span. The conductivity was measured using a SevenExcellence Multiparameter meter equipped with an Inlab 731 ISM probe. The probe was positioned 0.005 m from the bottom of the reactor. Measurements were taken at 1 second intervals and were obtained using the LabX direct pH software. As a precaution, all readings were taken after the meter reported stable temperature values. Photos of the probe and meter can be found in Figure 3.6a and Figure 3.6b respectively. Complete mixing was defined as the time in which the conductivity readings became constant from the time in which salt solution injection had first commenced. The time required for complete mixing was obtained by determining the point at which the column's conductivity first became constant from the onset of aqueous salt injection. This was obtained from a plot of instantaneous conductivity with time. The time required for the reactor to attain ninety percent mixing has been reported in the results section. Estimates of the axial dispersion coefficient were obtained from the method outlined in Ohki and Inoue (1970). No repeats were taken for this experiment due to time limitations. However, the experiment was carried out for each of the investigated internals.
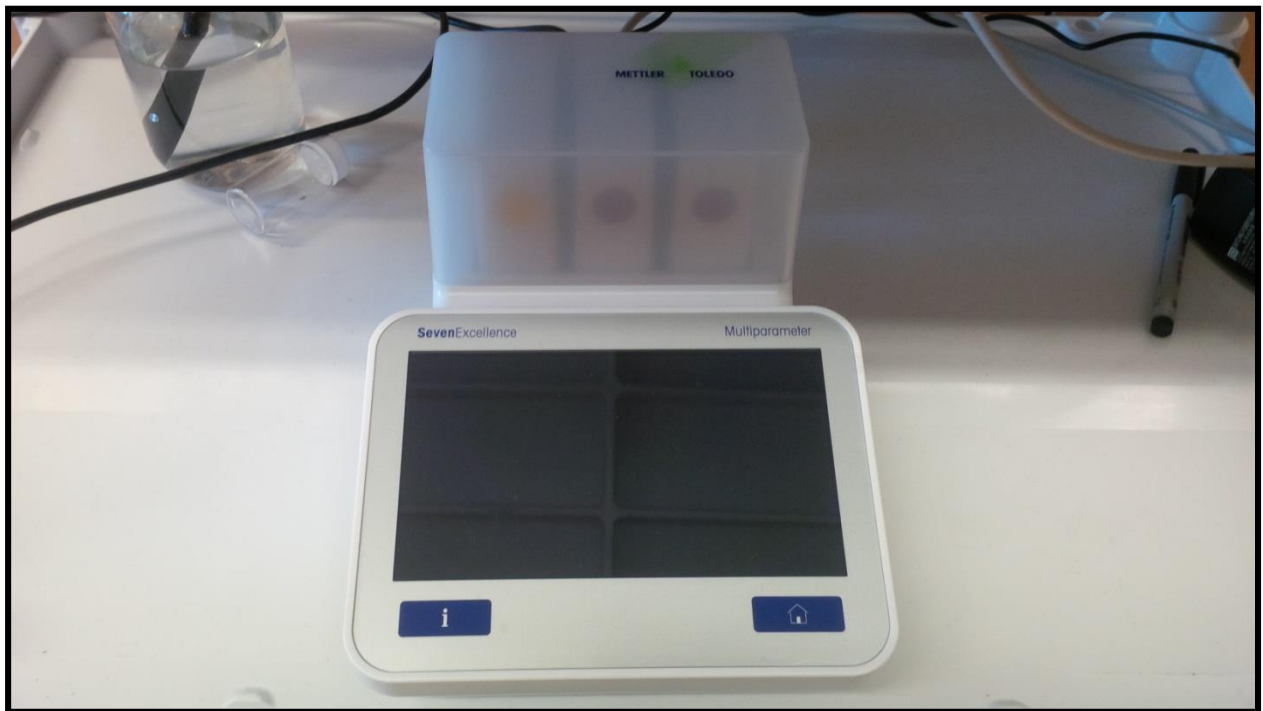
Figure 3.6: Picture of a) Inlab 731 ISM probe *(top)* and b) SevenExcellence Multiparameter

meter *(bottom)*

4.0 Results and Discussion

The results of this study are presented in three major sections (sections 4.1 to 4.3). Section 4.1 compares the effects of the CT and CTB internals on the local flow structure of the bubble column reactor. Bulk flow patterns, based on the local flow structures, are also proposed for both internals. Section 4.2 reviews the effect of the CT and CTB internals on the gas holdup experienced in a bubble column reactor. The effect of the internals on various bubble class properties (average bubble holdup, average rise velocity and small bubble size) is also reviewed. Lastly, a comparison between the effect of the CT and CTB internals on interfacial area is made. Section 4.3 compares the effect of the CT and CTB internals on mixing time and axial dispersion.

4.1 Local Flow Structures in the Presence of Internals

Bulk liquid circulation refers to the overall liquid circulation pattern that can be observed in a bubble column reactor under steady state operation. Although a single bulk circulation pattern exists for a particular reactor design under specific operating conditions, a variety of local flow structures can be observed. Local flow structures are quite complex since they can vary with both time and space. But like bulk circulation patterns, the nature of those local flow structures can be greatly influenced by the design of a bubble column reactor, particularly with the addition of internals. This section explores the effect of the CT and CTB internals on the local flow structures of a bubble column reactor. The local flow structures presented in this subsection were observed multiple times over several experimentation periods. The section will conclude with bulk liquid circulation propositions for the bubble column equipped with the CT and CTB internals respectively.

Local flow structures were observed through the use of near-neutrally buoyant beads, the design of which has been outlined in Appendix C. To accurately describe the observations, the column was separated into defined regions based on the internal used. When equipped with the CTB internal, the bubble column reactor was divided into six different regions – the distributor region, the baffle region, the tube bundle entrance region (called entrance region), the tube bundle inner core region (called core region), the tube bundle outer annular region (called annular region) and the tube bundle exit region (called exit region). These regions have been labelled regions 1 to 6 respectively in Figure 4.1a. When equipped with the CT internal, the bubble column reactor was divided into five different regions – the distributor region, the entrance region, the core region, the annular region and the exit region. These regions have been labelled region 1 to 5 respectively in Figure 4.1b.

The investigations carried out with the CT and CTB internals have yielded several interesting differences that can be qualitatively analysed through the use of neutrally buoyant particles. In general, the bubble column equipped with the CT internal could be described as containing two main circulation cells - cell one, the distributor region, and cell two, an amalgamation of the four remaining regions. This could be seen at all superficial gas velocities, although the circulation cells seem to merge at higher superficial gas velocities. Circulation cells were not observed in the bubble column when equipped with the CTB internal. Instead, the particles were seen randomly moving within the visible regions of the column. This difference implies that the presence of the baffle internal within the reactor disrupts overall liquid circulation and indirectly reduces backmixing.

Many interesting observations were made for the circulation cells which occurred during CT investigations. At low superficial gas velocities, the particles spent equal amounts of time in both cells, with the only exchange between cells occurring when the particles exited cell one through the core region and entered cell two through the annular region. As superficial gas velocity increased, the particles spent more time in circulation cell two over circulation cell one, and a breakdown of the two circulation cells developed. The breakdown was validated by increased occurrences of the particles exiting cell one and entering cell two via the annular region. This was first observed at a superficial gas velocity of 0.15 m/s, although the particles could be seen oscillating about the entrance region at a superficial gas velocity of 0.10 m/s. As superficial gas velocity increased, the distance traversed by the particles into the annular region experienced a general increase and the occurrences became more frequent.

Key:
1. Region 1 - Distributor
2. Region 2 - Baffle
3. Region 3 - Entrance
4. Region 4 - Core
5. Region 5 - Annular
6. Region 6 - Exit

Key:
1. Region 1 - Distributor
2. Region 2 - Entrance
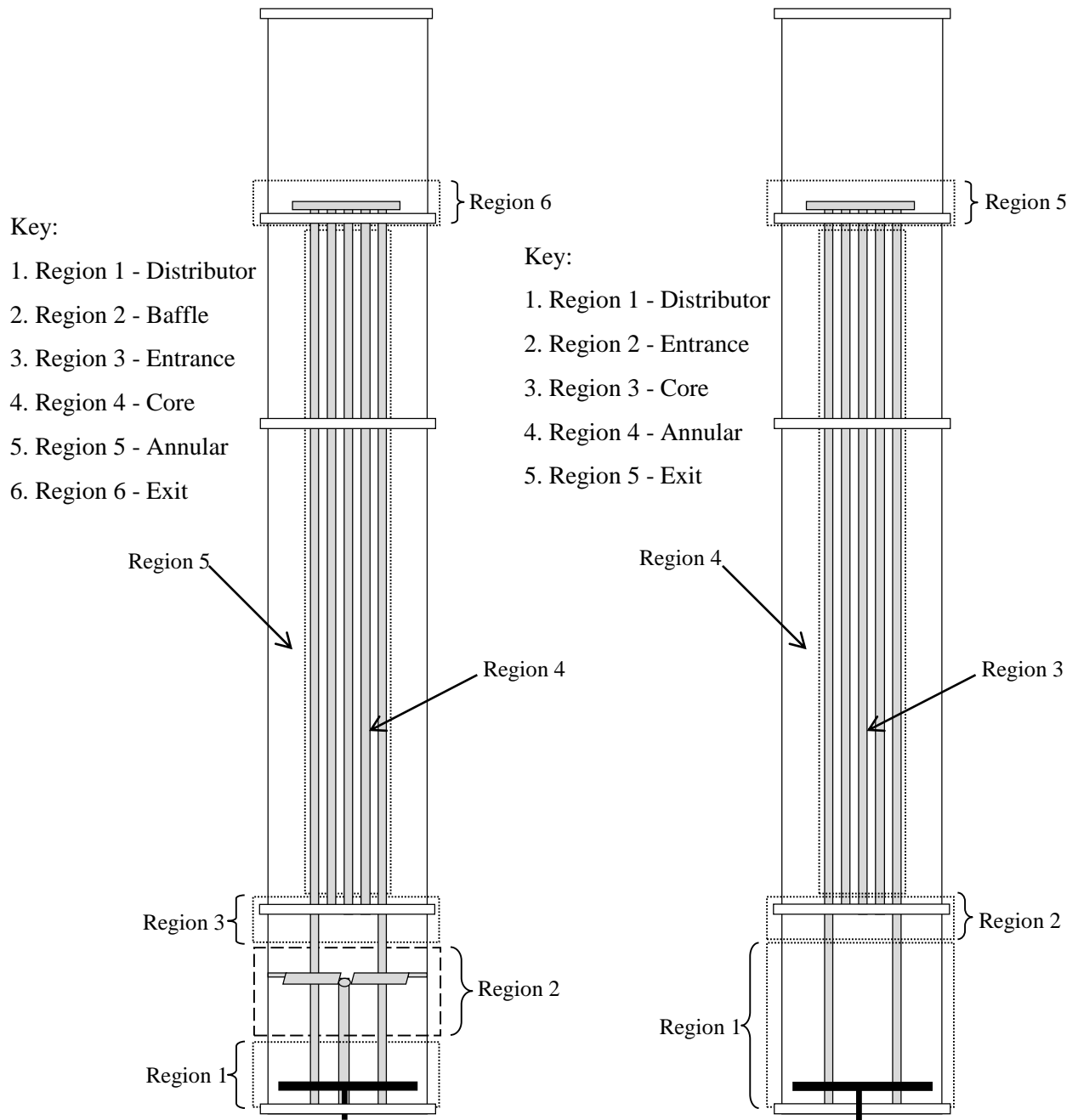3. Region 3 - Core
4. Region 4 - Annular
5. Region 5 - Exit

Figure 4.1: Regions in bubble column equipped with a) CTB internal (*left*) and b) CT internal

(*right*)

4.1.1 The Distributor and Baffle Regions

For all the flow conditions investigated with the CT and CTB internals, the residence time of the particles that entered the distributor region was typically very short, whether the particles settled to the reactor's bottom or remain suspended in the surrounding fluid. In both cases, the particles were re-suspended by streams of upward moving dispersion that had been reflected off of the reactor's bottom by the gas exiting the downward pointing sparger holes within a few seconds. This observation indicates the occurrence of substantial mixing in the distributor region which can be attributed to the sparger's specific design and orientation. A picture series outlining the particle movements can be seen in Figure 4.2. A typical trajectory is shown in Figure 4.3. It is important to point out that the particles approached the distributor from all sides during investigations with both internals. This occurrence may indicate symmetrical flow in this region.

After leaving the immediate vicinity of the distributor, the particles enter the baffle region during CTB investigations or remain in the upper part of the distributor region during CT investigations. The following paragraphs summarizes the observations made for each case.
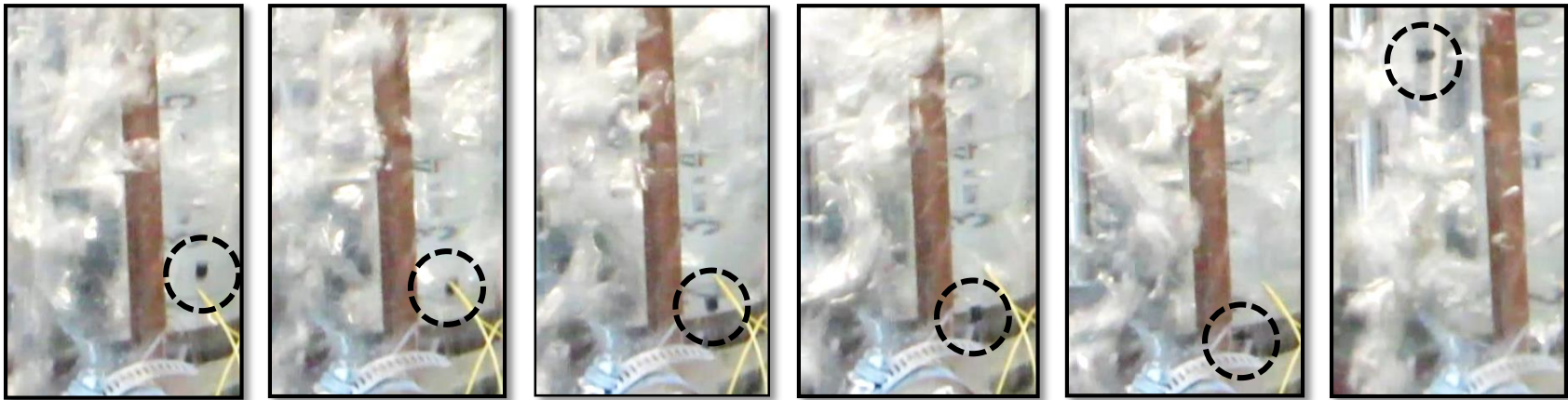
Figure 4.2: Picture series of particle in distributor region (V_g ~ 0.02 m/s, magnification: ~ 0.35%)
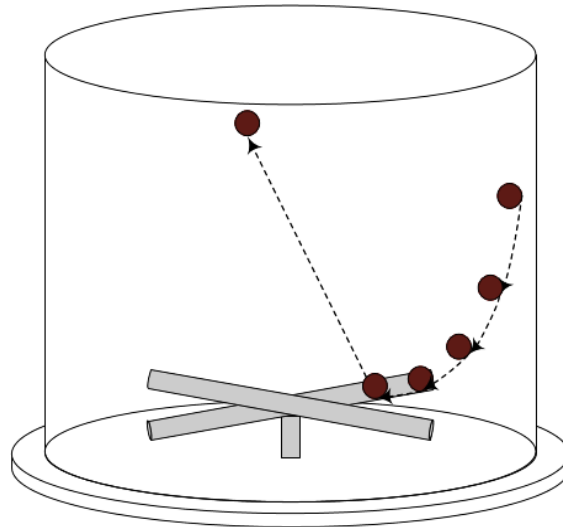
Figure 4.3: Schematic of particle in distributor region ($V_g \sim 0.02$ m/s)

The baffle region was the most turbulent of all the regions outlined in the bubble column equipped with the CTB internal. In this region, the particles traversed the column axially, radially and azimuthally in a random manner. At low superficial gas velocities, particle movements were relatively circular in nature. However, as superficial gas velocity increased, the particles changed directions more frequently in an angular, random manner, as can be seen in Figure 4.4. At all investigated gas velocities, the particles were seen vertically oscillating between a variety of points above and below the baffle. This oscillatory motion was irregular since the particles seemed to spend more time in the area below the baffle. At low superficial gas velocities, particle oscillations were primarily contained within the baffle region. However, as superficial gas velocity increased, the particles travelled to the lower annular region before rapidly dropping beneath the baffle once again. In general, the particles spent significant amounts of time in the baffle region in spite of its relatively small volume. However, the time spent travelling this region decreased slightly with increases in superficial gas velocity.
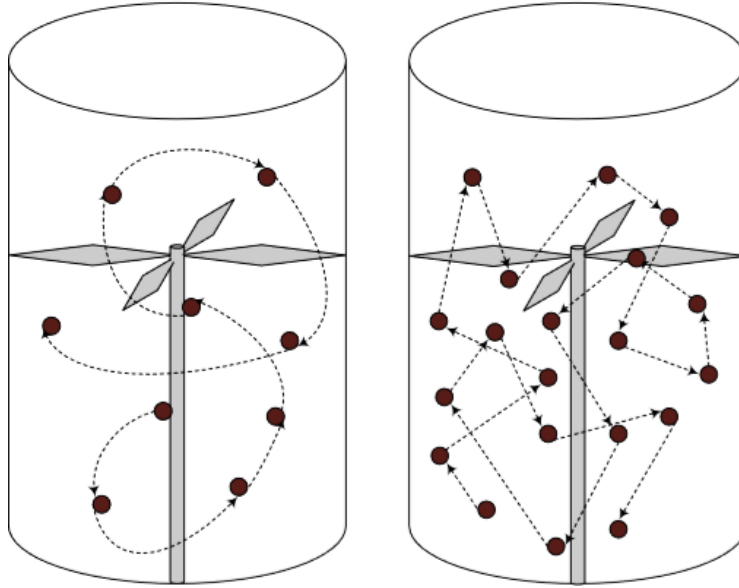
69

Figure 4.4: Schematic of particle in baffle region ($V_g \sim 0.02$ m/s *(left)* and ~ 0.15 m/s *(right)*)

After re-suspension, the particles could be seen making a variety of smooth but random movements within the upper portions of the distributor region during experimentation with the CT internal. As superficial gas velocity increased, those movements became quicker and shorter, but remained smooth. This could be seen in Figure 4.5. The particles could also be seen making quick, vertical drops within this region at higher superficial gas velocities.

Several differences exist between the observations for the baffle/upper distributor regions when equipped with the CT and CTB internals respectively. As seen above, the particle movements at high superficial gas velocities were angular (baffle region) during CTB investigations and remained rounded (distributor region) during CT investigations. However, the major difference observed between the baffle/distributor regions when equipped with the different internals was that equipment with the CT internal seemed to separate the reactor into two separate circulation

cells while equipment with the CTB internal did not. The details of the circulation cell behavior have been addressed in the previous subsection.
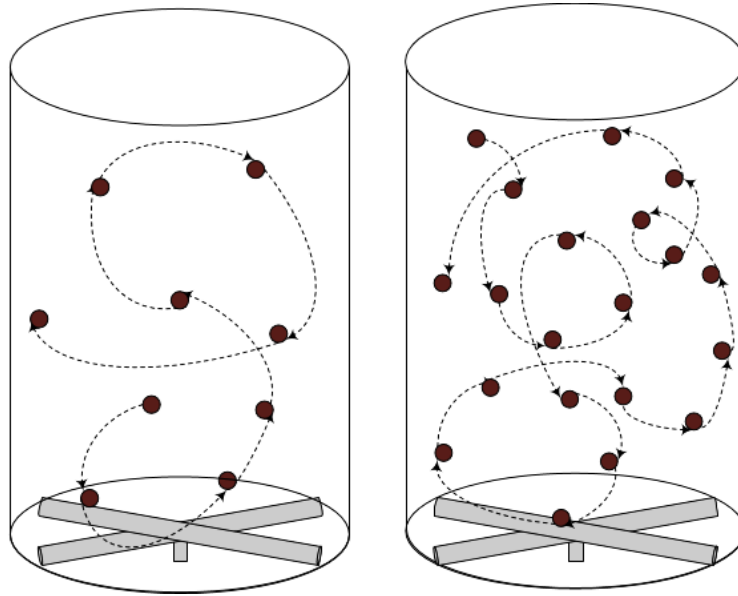

Figure 4.5: Schematic of particle in the distributor region (V_g ~ 0.02 m/s *(left)* and ~ 0.20 m/s *(right)*)

4.1.2 The Entrance Region

The entrance region, amongst having its own properties, is the site at which the particles enter either the core or the annular regions. Unfortunately, clear observations could not be made for neither the CTB nor the CT internals due to visibility that resulted from the system's design. However, at higher superficial gas velocities, the particles were found around the exit region more frequently for both internals. This can be attributed to an increase in the frequency with which the particles entered the baffle/upper distributor regions.

4.1.3 The Core Region

Although particle motion could not be tracked while the particles traversed the core region (due to visibility and design limitations), a few important observations were made. For both internals, the time spent by the particles travelling the core region seemed to decrease with increases in superficial gas velocity. At moderate superficial gas velocities however (0.08 – 0.12 m/s), particles in the CTB equipped column could be seen making their way to the exit region through the annular region. Disfavor for the core region route may be due to the transient nature of the column under these conditions. No such observations were made in the bubble column reactor equipped with the CT internal.

At the lowest superficial gas velocity, smaller particles (with maximum radius less than 4.4 mm) were seen entering and exiting the core region through the spaces of the tube-bundle internal, primarily at its ends. This was observed for both of the investigated internals, although more frequent during CTB investigations. The occurrence indicates an exchange of material between the core and annular regions and can be seen in Figure 4.6 to Figure 4.8. When superficial gas velocity is high, passage of the small particles through the spaces of the tube bundle was nonexistent for both the CT and CTB internals. This indicates more structured exchanges between the core and annular regions (via the exit region).
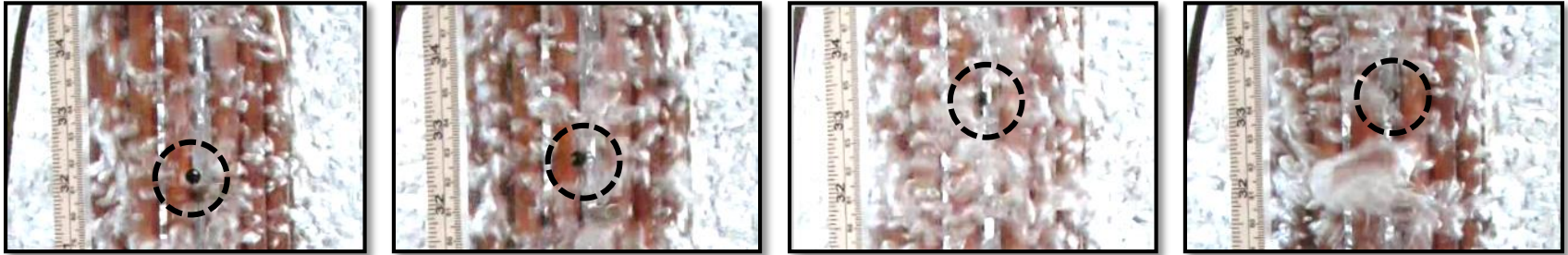
Figure 4.6: Picture series of particle entering core region ($V_g \sim 0.02$ m/s, magnification: $\sim 0.35\%$)
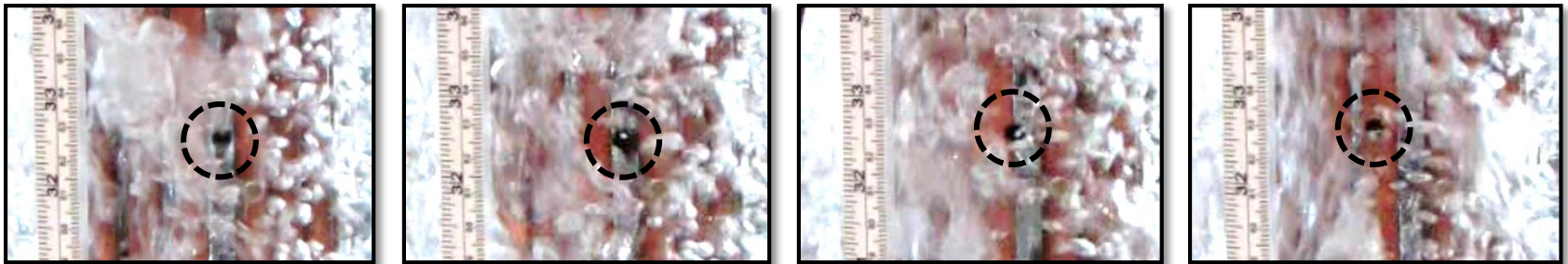

Figure 4.7: Picture series of particle exiting core region ($V_g \sim 0.02$ m/s, magnification: $\sim 0.50\%$)
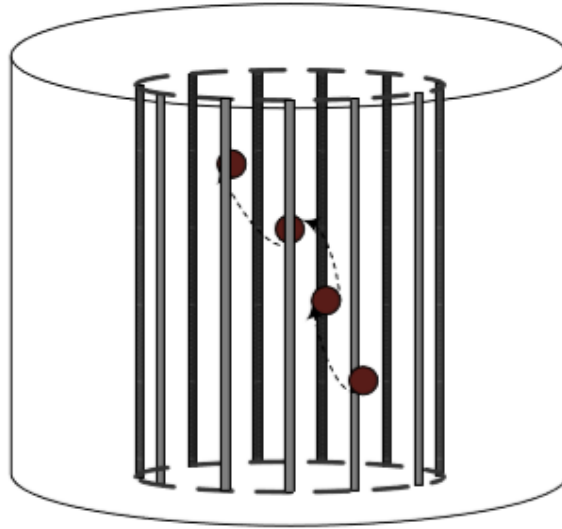
Figure 4.8: Schematic of particle entering core region ($V_g \sim 0.02$ m/s)

4.1.4 The Annular Region

Each superficial gas velocity investigated was associated with a few characteristic particle motions. These particle motions are due to the existence of eddies which are created by the rapidly moving bubbles that traverse the system. Eddies can be generated within bubble columns through two major means – shear instabilities and wake shedding. Eddies generated by the first means, shear instabilities, are created at the interface of two fluids of different densities moving past each other at different velocities. Thus, passage of the gaseous phase within the continuous phase naturally creates eddies in bubble column systems. The second means through which eddies can be generated in a bubble column is through bubble wake shedding. When a bubble rises, a region of low pressure is created behind that bubble and any surrounding liquid is pulled into its energetic wake. As the bubble continues to rise, liquid is constantly absorbed into the bubble's wake until the wake becomes too heavy for the bubble to carry. The wake of that bubble is then shed and it exists as a high energy eddy within the system.

The nature of the eddies dominating the annular region can be affected by both the continuous phase and discontinuous phase properties. In this system, variations in the superficial gas velocity of the discontinuous phase affects a bubble's size, shape, rise velocity, trajectory and eventually, the type of eddy dominating the annular region of the column. The following subsections discuss the most frequently observed characteristic 'near-linear' and 'non-linear' particle movements at specific superficial gas velocities in the presence of the CT and CTB internals respectively.

4.1.4.1 Near-linear Particle Movements

'Near-linear' particle movements refer to all observed particle movements that were straight or at worst, mildly curved in appearance. These observations were made for both the CT and CTB internals, although the specifics surrounding the particle movements in each case were quite different. During CTB investigations, at all superficial gas velocities, the particles could be seen rapidly making independent upward or downward linear movements at a variety of trajectories. Quick, upward movements were frequently observed when operating at a superficial gas velocity of 0.02 m/s and suggests the existence of a weakly developed flow pattern. The rapid downward movements of the particles were observed to last the entire length of the annular region at times, particularly at low superficial gas velocities. This observation is suggestive of gulf streaming. In general, the distance traversed by particles during upward and downward movements decreased with increases in superficial gas velocity. This may be due to the existence of high energy eddies that are able to intercept gulf streams at those gas velocities.

Many phenomena were observed within the annular region during investigations with the CT internal. For most superficial gas velocities, the primary direction of flow within the annular region

was observed to be downward. However, as superficial gas velocity increased, upward flow within the annular region increased. At all superficial gas velocities, the particles could frequently be seen making a large, single loop. This has been illustrated in Figure 4.9c. As superficial gas velocity increased, the overall diameters of the loops increased while the number of loops created seemed to decrease slightly.

At lower superficial gas velocities ($V_g \leq 0.10$ m/s), the maximum velocity at which particles moved upward was observed to be slightly higher than that at which they moved downward during CTB investigations. This can be seen in Table 4.1. When superficial gas velocity exceeded 0.10 m/s however, the downward moving particles generally traversed the reactor at higher velocities than their upward moving counterparts. During CT investigations, no near-linear upward particle movements were observed for the lowest superficial gas velocity investigated. Also, the downward particle velocities tended to be higher than their upward moving counterparts. This can be seen in Table 4.1. It is important to point out that these values are only rough estimates since the measurement method was subjected to visibility limitations and particle trajectory changes.

Table 4.1: Summary of measured liquid velocities

Maximum Liquid Velocities, m/s				
Vg	CT		CTB	
	Upward	Downward	Upward	Downward
0.01	0.00	-0.32	0.49	-0.25
0.10	0.63	-0.66	0.61	-0.31
0.15	0.61	-0.61	0.61	-0.76
0.20	0.46	-1.09	0.53	-0.70
0.25	0.53	-0.51	0.51	-0.53

The type of internal used was found to significantly affect the behavior of the particles and thus, the hydrodynamics of the reactor's system. During CTB investigations, the particles experienced more frequent, near-linear upward motions at all superficial gas velocities. During CT investigations however, the particles only made individual upward movements during operation at high superficial gas velocities. Several non-linear particle movements were observed in the annular region during investigations with the CTB internal at low to intermediate gas velocities. However, during CT investigations at comparable gas velocities, more structured, downward flows were observed. These differences indicate reduced backflow during CTB investigations, a desired property for certain bubble column applications.

4.1.4.2 Non-linear Particle Movements

"Non-linear" particle movements refer to all observed particle movements that deviated significantly from a straight-line motion. The behavior of the particles in the presence of the CT and CTB internals was quite different with respect to the non-linear movements observed, although particle behavior became more similar at higher gas velocities. At the lowest superficial gas velocity investigated with the CTB internal (about 0.02 m/s), particles were seen moving upwards or downwards and then returning to the initial start in a circular manner, for several revolutions. This movement suggests the prevalence of vortexes at low superficial gas velocities and can be seen in Figure 4.9a. The particles were also observed to be relatively stagnant for about a second or two before moving off at a tangent with substantial velocity. This stagnation period indicates that the particles may have been caught between opposing eddies of near-equal magnitudes. Lastly, the particles were seen moving in a helical manner, as can be seen in Figure 4.9b. A series of pictures outlining a particle's helical motions can be seen in Figure 4.10.

77

During CT investigations, the only characteristic particle movement observed at a superficial gas velocity of 0.02 m/s was the wide loop. This can be seen in Figure 4.9c.
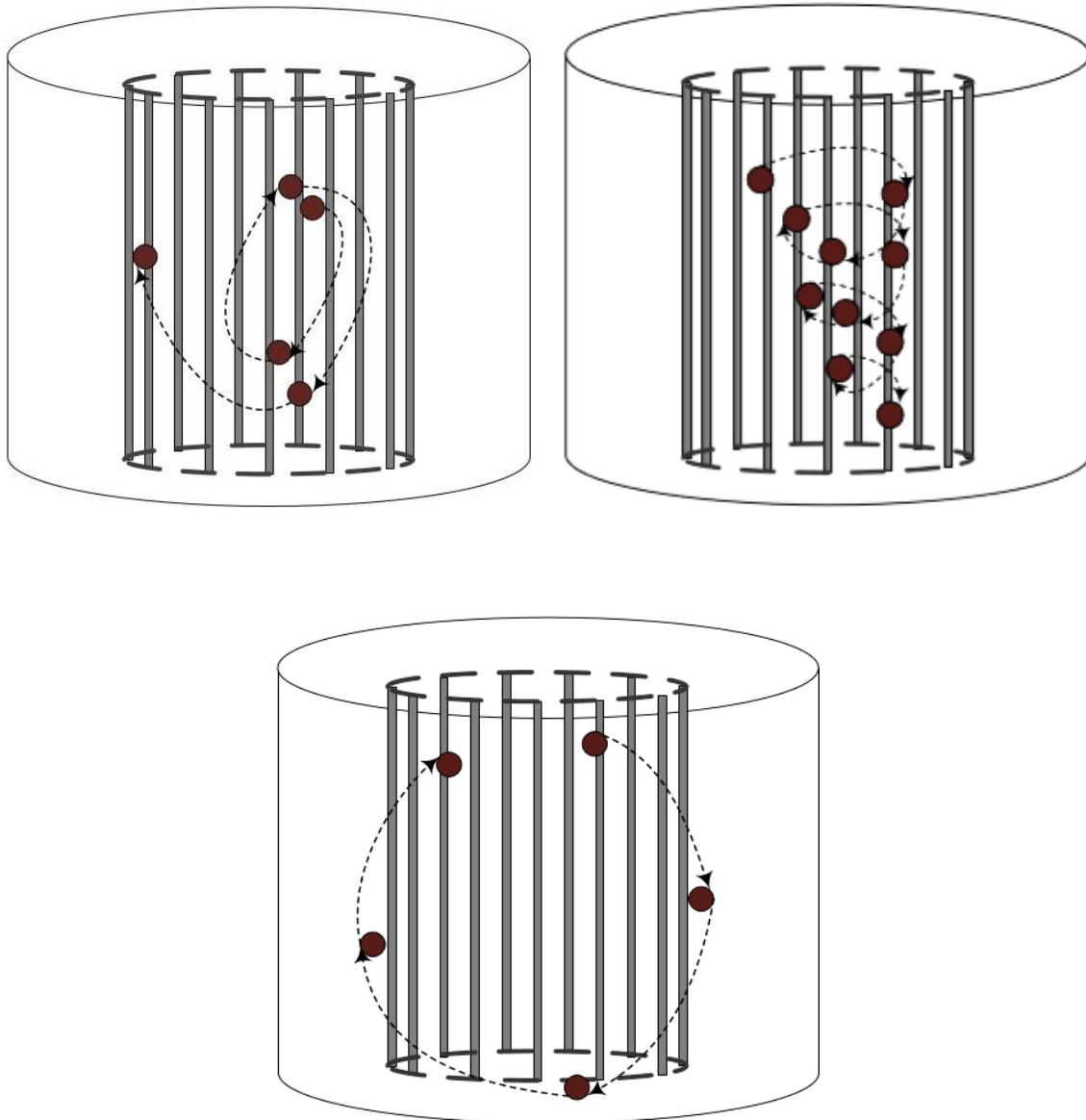

Figure 4.9: Schematic of a) particle caught in vortex ($V_g \sim 0.02$ m/s) *(top, left)* and b) helical particle movements ($V_g \sim 0.02$ m/s) *(top, right)* c) wide loop ($V_g \sim 0.02$ m/s) *(bottom)*
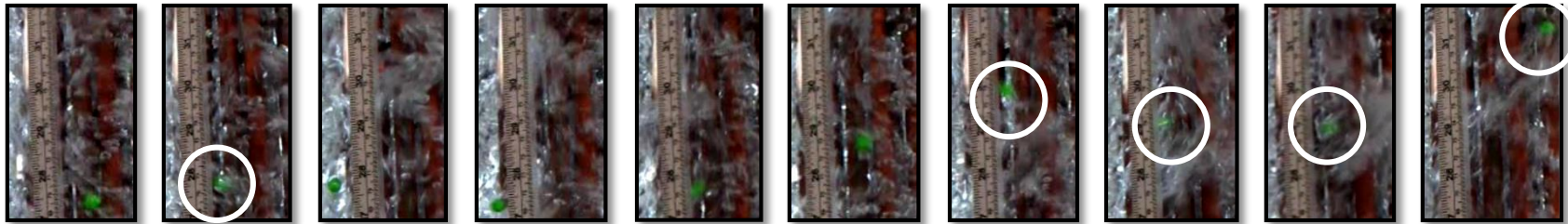
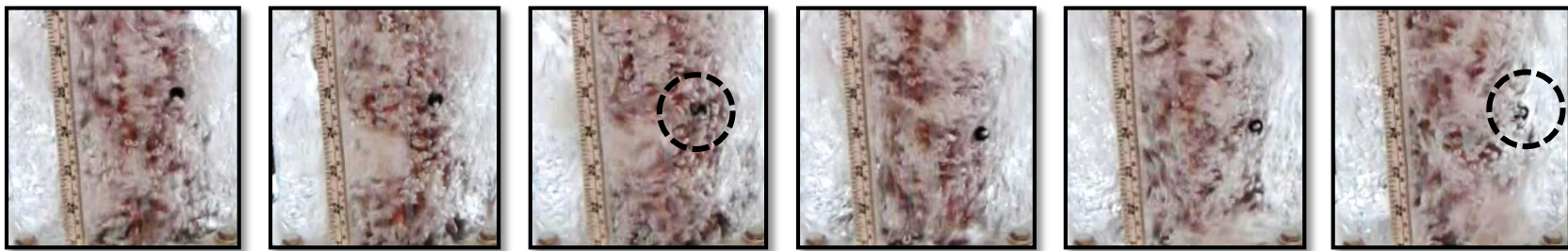Figure 4.10: Picture series of helical particle movements ($V_g \sim$ 0.02 m/s, magnification: ~ 0.35%)

Figure 4.11: Picture series of particle making short, random movements ($V_g \sim$ 0.10 m/s, magnification: ~ 0.20%)

At superficial gas velocities of about 0.10 m/s, the aforementioned upward and downward movements of the particles was the major observation made during CTB investigations. However, the particles were periodically caught making short, random movements and occasionally displayed mild 'bouncing' characteristics while moving. The schematic showing the particle caught making the short, random movements can be seen in Figure 4.12a while a picture series of the same occurrence can be seen in Figure 4.11.

During CT investigations, superficial gas velocities of about 0.10 m/s were characterized by wide loops within the annular region along with oscillations about the entrance region. While this superficial gas velocity could be considered the true point of circulation cell breakdown, the particles never entered cell two through the annular region. Instead, the particles would return to the distributor region after a series of oscillations where they would remain for some time before entering the core region. The major characteristic particle movement observed at this superficial gas velocity was the occurrence of the wide loop depicted in Figure 4.9c. In addition to the wide loops, the particles were also seen making a series of smaller loops as they neared the lower end of the annular region.

At superficial gas velocities near 0.15 m/s, particles may be seen making full 'bouncy' movements superimposed on tangential and erratic upward or downward movements during CTB investigations. This 'bounciness' could also be seen superimposed on relatively horizontal particle motions and is depicted in Figure 4.12b and Figure 4.14. In addition to the bouncy movements, particles were occasionally trapped in small vortexes, particularly in the entrance and lower annular regions.
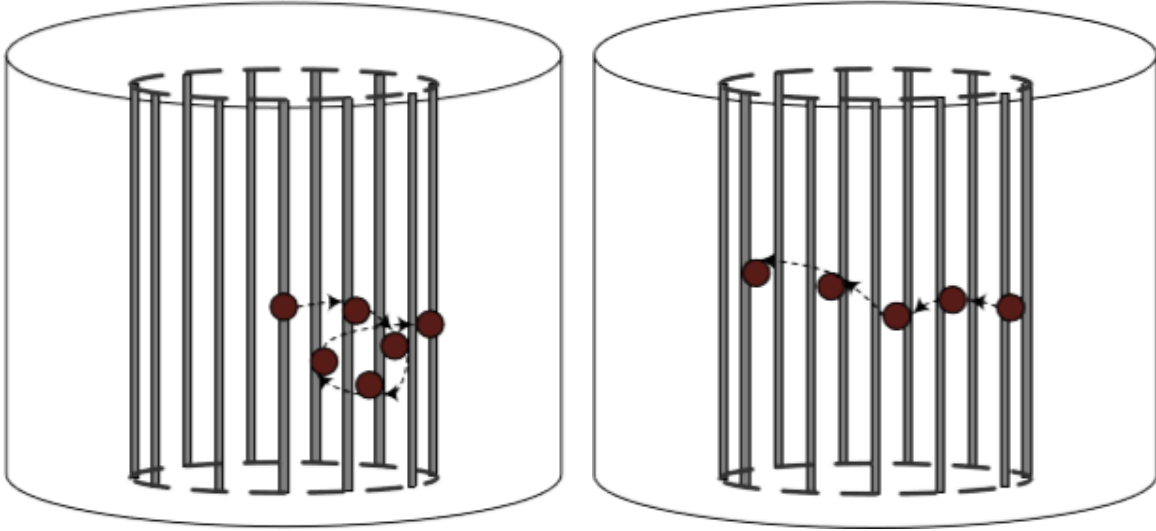
Figure 4.12: Schematic of a) particle making short, random movements ($V_g \sim 0.10$ m/s) *(left)* and

b) bouncing movements ($V_g \sim 0.10$ m/s) *(right)*

At 0.15 m/s during investigations with the CT internal, particle movements were similar to that observed at 0.10 m/s, but more intense. The particles were seen making larger, wider loops within the annular region, while particle passage through the core region at this superficial gas velocity was perceived to be the most frequent of all the superficial gas velocities investigated.

During CTB investigations, superficial gas velocities of about 0.20 m/s were characterized by the vortexes and bouncy movements observed in the column operating at 0.15 m/s as well as moderate 'S – like' movement superimposed on relatively vertical, upward or downward motions. The downward 'S – like' motions were observed to be longer than their upward counterparts. This can be seen in Figure 4.13a. At 0.25 m/s, particle movements in the annular region were characterised by exaggerated, conjoined 'S – like' motions that ranged from completely horizontal to completely vertical in orientation. This could be seen in Figure 4.13b and Figure 4.15.
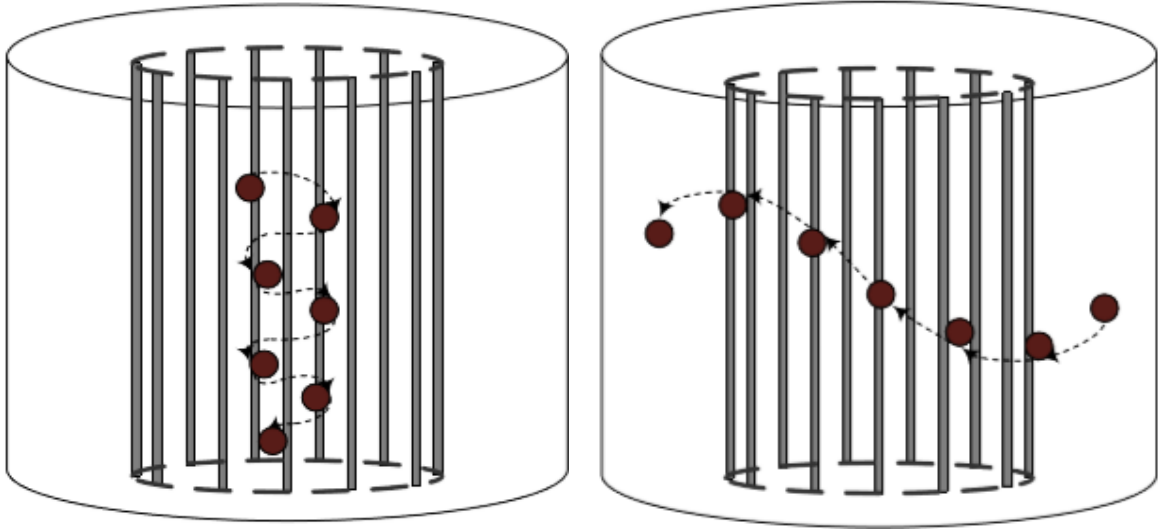
Figure 4.13: Schematic of a) moderate "S" - movements (V$_g$ ~ 0.25 m/s) *(left)* and b) exaggerated "S" - movements (V$_g$ ~ 0.25 m/s) *(right)*

During CT investigations, superficial gas velocities of 0.20 m/s were characterized by oscillations about the entrance region while superficial gas velocities of 0.25 m/s were characterized by zigzag movements. A schematic of the zigzag movements can be seen in Figure 4.16. However, despite those differences, the last two superficial gas velocities investigated shared several commonalities. At both gas velocities, the bubble column reactor began to exhibit a wide range of flow phenomena that were not present at any of the lower gas velocities. One of the most frequently observed phenomena was that the particles displayed an excessive amount of horizontal movements. At superficial gas velocities of 0.20 m/s, the horizontal particle movements were relatively straight. At 0.25 m/s however, the horizontal movements took on a 'bouncy' appearance, such as that illustrated in Figure 4.12b. A second commonality was that independent, near-linear upward particle movements were observed for the two latter superficial gas velocities. These particle movements could be seen at various trajectories and normally occurred over short distances.
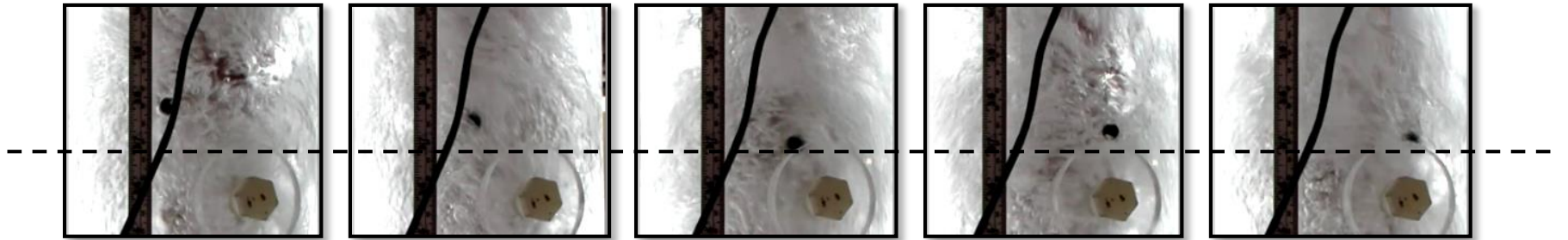
Figure 4.14: Picture series of bouncing movements ($V_g \sim 0.20$ m/s, magnification: $\sim 0.25\%$)
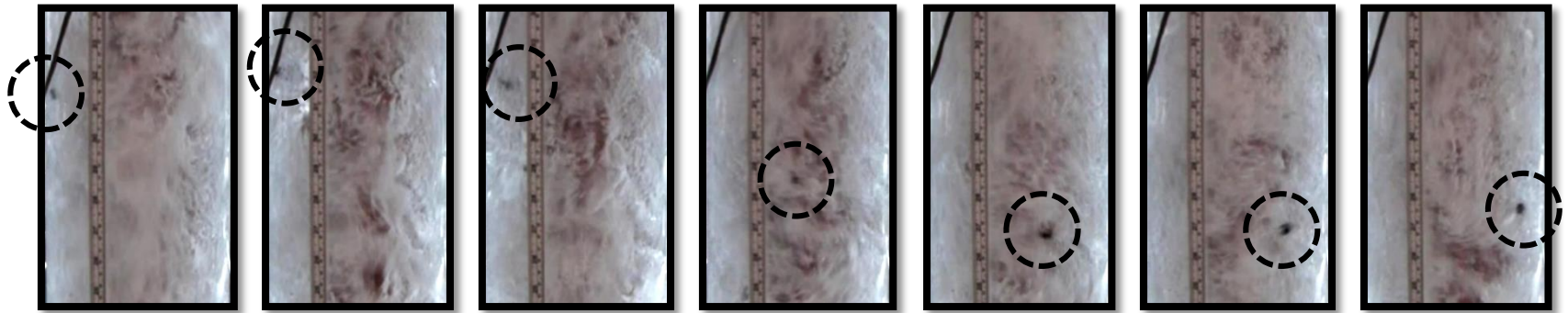

Figure 4.15: Picture series of exaggerated "S" - movements ($V_g \sim 0.25$ m/s, magnification: $\sim 0.20\%$)
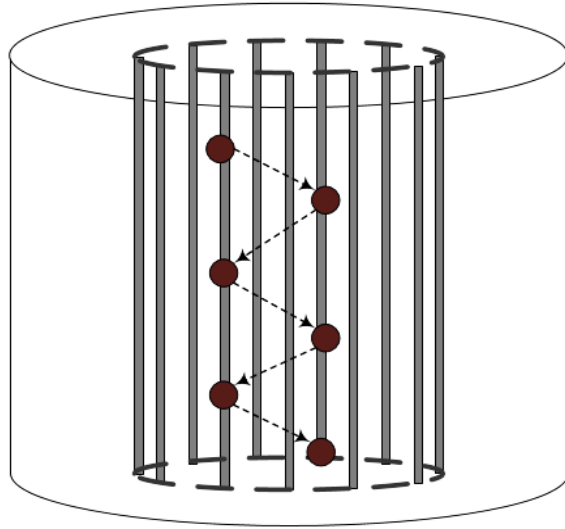
83

Figure 4.16: Schematic of zigzag movements ($V_g \sim 0.25$ m/s)

In general, the length of the annular region travelled by the particles tended to decrease with increases in superficial gas velocity during CTB investigations. At the lowest superficial gas velocity studied, the particles could be seen travelling from the entrance to the exit regions by way of the annular region. However, at the highest superficial gas velocity, the particles were only seen travelling from the entrance region to a point that lie about halfway the annular region. During CT investigations, the annular region experienced an increase in particle activity at higher superficial gas velocities. As a result, the particles tended to spend more time within circulation cell two over circulation cell one at those superficial gas velocities.

4.1.5 The Exit Region

As mentioned earlier, particles were seen in the exit region (without taking any visible paths) more frequently at higher superficial gas velocities in the presence of both the CT and CTB internals. This occurrence is believed to be due to the existence of well-defined flow fields at higher

superficial gas velocities which move upward in the core region and downward in the annular region.

4.1.6 Combined Flow Patterns

Plausible liquid circulation patterns have been proposed for the modified bubble column systems that have been investigated in this study, the justification of which originating from the observations made during the neutrally buoyant particle experiments. The suggested flow patterns can be found in Figure 4.17 and are valid for intermediate to high superficial gas velocities. The flow pattern observed during CT investigations can be justified from the following. Circulation between the core and annular regions is proposed based on the repeated occurrence of downward particle movements in the annular region and upward particle movements in the core region, both of which spanning the entire length of the tube bundle internal. Circulation within the distributor region is based on the random, upward and downward movements displayed by the particles over short distances. At superficial gas velocities of 0.15 m/s, direct exchange between the distributor and core regions were observed. Figure 4.17a accounts for this through the use of orange arrows that indicate the direction of fluid flow from the distributor region into the annular region and through weak circulation patterns (indicated by broken lines) in the annular region.

The flow structure observed with the CTB internal was more complex in comparison to that observed with the CT internal. This comparison can also be seen in Figure 4.17. Circulation within the mid-section of annular region is supported by the occurrence of both upward and downward particle movements in this region. Upward flow within the core region is proposed since the particles were never seen directly entering the baffle region from the core region. However, flow

through the core region is expected to be weaker than that experienced during CT investigations since more frequent exchanges between the core and annular regions (by way of the exit and entrance regions) were observed with the CT internal. This is indicated by a thinner arrow in Figure 4.17. Weak circulation between the distributor and baffle regions is proposed based on the random, upward and downward particle movements that were observed. Direct exchange between the baffle and annular regions was a frequent occurrence at higher superficial gas velocities. This is depicted using solid green arrows in Figure 4.17b. The deflection of larger bubbles into the annular region was encouraged by the presence of the baffle internal. This is depicted by the red arrows in Figure 4.17b.
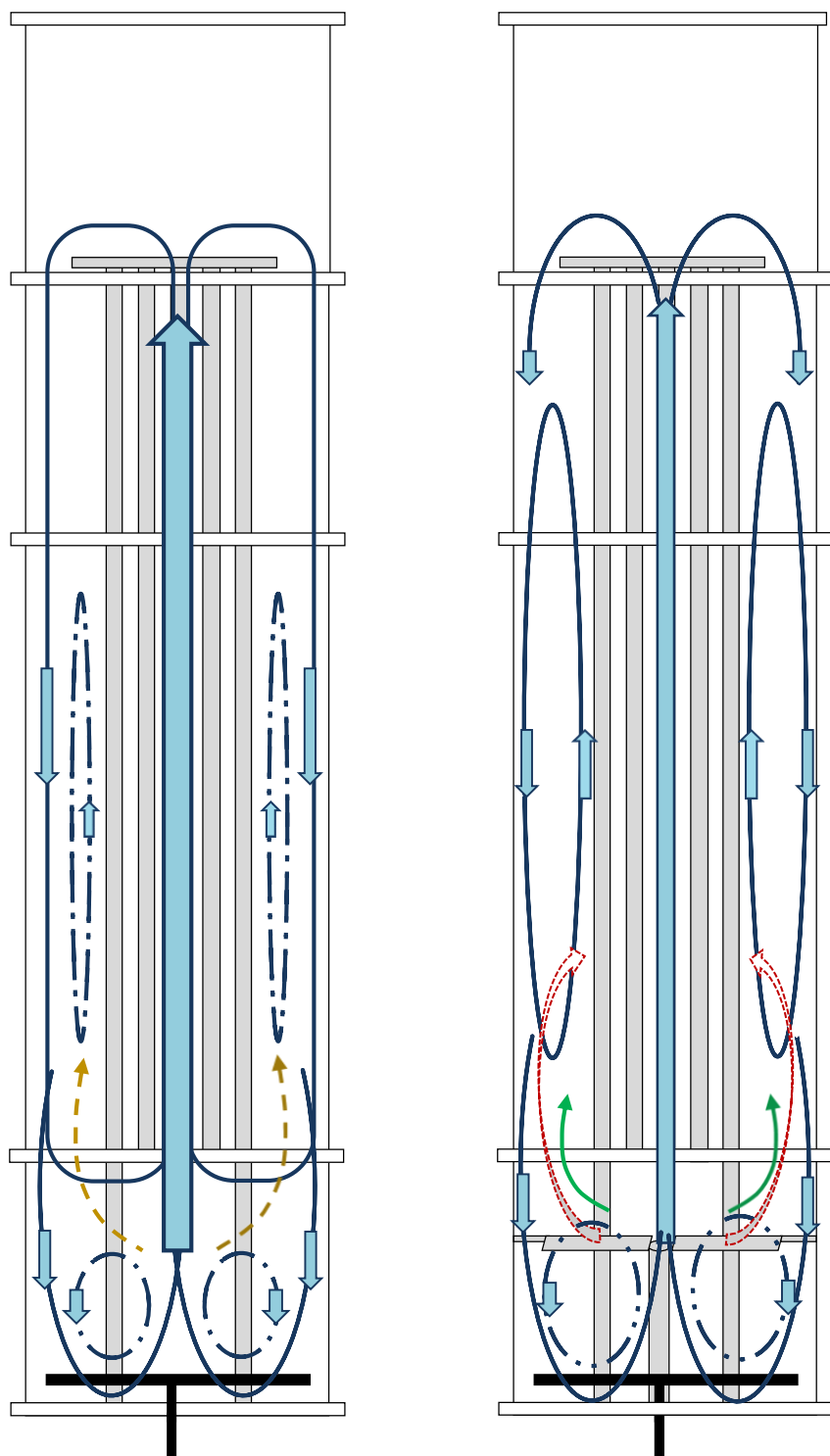
Figure 4.17: Gross flow patterns in presence of a) CT internal (*left*) and b) CTB internal (*right*)

4.2 Interfacial Area and Gas Holdup Structure

Interfacial area can be defined as the amount of area contact between the phases contained within a system. It is an important design parameter in all multi-phase reactors because it influences the amount of heat, mass and momentum that can be transferred between phases. Interfacial area can be related to the properties of the bubbles in a bubble column reactor. In general, two classes of bubbles exist within a bubble column – the small and large bubble classes. Bubbles are assigned to either class based on their bubble rise velocities (Daly et al., 1992, Schumpe and Grund, 1986). Small bubbles can have diameters which range from 3 mm to 6 mm while the smallest large bubble has a diameter greater than 1 cm.

The interfacial area can be estimated using equation 4.1 in which a is interfacial area, ε_b is bubble class holdup and d_b is the average bubble class size (Li et al., 2003). The subscripts S and L refer to that of the small and large bubble classes respectively. From this equation, it could be seen that interfacial area increases with increases in bubble holdup and decreases with bubble size. The small bubbles have been found to contribute most to the interfacial area of a bubble column reactor. This is intuitive since the surface area-to-volume ratio of a body increases with a decrease in its volume.

$$a = \frac{6\varepsilon_{b,L}}{d_{b,L}} + \frac{6\varepsilon_{b,S}}{d_{b,S}} \tag{4.1}$$

The properties of the bubbles formed in a bubble column can be altered by the design of the reactor, particularly with the addition of internals to the system. The effect of the CT and CTB internals on the gas holdup, average bubble holdup, average bubble rise velocity and average bubble size

will be explored in the subsequent subsections. This section will conclude with a discussion on the effect of the two internals on interfacial area.

4.2.1 Gas Holdup

In general, gas holdup was found to increase with increases in superficial gas velocity for various internal conditions. Gas holdup was also found to increase with the addition of internals to the bubble column reactor. Figure 4.1 compares the gas holdup of a comparable hollow bubble column system (Jhawar, 2011) with that obtained during CT and CTB investigations respectively. Equipment with the CT internal yielded the higher increase in gas holdup when compared to that of the CTB internal. The increase experienced with the CTB internal was significant and comparable to that already existing in the literature (Jhawar, 2011). Figure 4.1 can easily be divided into the three major flow regimes – the bubbly (I), transition (II) and coalesced bubble flow (III) regimes. The divisions are shown in Figure 4.18. As can be seen, the bubbly and coalesced bubble flow regimes are both characterized by near-linear increases in gas holdup with superficial gas velocity, with the rate of increase occurring within the bubbly flow regime exceeding that of the coalesced bubble flow regime. The transition regime is characterized by non-linear increases in gas holdup.

4.2.2 Bubble Fractions

The data obtained from gas holdup measurements provides information that is useful in both defining and designing a bubble column reactor. However, much more could be learnt about gas holdup structures from methods such as the dynamic gas engagement technique. In this technique,
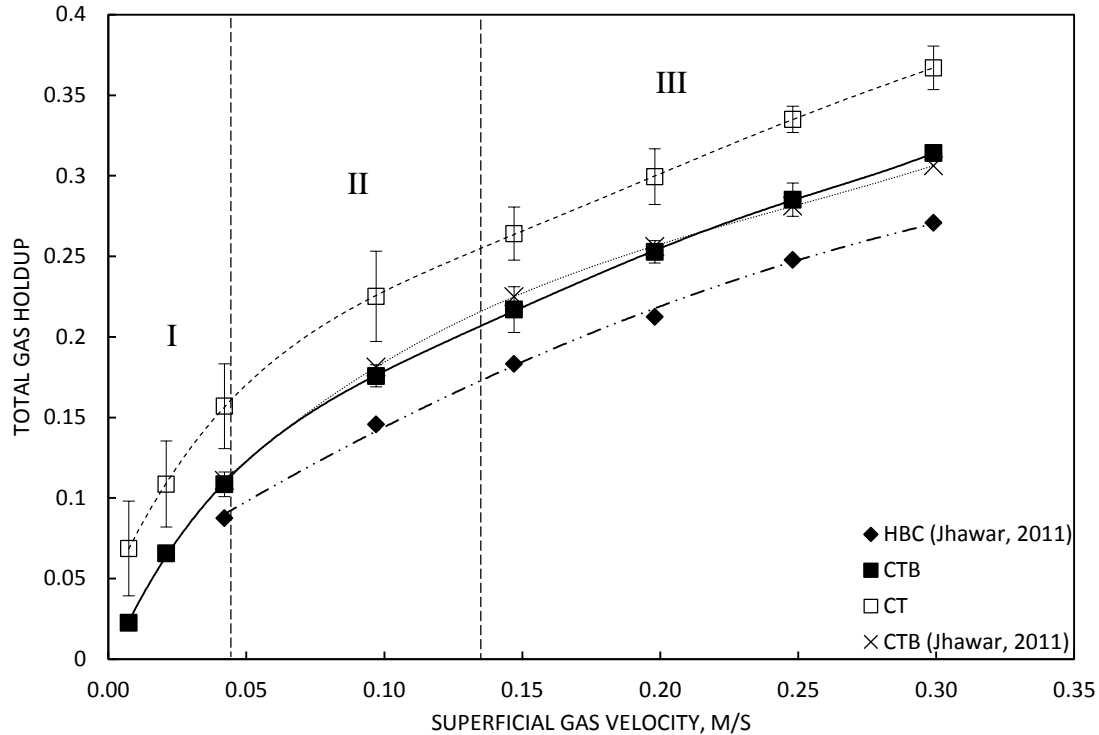
Figure 4.18: Effect of internals on hollow bubble column systems

bubbles are loosely classified by size into two general groups – the large and small bubble classes – based on their bubble rise velocities. Execution of this technique results in the initial escape of the larger bubbles from the column within a relatively short amount of time. This causes a set of intense pressure fluctuations which form the first disengagement period of the dynamic gas disengagement curve in Figure 4.19. The second disengagement period (also seen in Figure 4.19) results from the escaping of smaller bubbles from the column. These smaller bubbles have smaller bubble rise velocities and do not create large fluctuations in bed pressure drop. As a result, more time is required for small bubble travel and its disengagement period increases.
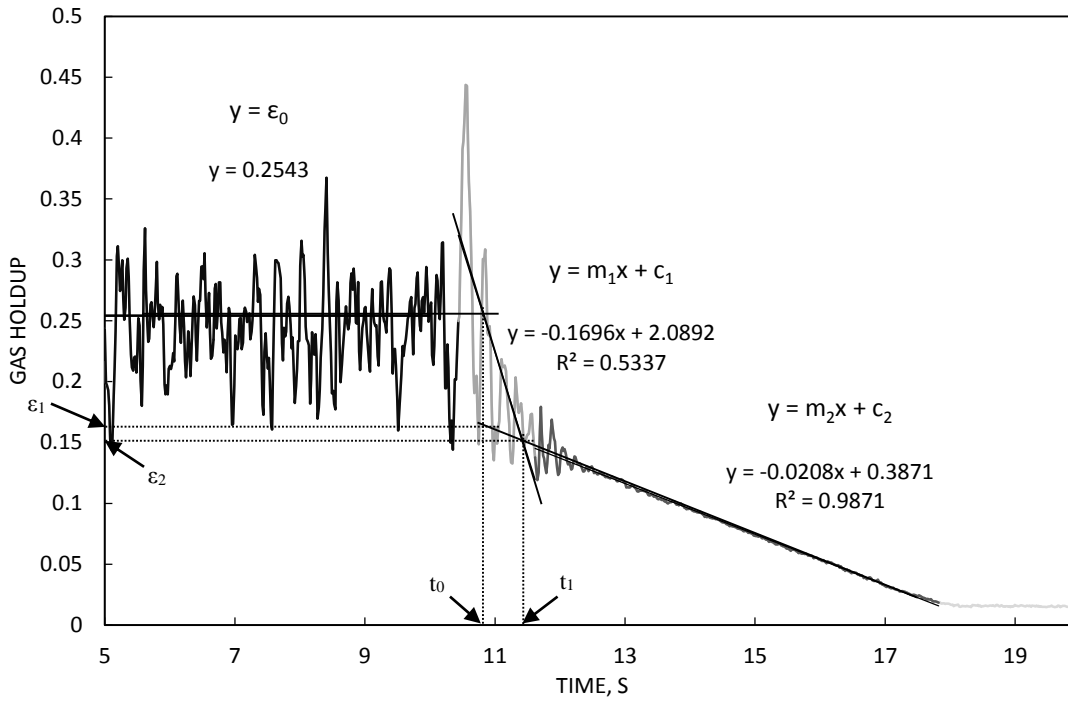
Figure 4.19: Sample of dynamic gas disengagement curve (Vg ~ 0.20 m/s, CTB)

Several different dispersed bubble phase properties may be obtained from the analysis of a
dynamic gas disengagement curve. These include 1) small and large bubble class contributions to
gas holdup and 2) the average bubble rise velocities of each bubble class (Li and Prakash, 2000).
A summary of the major equations used is presented below.

$$V_{g,sm} = \frac{-\Delta H m_2}{t_1 - t_0}$$

(4.2)

$$V_{g,l} = V_g - V_{g,sm}$$

(4.3)

$$\varepsilon_{b,sm} = \varepsilon_1 = m_2 t_0 + c_2$$

(4.4)

91

$$\varepsilon_{b,l} = \varepsilon_0 - \varepsilon_{b,sm} \tag{4.5}$$

$$u_{b,lg} = \frac{V_{g,lg}}{\varepsilon_{b,lg}} \tag{4.6}$$

$$u_{b,sm} = \frac{V_{b,sm}}{\varepsilon_{b,sm}} \tag{4.7}$$

In the above equations, ε_0 is total gas holdup, V_g is superficial gas velocity, ε_b is bubble class holdup, u_b is bubble rise velocity and ΔH is the distance between the pressure transducers. ε_1, t_1, t_0, m_2 and c_2 are shown in Figure 4.19. The subscripts sm and lg pertain to the small and large bubble classes respectively. The effect of the CT and CTB internals on the small bubble holdup within bubble column systems can be seen in Figure 4.20. From this figure, the presence of internals significantly increases small bubble holdup when compared to that of the hollow bubble column reactor. Larger increases were obtained when the reactor was equipped with the CT internal.

The corresponding data for the large bubble class can be found in Figure 4.21. Large bubble holdup decreased significantly in the presence of internals. However, the CTB internal offered a slightly lower large bubble holdup than the CT internal.
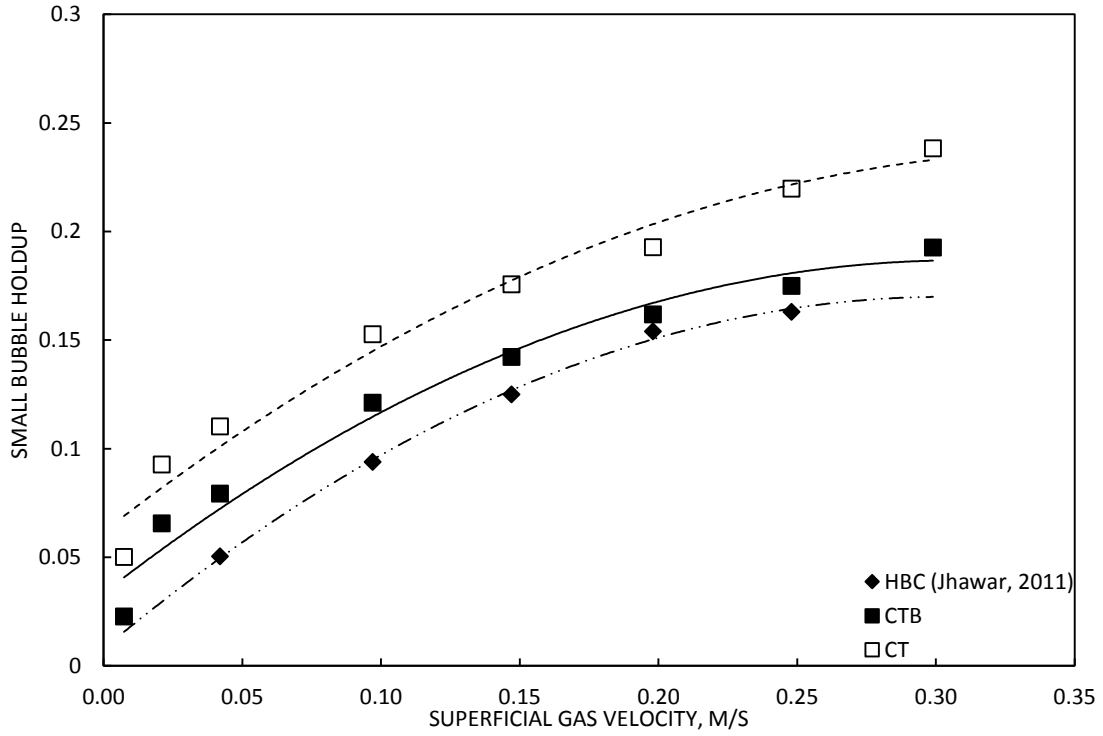
Figure 4.20: Effects of internals on small bubble holdup
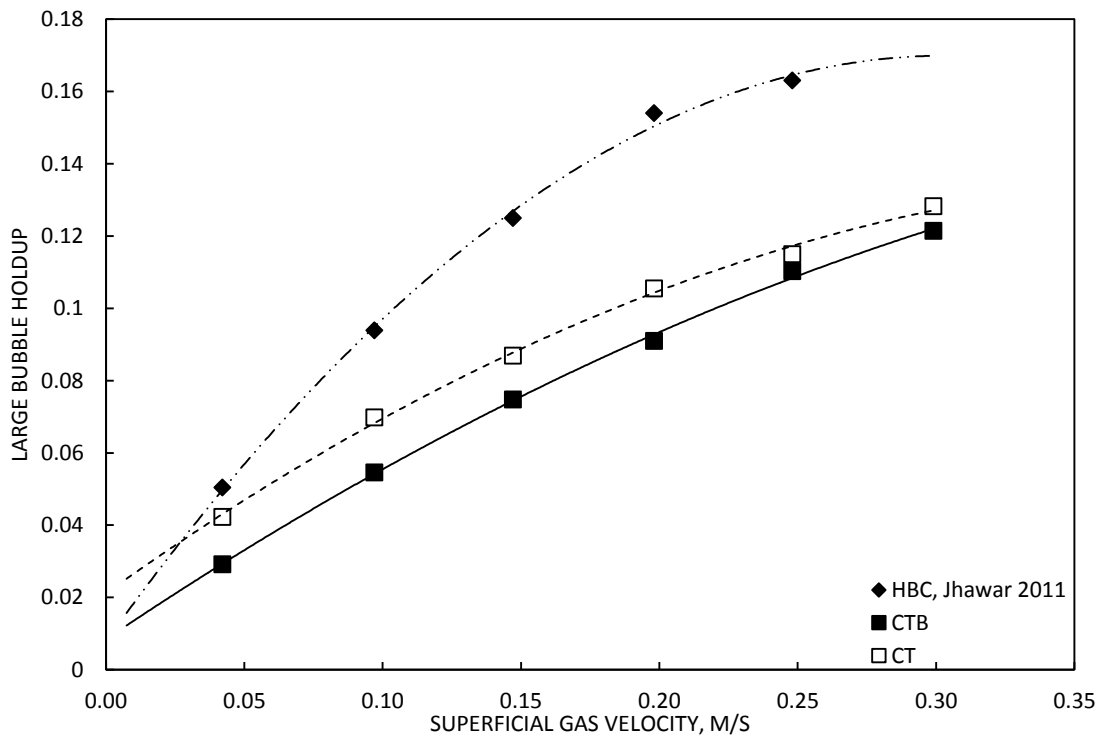
Figure 4.21: Effect of internals on large bubble holdup

Figure 4.22 shows the relationship between the bubble rise velocities of the two bubble classes with superficial gas velocity in the presence of the CT and CTB internals. From this figure, the rise velocity of the small bubble class shows a slight decreasing trend while that of the large bubble class increases rapidly, for both internals. The rise velocities in the bubble column reactor equipped with the CT internal were found to be lower than that observed with the CTB internal, particularly for the case of the small bubble class.
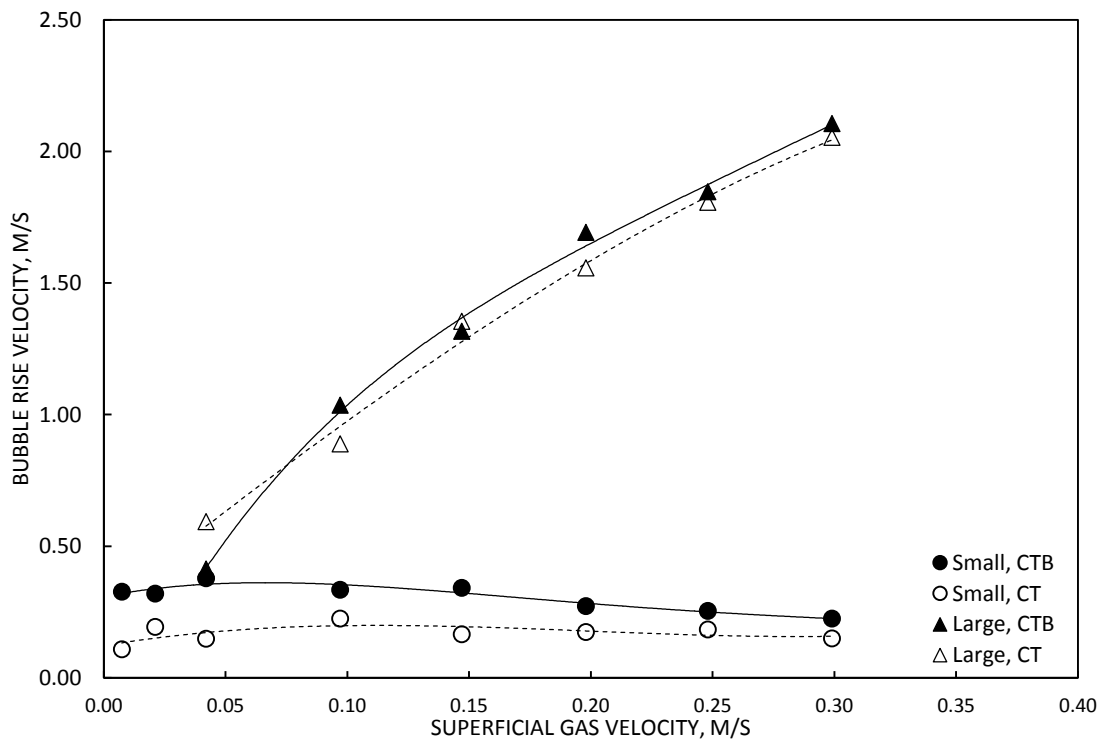
Figure 4.22: Effect of internals on small and large bubble rise velocities

4.2.3 Small Bubble Sizes

Several correlations to estimate bubble size from bubble rise velocity have been reported in the literature. For the large bubble class, the correlation by Kim et al. (1977) has been recommended

by Li et al. (2003). In this equation, $d_{b,L}$ is the average large bubble diameter prediction and $U_{b,L}$ is the average large bubble rise velocity. The equation is shown below. The average large bubble size prediction can be found in Figure 4.23.

$$d_{b,L} = \left(\frac{U_{b,L}}{17.1}\right)^{1.011} \tag{4.8}$$
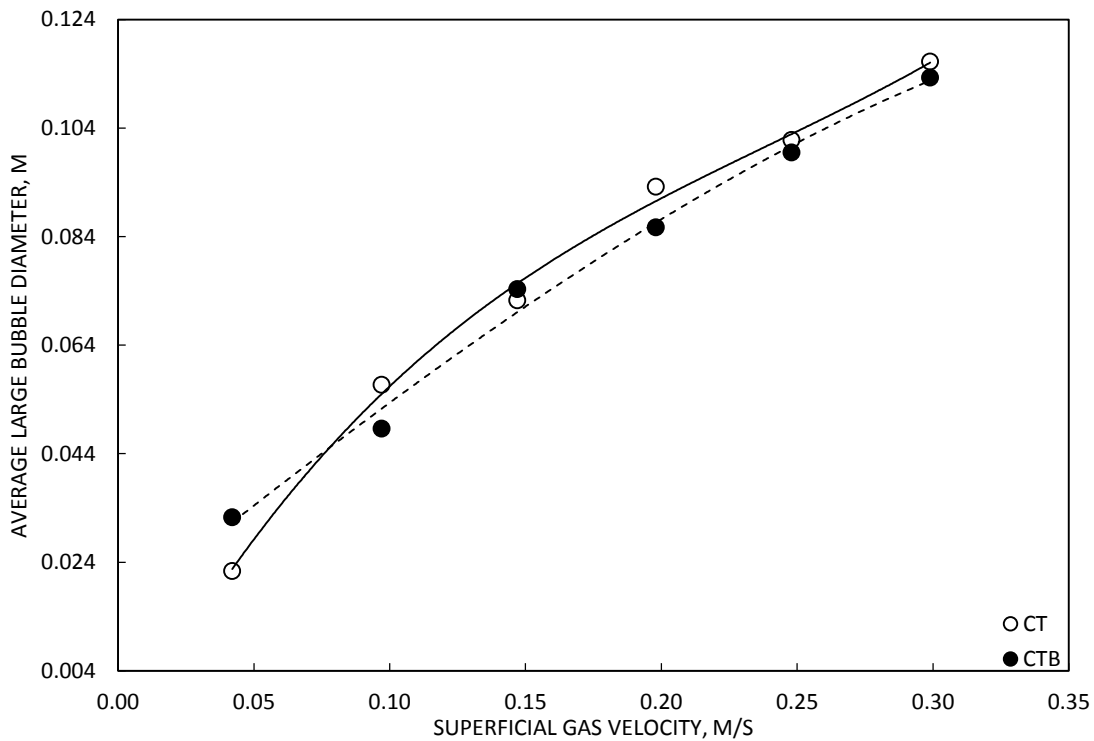
Figure 4.23 Effect of Internals on the theoretical size estimates of the large bubble class

The effect of the CT and CTB internals on small bubble diameter was investigated at several superficial gas velocities through correlations recommended by Li et al. (2003) and through direct measurement using a photography-based method. The correlations used are listed below. The results from the correlations are not presented because they were significantly smaller than the

measured values. A summary of the small bubble size estimations from direct measurement can be found in Figure 4.24. It could be seen that the average small bubble sizes range from 4.5 mm to 5.5 mm and agrees with what already exists in the literature (Daly et al., 1992, Schumpe and Grund, 1986). Higher diameters were obtained with the CTB internal when compared to that of the CT internal. This observation agrees closely with previous findings since increases in bubble size are associated with higher bubble rise velocities.

$$U_b' = \left\{ \left[\frac{Mo^{-\frac{1}{4}}}{K_b} \left(\frac{\Delta\rho}{\rho_l} \right)^{\frac{5}{4}} d_b'^{\,2} \right]^{-n} + \left[\frac{2c}{d_b'} \left(\frac{\Delta\rho}{\rho_l} \right) \frac{d_b'}{2} \right]^{-\frac{n}{2}} \right\}^{-\frac{1}{n}} \tag{4.9}$$

$$U_b' = U_b \left(\frac{\rho_l}{\sigma g} \right)^{\frac{1}{4}} \tag{4.10}$$

$$d_b' = d_b \left(\frac{\rho_l g}{\sigma} \right)^{\frac{1}{2}} \tag{4.11}$$

$$n = 0.8, \quad c = 1.2, \quad K_b = \max(14.7 Mo^{-0.038}, 12) \tag{4.12}$$

In the above equations, U_b' is dimensionless average bubble rise velocity, U_b is average bubble rise velocity, d_b' is dimensionless average bubble diameter, d_b is average bubble diameter, $\Delta\rho$ is the difference in phase densities, ρ_l is liquid phase density, σ is liquid phase surface tension, Mo is Morton Number and g is acceleration due to gravity. n, c and K_b are given by equation 4.12.
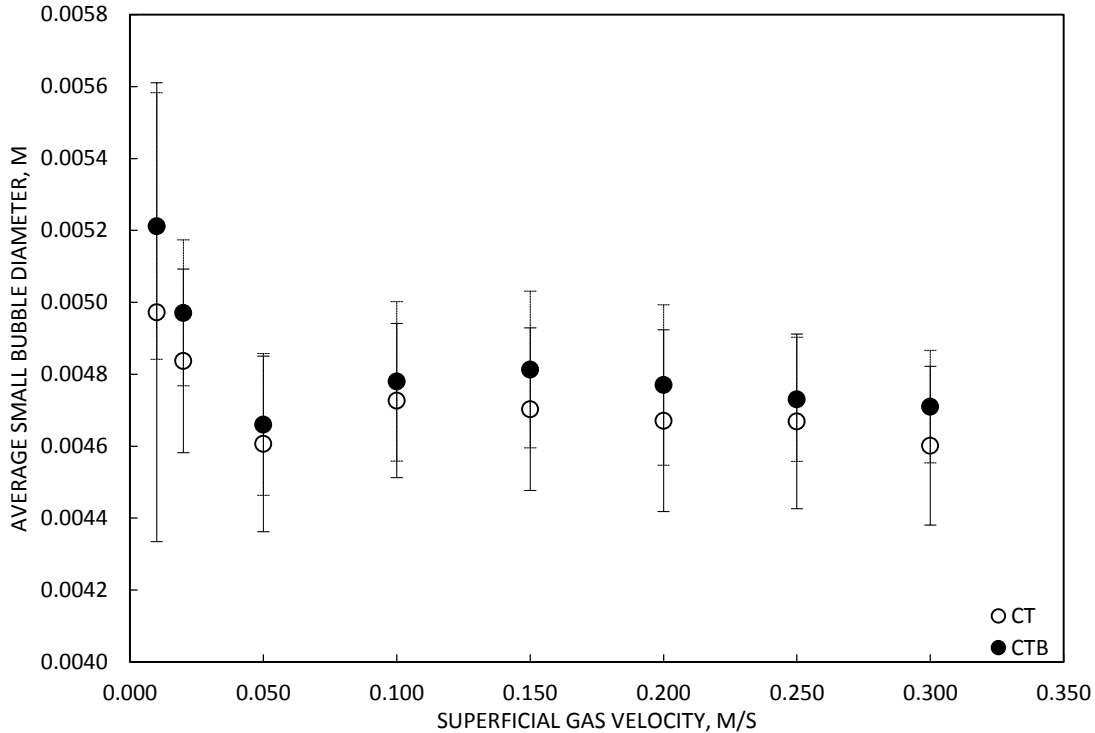
Figure 4.24: Effect of internals on small bubble class size measurements

Histograms of the small bubble size measurements were constructed for samples at high (0.25 m/s) and low (0.02 m/s) superficial gas velocities, for both internals. This can be seen in Figure 4.25. In general, the size measurements obtained during CT investigations were subject to greater variability given the broader width of its histograms at both the high and low gas velocities. However, lower variances in size measurements were obtained at the higher superficial gas velocity, for both internals.

To ensure that accurate small bubble size estimates were obtained, all size measurements were taken during the disengagement of the small bubble class. Measurements taken during this period are believed to be less affected by the distortion associated with regular operation.
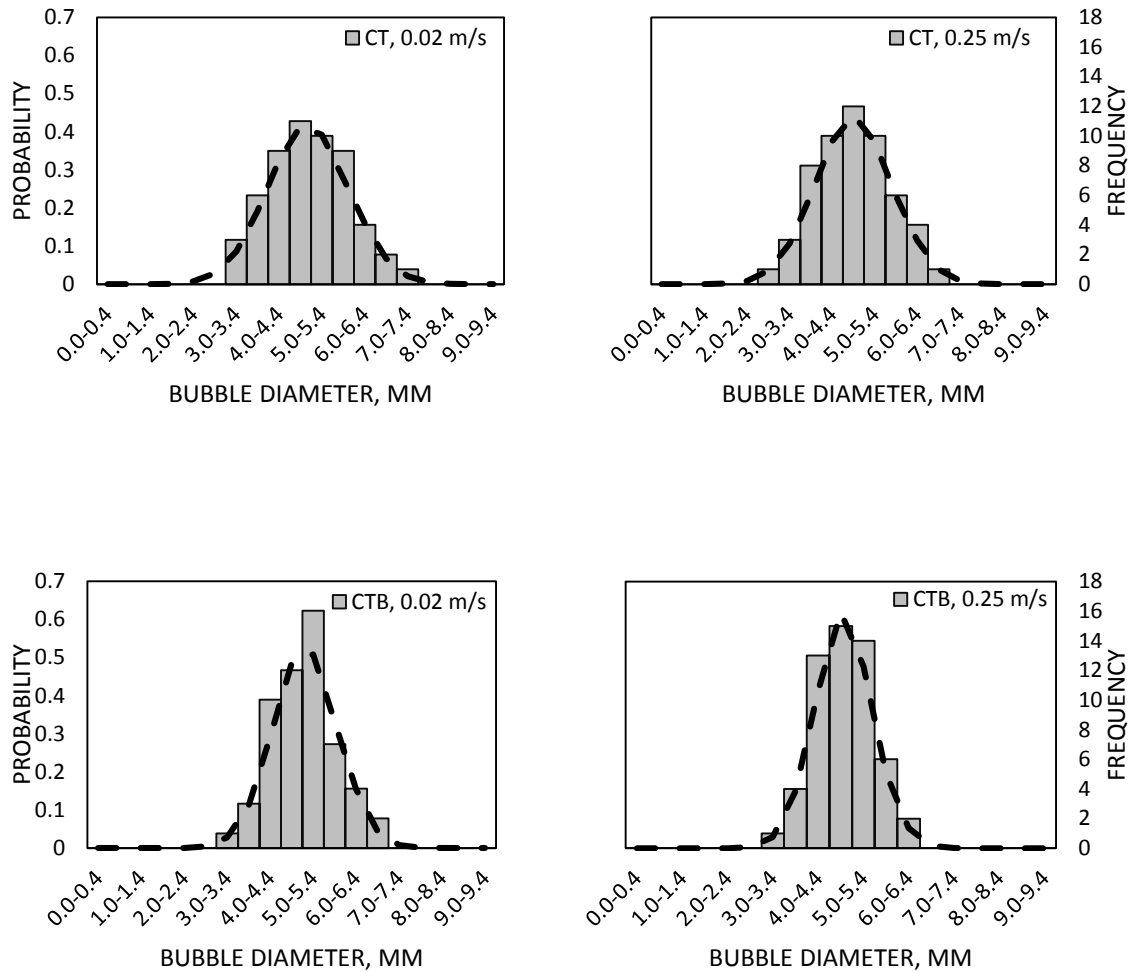
Figure 4.25: Effect of internals on small bubble size distributions at high and low gas velocities

4.2.4 Interfacial area

As discussed earlier, increases in small bubble holdup are advantageous because small bubble holdup greatly influences the interfacial area of bubble column systems. Interfacial area is a good indicator of the gas-liquid mass transfer capabilities of a bubble column system. Figure 4.26 and Figure 4.27 summarize the effects of the CT and CTB internals on total interfacial area, as well as the small and large bubble contributions to interfacial area. For both internals, the small bubble

contributions to interfacial area were much greater than that of the large bubbles. This can be seen in Figure 4.27. The small bubble interfacial area contributions also increased rapidly with superficial gas velocity while that of the large bubble tended to decrease. As a result, total interfacial area, which can be seen in Figure 4.26, was found to increase with superficial gas velocity for both internals. However, larger total interfacial area values were obtained with use of the CT internal over the CTB internal. This is expected since interfacial area is favoured by higher small bubble holdup values and reduced small bubble diameters, both of which were obtained with the CT internal.
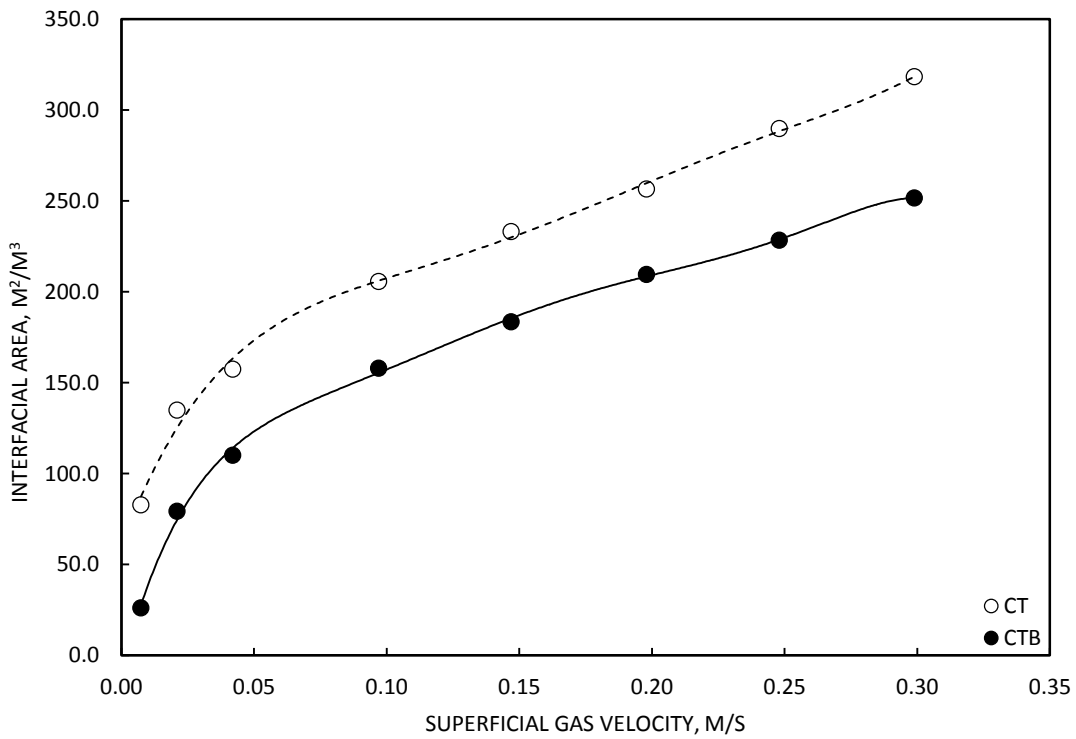
Figure 4.26: Effect of internals on total interfacial area
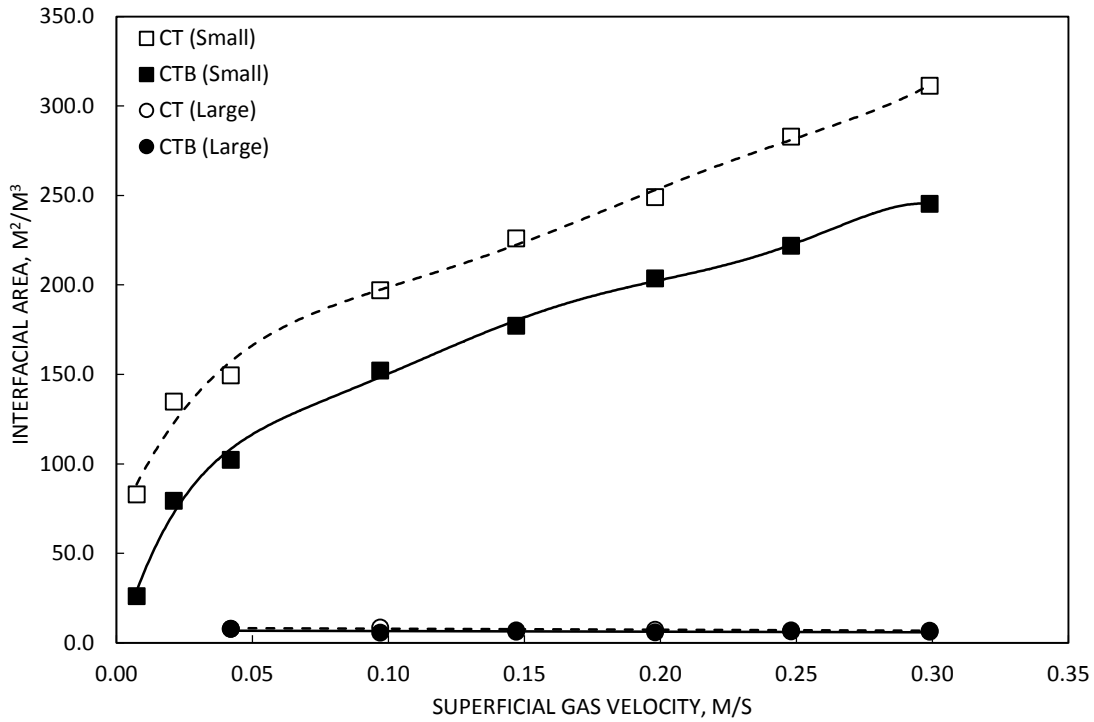
Figure 4.27: Effect of internals on large and small bubble contributions to interfacial area

The increases in interfacial area are believed to be mainly due to an accumulation of small bubbles in the system and thus, an increase in small bubble holdup. This can be explained by considering the effect of each internal on liquid circulation. During CT investigations, most large bubbles and their wakes are directed to the center of the concentric tube bundle. After reaching the top of the bundle, the large bubbles erupt and the fluids they entrained flow down the annular region. The structured downward flow of fluid in the annular region provides resistance to the small bubbles, which primarily traverse this region. This resistance slows down the small bubbles and thus, increases small bubble holdup. The behavior can be seen in Figure 4.28a. Although increased small bubble holdups were obtained when using the CTB internal, smaller values were recorded when compared to that of the CT internal. The difference in small bubble holdup may be attributed to the presence of the baffle during CTB investigations. The baffle internal can deflect larger bubbles

into the annular region that are able to re-entrain small bubbles and other surrounding fluid as they rise. This partially counters the downward fluid flow in the annular region which has already been weaken due to the reduced passage of large bubbles through the core of the tube bundle. The behavior can be seen in Figure 4.28b.

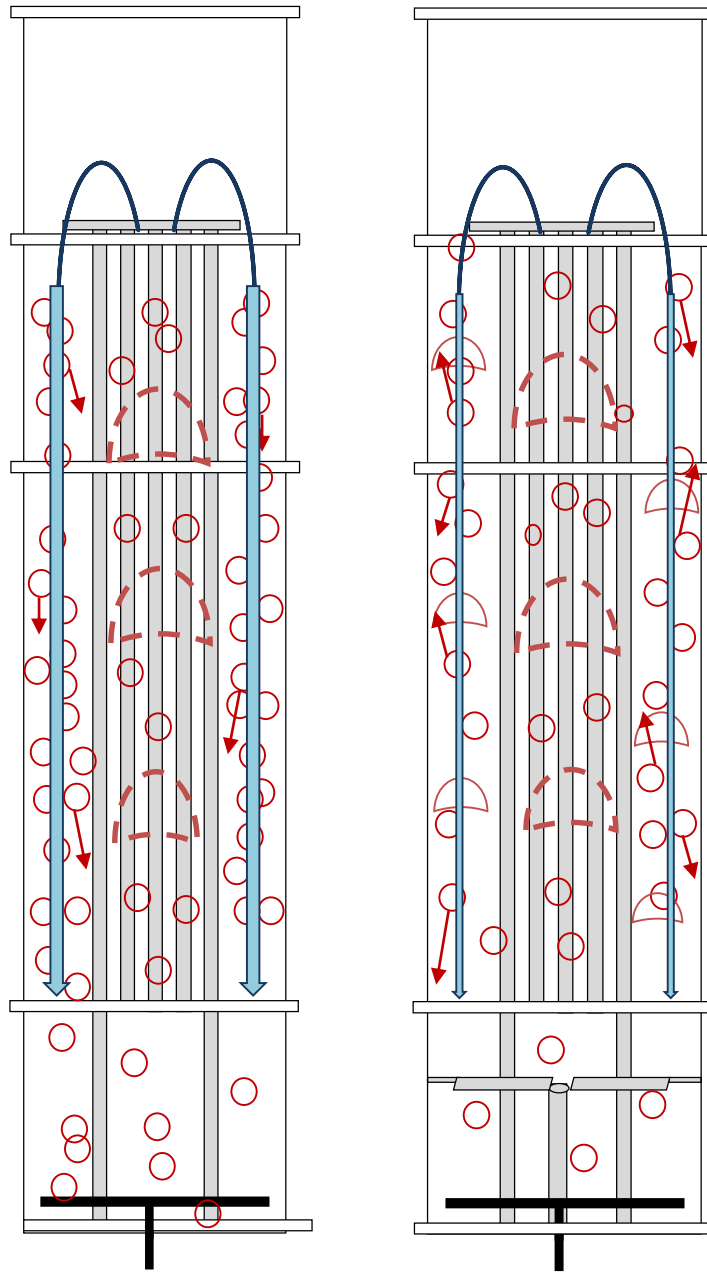Figure 4.28: Visualization of a) CT (*left*) and b) CTB (*right*) internals on small bubble holdup

4.3 Liquid Phase Mixing

Liquid phase mixing is a phenomenon that results from the hydrodynamic interactions between the gaseous and liquid phases contained within a bubble column reactor. It is scale dependent and varies between two theoretical ideals, namely the plug flow and complete mixedness ideals. The extent of liquid phase mixing in a reactor can be quantified through two global mixing indexes – mixing time and axial dispersion coefficient. These parameters are inversely related and are sensitive to a reactor's design, particularly the addition of internals. The effect of the CT and CTB internals on liquid phase mixing time and axial dispersion coefficient will be investigated in the following subsections. Comparisons will be made between the obtained results.

4.3.1 Liquid Phase Mixing Time

Mixing time was estimated using dye and salt tracers, the results of which can be found in Figure 4.29. Estimates of complete mixing were reported for the dye tracer studies while estimates of ninety percent mixing were reported for the salt tracer studies. From Figure 4.29, it could be seen that comparable mixing time trends were obtained for both methods although higher values were obtained with the salt tracer method. This difference in mixing time can be attributed to visual limitations since the human eye is unable to pick up subtle changes in colour that occur over long periods of time. Complete mixing with the dye tracer was determined visually and was thus subject to this limitation. More accurate results with dye tracers may be obtained by using devices such as spectrophotometers.
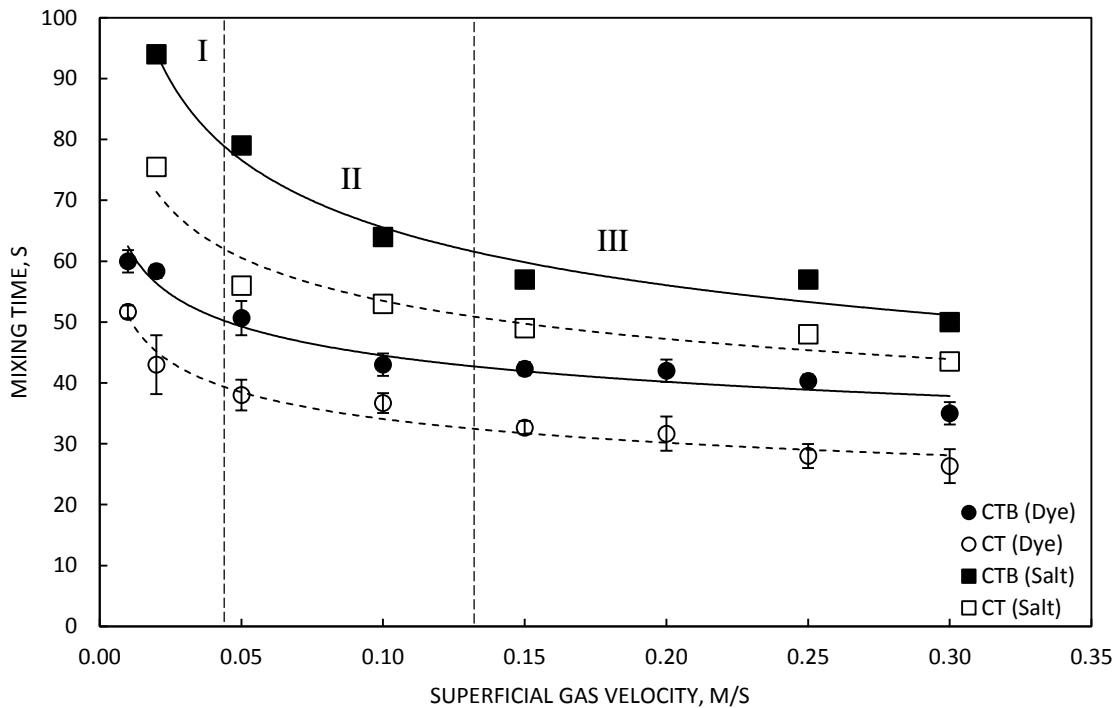
Figure 4.29: Comparison of liquid mixing obtained by two methods for two respective internals

Although significant differences exist between the results obtained from the two tracer methods, the mixing times obtained with the CTB internal were consistently higher than that obtained with the CT internal. The average mixing time differences were 12 seconds with the salt tracer technique and 10 seconds with the dye tracer technique. The increase in mixing time during CTB investigations strongly suggests a reduction in liquid backmixing since backmixing is inversely proportional to mixing time. For all cases, mixing time decreased with increases in superficial gas velocity in a manner indicating flow regime transitions. This allows Figure 4.29 to be divided into three major regions, based on the rate of decrease of mixing time with superficial gas velocity. The initial, near-linear drop in mixing time observed in this figure is associated with a sudden increase in liquid mixing. This is due to growth of the small bubbles in the homogenous flow regime. Throughout transition, rate at which mixing time decreases continues to slow down as the number

103

of large bubbles within the system continues to increase. Beyond transition, mixing time decreases in a near-linear manner with superficial gas velocity and indicates operation within the coalesced bubble flow regime.

4.3.2 Axial Dispersion Coefficient

The axial dispersion coefficient can be used to quantify backmixing in the axial plane. As explained earlier, backmixing refers to the random movement of fluid that has been superimposed on the direction of major flow within a system (Moustiri at al., 2001, Shah et al., 1978). The axial dispersion coefficient is an important design parameter for bubble column reactors (Sanchez Miron et al., 2000, 1999). Lower axial dispersion coefficients are desirous for reaction-containing systems since larger backmixing (higher axial dispersion coefficients) reduce reactant and product concentration gradients through dilution. This property affects mass transfer and thus, the reactor's productivity. Higher axial dispersion coefficients are desirous in applications that require constant equilibrium despite continuous disturbance. These include biological applications as well as reactors requiring temperature control due to their contained endothermic or exothermic reactions.

Theoretically, the axial dispersion coefficient, D_a, can be obtained from the mass balance of the injected tracer into the system. The simplest, one-dimensional dispersion model and its associated boundary conditions can be seen below (Ohki and Inoue, 1970). It is important to point out that model has been verified by others (Deckwer et al., 1974).

Model:

$$\frac{\partial C}{\partial t} = D_a \frac{\partial^2 C}{\partial z^2}$$

(4.13)

Boundary condition:

$$\frac{\partial C}{\partial z} = 0 \; at \; z = 0 \; and \; z = L$$

(4.14)

Initial conditions:

$$C(z, 0) = C_0 \; for \; 0 \leq z \leq \lambda$$

(4.15)

$$C(z, 0) = 0 \; for \; z \geq \lambda$$

(4.16)

where C is the instantaneous tracer concentration, z is axial displacement, D_a is the axial dispersion coefficient, λ is the height filled with tracer and t is time. The solution to this differential equation can be seen below.

$$\frac{C}{C_E} = 1 + \frac{2L}{\pi \lambda} \sum_{n=1}^{\infty} \left[\frac{1}{n} \cdot \sin \frac{n\pi}{L} \lambda \cdot \cos \frac{n\pi}{L} z \cdot exp\left(-\left(\frac{n\pi}{L}\right)^2 D_a t \right) \right]$$

(4.17)

where $C_E L = C_0 \lambda$. When $\lambda n \ll L$, equation 4.17 approximates to the following,

$$\frac{C}{C_E} = 1 + 2 \sum_{n=1}^{\infty} \left[\cos \frac{n\pi}{L} z \cdot exp\left(-\left(\frac{n\pi}{L}\right)^2 D_a t \right) \right]$$

(4.18)

In a more practical sense, estimates of the axial dispersion coefficient can be obtained without the solution to a dispersion model. According to Ohki and Inoue (1970), six terms are sufficient to obtain estimates of the axial dispersion coefficient with less than 1 percent error. Equation 4.19 shows the equation used for this calculation.

$$D_a = \left(\frac{L_{dyn}}{\pi}\right)^2 \frac{\Delta\theta}{\Delta t} \tag{4.19}$$

In equation 4.19, L_{dyn} is the dynamic height of the fluid in the reactor and Δt is the time within which the dimensionless tracer concentration changes from 0.3 to 0.7. $\Delta\theta$ is a dimensionless number that can be obtained from Figure 4.30. It is obtained from the dimensionless tracer concentration as well as the dimensionless distance between the conductivity probe and injection point. An obtained tracer concentration curve can be seen in Figure 4.31.
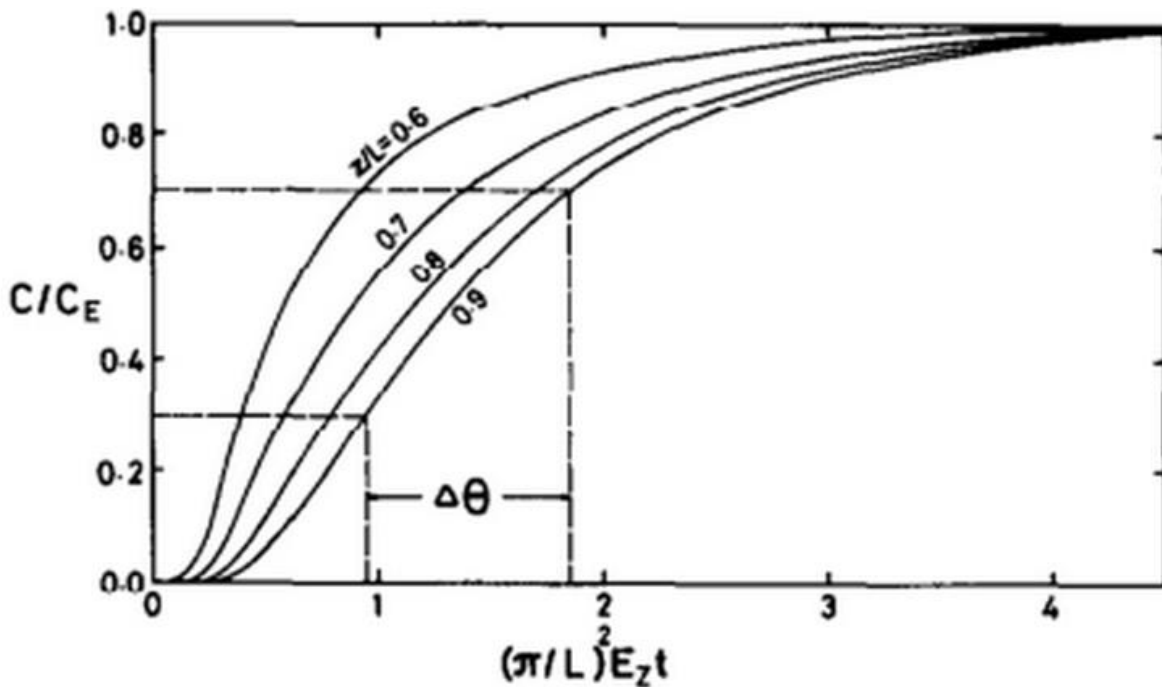
Figure 4.30: Tracer response curves derived from the diffusion model (Ohki and Inoue 1970)

106
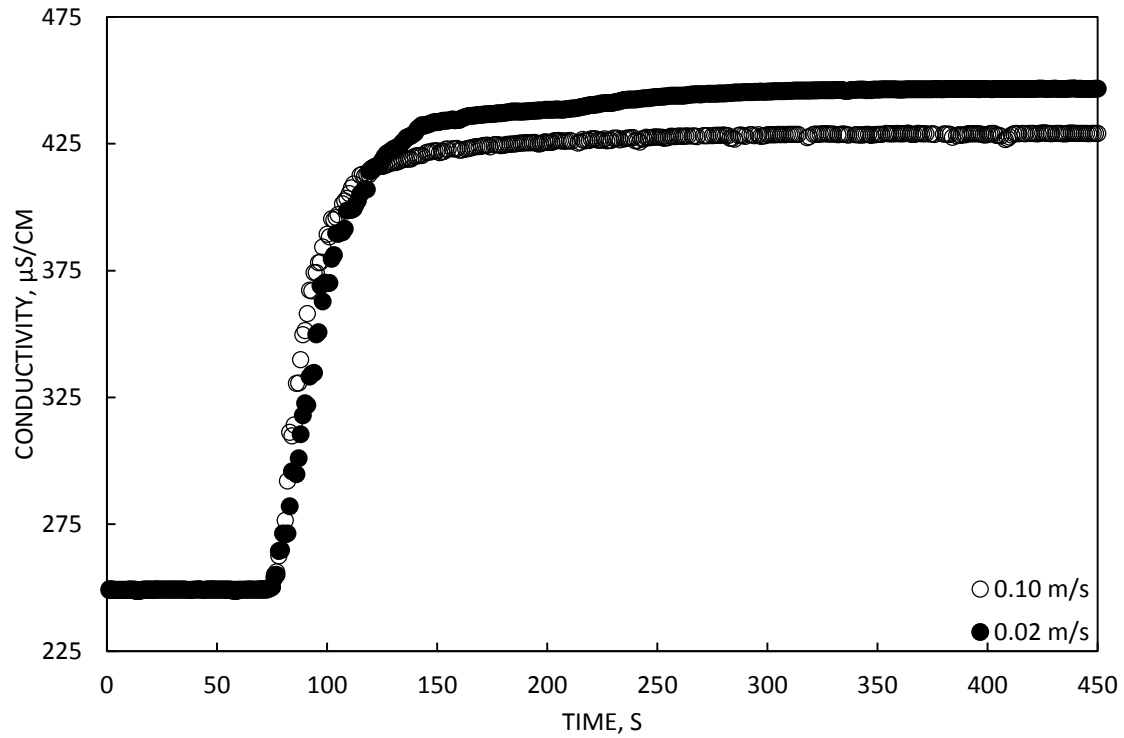
Figure 4.31: Sample of conductivity-time curve (CT)

Figure 4.32 summarizes the effect of the CT and CTB internals on the axial dispersion coefficients of a bubble column reactor. For this figure, axial dispersion coefficient increases with increases in superficial gas velocity for both internals in a similar manner. The axial dispersion coefficients obtained with the CT internal were consistently higher than those obtained during CTB investigations. This confirms reduced backmixing with the CTB internal.
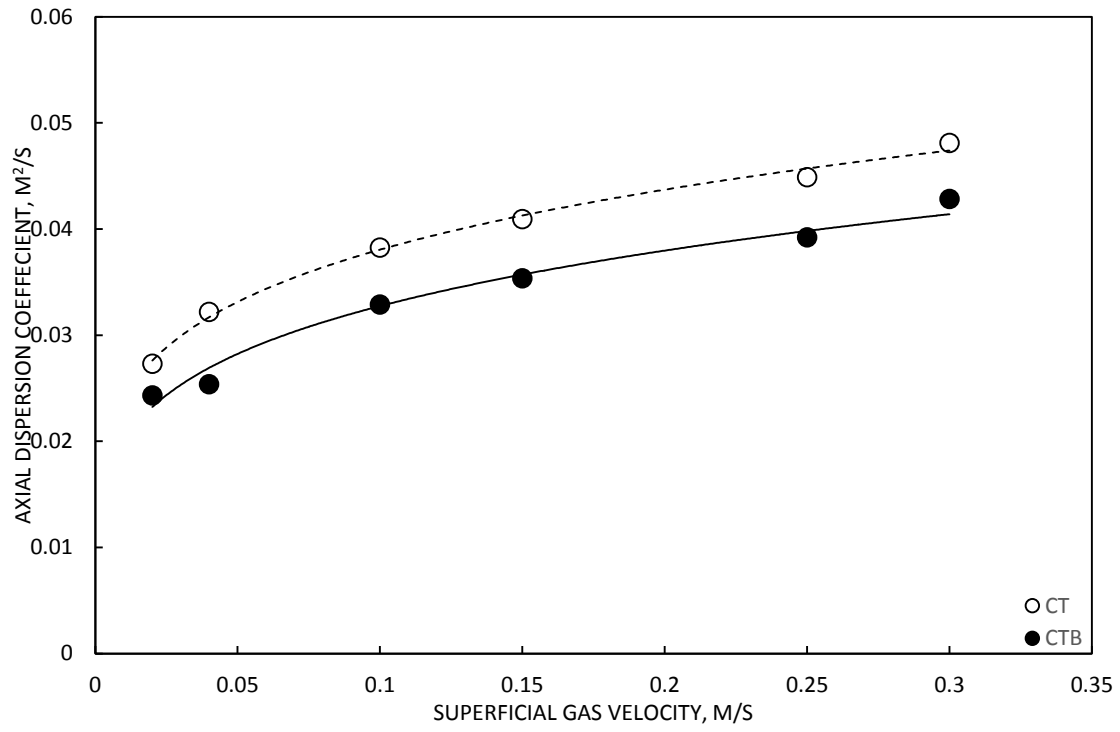
Figure 4.32: Effect of internals on axial dispersion

5.0 Conclusions and Recommendations

5.1 Conclusions

1. The tube bundle internal (CT) and the novel tube bundle/baffle internal combination (CTB) provide useful insights into the role of internal design on bubble column hydrodynamics. These observations can be the basis for further improvements and other practical applications.

2. The observations made with the neutrally buoyant particles demonstrates the complexity and variations in local flow structure in a bubble column equipped with the CT and CTB internals respectively. These observations are also used to construct the bulk liquid circulation flow patterns for the system equipped with each internal respectively. The presence of the baffle in the CTB internal significantly increases upward particle movements in the annular region when compared to that observed with the CT internal. Several interesting non-linear particle movements are observed during neutrally buoyant particle experimentation for each of the investigated internals.

3. The addition of internals to a bubble column significantly increases the gas holdup of the system. This is mainly attributed to an increase in small bubble holdup. Higher gas holdups are achieved with the CT internal over the CTB internal. The difference is attributed to the deflection of larger bubbles into the annular region during CTB investigations, due to the baffle internal. These larger bubbles entrain smaller bubbles and surrounding liquids with them as they rise, which lowers gas holdup.

4. Interfacial area is estimated for both the CT and CTB internals. Larger interfacial area values are obtained with the CT internal due to the higher small bubble holdup and slightly lower small bubble diameters obtained with its use.

5. Mixing time and axial dispersion measurements provide further quantification of the differences between the CT and CTB internals.

   - The mixing times obtained with the CTB internal are consistently higher than those obtained with the CT internal.

   - The axial dispersion coefficients obtained with the CT internal are consistently higher than those obtained with the CTB internal.

5.2 Recommendations

1. More detailed investigation on the liquid circulation patterns observed with the internals should be carried out to confirm the proposed flow structures using suitable tracer techniques.

2. More accurate and detailed bubble size measurements should be obtained for the different regions of the internal-equipped bubble column using needle probes.

3. Other internal parameters (e.g. position of each internal within the column and the width of the spaces between the tubes of the tube bundle internal) should be investigated in order to gain a better understanding of their effects on bubble column systems.

4. Further optimization of the internal designs should be achieved with CFD modeling.

Appendix A – Calibration of Sonic Nozzles
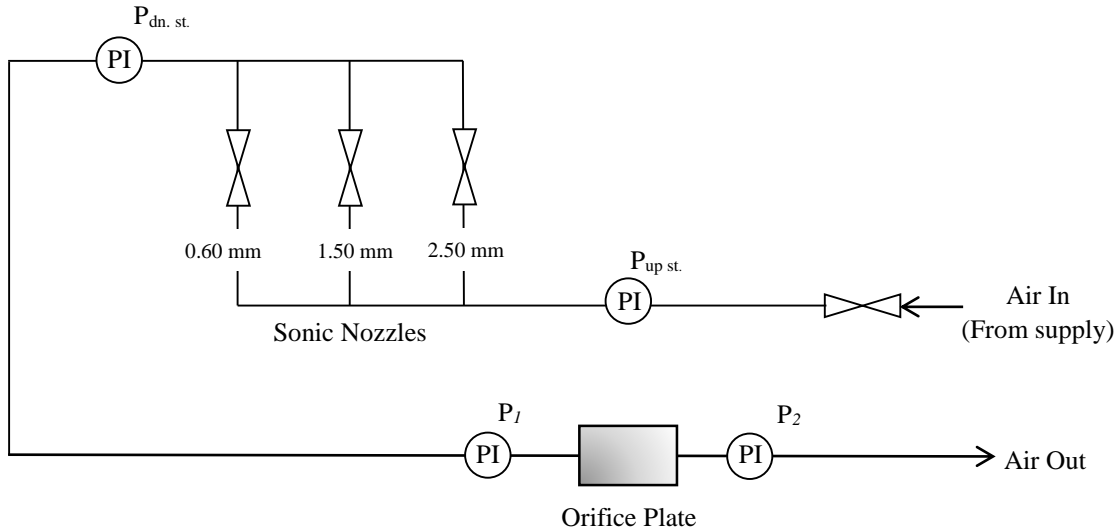
Figure A.1: Schematic showing experimental layout

Gas flow through the system was calibrated using the experimental setup outlined in Figure A.1 above. Initial measurements for P_1 and P_2 were made using relatively inaccurate pressure gauges (operation ranges: 0 to 639 kPa/0 to 100 psig, graduation: 7 kPa/1 psi) to obtain an estimate of the upstream pressure as well as the corresponding orifice plate meter pressure drop for a maximum column superficial gas velocity of 0.30 m/s. This estimate was initially carried out using 2.5 mm and 4.8 mm orifice plates. When using the stated orifice plates, the upstream pressures required to attain the desired column superficial gas velocities were too high and thus more suitable orifice plates were required. After further investigation of past literature, it was decided that the most ideal orifice plate should have an orifice diameter of 6.4 mm. For cost efficiency purposes, it was decided that the orifice of the 2.5 mm orifice plate should be extended to 6.4 mm without altering its orifice edge angle. After its expansion, the modified orifice plate was installed and estimates of

the pressure drops across the orifice plate meter were obtained. These estimates revealed that for an upstream pressure of about 648 kPa (94 psig), the pressure drop across the orifice plate meter was about 41 kPa (6 psig) and the superficial gas velocity within the column was about 0.31 m/s. Based on this information, more accurate pressure gauges for P_1 and P_2 were purchased and installed. These new gauges are operable for pressures between 0 to 69 kPa (0 to 10 psig) and have graduations of 7 Pa (0.001 psi). Measurements for column superficial gas velocities of about 0.10 to 0.30 m/s were taken with the 2.5 mm throat sonic nozzle and 6.4 mm orifice plate. Measurements for column superficial gas velocities of about 0.04 to 0.11 m/s were taken with the 1.5 mm throat sonic nozzle and 6.4 mm orifice plate. Measurements for column superficial gas velocities of about 0.007 to 0.02 m/s were taken with the 0.06 mm throat sonic nozzle and 4.8 mm orifice plate. From these measurements, the pressures corresponding to superficial gas velocities of about 0.007, 0.02, 0.04, 0.10, 0.15, 0.20, 0.25 and 0.30 m/s were obtained, using the appropriate sonic nozzles. Table A.1 summarizes this relationship.

Table A.1: Summary of sonic nozzles, upstream pressures and superficial gas velocities

Nozzle Diameter, mm	Upstream Pressure (kPa)	Superficial Gas Velocity (m/s)
0.60	165	0.007
1.50	69	0.021
1.50	207	0.042
2.50	165	0.097
2.50	269	0.147
2.50	372	0.198
2.50	476	0.248
2.50	579	0.299

Sonic nozzles are special types of metering devices which facilitate the control of a gas's velocity through manipulation of its inlet temperature or pressure. Sonic nozzles achieve this through their unique design, as can be seen in Figure A.2 below:
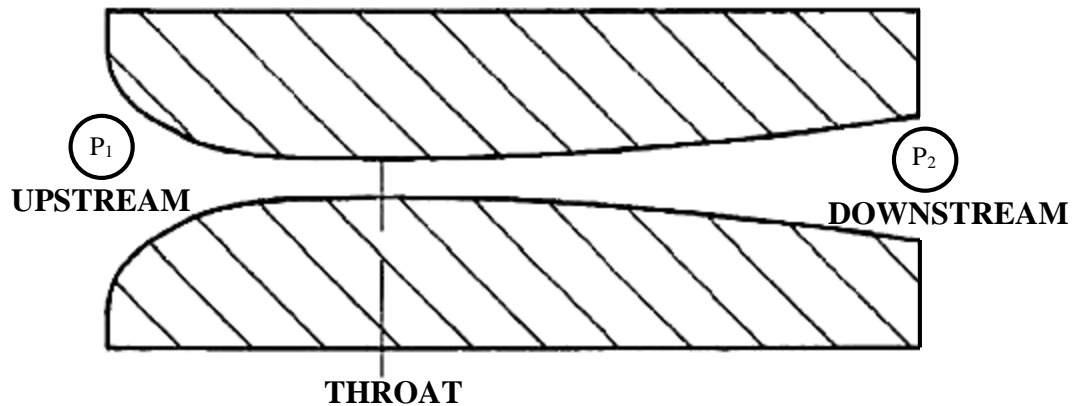

Figure A.2: Schematic of sonic nozzle, modified (Baker 2005)

After the gas enters the inlet of a sonic nozzle (at 1), it is constricted upon reaching the minimum in the nozzle's convergent-divergent design, called the throat. At that point, the gas' velocity is increased due to the inverse relationship between gas velocity and pipe cross-sectional area for a constant gas flow rate. As upstream pressure is increased, the gas velocity increases in a non-linear manner until gas velocity at the throat approaches and surpasses the speed of sound. At those instances, gas flow is described as being 'sonic' or 'critical' and is a linear function of upstream pressure for a given temperature. Operation within this sonic state is advantageous because downstream disturbances do not affect the upstream environment and thus, limit fluctuations and errors.

The point at which gas flow at the nozzle throat becomes sonic can be identified by a certain downstream/upstream pressure ratio called the critical ratio, r_c. The following equation from Flow Measurement Handbook: Industrial Designs, Operating Principles, Performance, and Applications can be used to locate r_c in sonic nozzles systems (Baker 2005).

$$r_c = \frac{P_{dn.st.}}{P_{up\ st.}} = \left(\frac{\Upsilon + 1}{2}\right)^{\frac{-\Upsilon}{\Upsilon - 1}} \tag{A.1}$$

Assuming that air behaves as an ideal gas and losses due to friction are negligible within the metering device, Equation A.1 can be solved to achieve $r_c = 0.528$, where $\Upsilon = 1.4$ for air. Thus, the downstream pressure must be at maximum half of the upstream pressure for critical flow to exist in sonic nozzles measuring air flow.

The mass flow rate of gas through a sonic nozzle can be determined using a correlation recommended by Briens (1993):

$$F_g = 1000 \left(1000 \times Y P_{up\,st.} A_T^2 \left(\frac{2}{Y} + 1 \right)^{\frac{Y+1}{Y-1}} \right) \tag{A.2}$$

For air, this correlation may be reduced to:

$$F_g = 685.2 A_t (\rho P_{up\,st.})^{0.5} \tag{A.3}$$

For the experiments carried out, a sonic nozzle with a throat diameter of 2.5 mm was used and was calibrated for pressures ranging from 138 to 189 kPa (20 to 100 psig). A summary of this calibration can be found in Table A.1.

To validate the results obtained from the theoretic sonic nozzle gas flow correlation, the gas flow through the nozzle was measured using a second type of metering device called an orifice plate meter. A schematic of a typical orifice plate meter can be seen in Figure A.3.
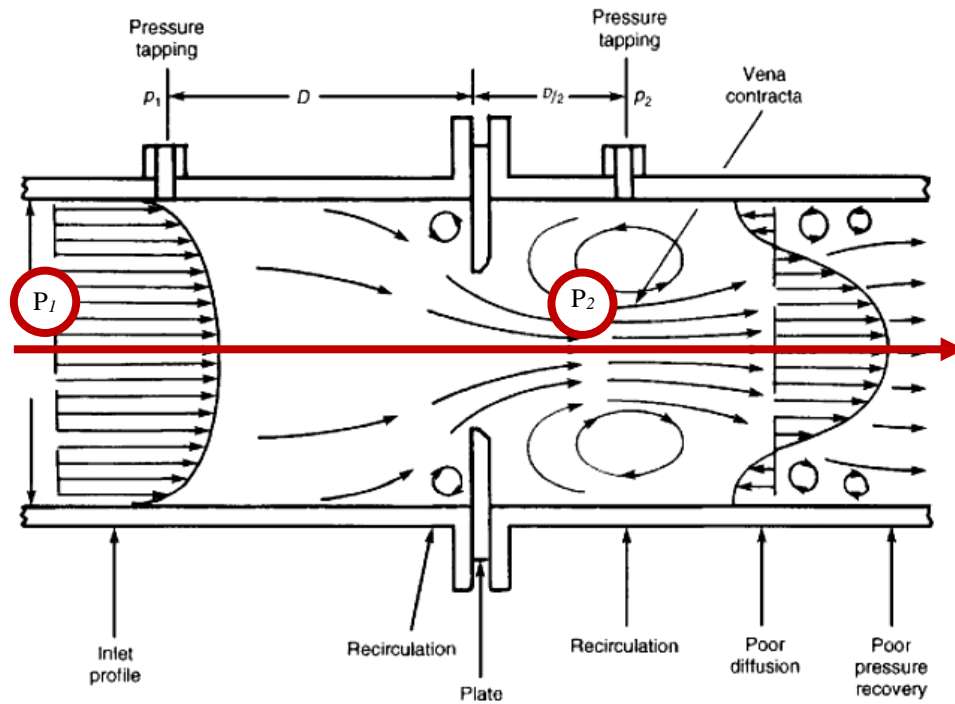
Figure A.3: Schematic of orifice plate, modified (Baker 2005)

Orifice plate meters, like Venturi meters, are based on Bernoulli's principle which simply states that the velocity of an invicid fluid decreases when the pressure on that fluid and/or the potential energy of that fluid increases. When a stream of gas is steadily passed through the typically sharp-edged orifice of an orifice plate, the stream is forcefully converged as can be seen in Figure A.2. Interestingly, the stream is not its most converged at the orifice, but at a point shortly downstream of the orifice called the vena contracta. After the vena contracta, the fluid is fully expanded once again. If the fluid through the pipe is assumed to be invicid, the volumetric flow rate of the fluid could be found using Bernoulli's Equation provided that the pressure difference between the upstream gas flow and the vena contracta is known. For a horizontal system configuration, potential energy is constant and Bernoulli's Equation is reduced to the following:

$$P_1 - P_2 = \frac{1}{2}(V_2^2 - V_1^2) \tag{A.4}$$

Acknowledging the fact that volumetric flow through the system is constant and that fluid velocity through an opening is equal to volumetric flow rate divided by the area of that opening (continuity equation), Equation A.4 can be rewritten as follows:

$$P_1 - P_2 = \frac{\rho Q^2}{2}\left(\frac{1}{A_2^2} - \frac{1}{A_1^2}\right) \tag{A.5}$$

Rearranging Equation A.5 yields:

$$Q = \sqrt{\frac{2(P_1 - P_2)}{\rho} \times \left(\frac{1}{A_2^2} - \frac{1}{A_1^2}\right)^{-1}} = \sqrt{\frac{2(P_1 - P_2)}{\rho} \times \left(\frac{A_2^2}{1 - A_2^2/A_1^2}\right)^{-1}}$$

$$= A_2\sqrt{\frac{2(P_1 - P_2)}{\rho\left(1 - A_2^2/A_1^2\right)}} \tag{A.6}$$

If the orifice and pipe are perfectly circular, the following simplification can be made:

$$\frac{A_2^2}{A_1^2} = \frac{D_2^2}{D_1^2} = \left(\frac{D_2}{D_1}\right)^2 = (\beta_1)^2 = \beta_1^2 \tag{A.7}$$

Substituting Equation A.7 into Equation A.6 yields the final equation for volumetric flow of a fluid through a pipe, Equation A.8. The coefficient C_d has been added to account for the non-ideality of fluid flow in real flow systems. The value of C_d used in the orifice plate calculation was 0.61.

$$Q = A_2 \sqrt{\frac{2(P_1 - P_2)/\rho}{(1 - \beta_1^4)}}$$

(A.8)

The mass flow of the fluid can be obtained by multiplying the results from Equation A.8 by the density of the fluid, where

$$\rho = \frac{P_{up\,st.} MW_{air}}{8.314 T_{up\,st.}}$$

(A.9)

A summary of the orifice plate meter measurements made on the 2.5 mm throat sonic nozzle can be found in Table A.1. The diameter of the orifice in the orifice plate was 6.4 mm. A plot of column superficial gas velocity from orifice plate measurements vs. column superficial gas velocity from sonic nozzle measurements can be seen in Figure A.4 below. Figure A.5 shows the relationship between upstream pressure and column superficial gas velocity for the 2.5 mm throat sonic nozzle. All calculations were carried out using an excel spreadsheet.
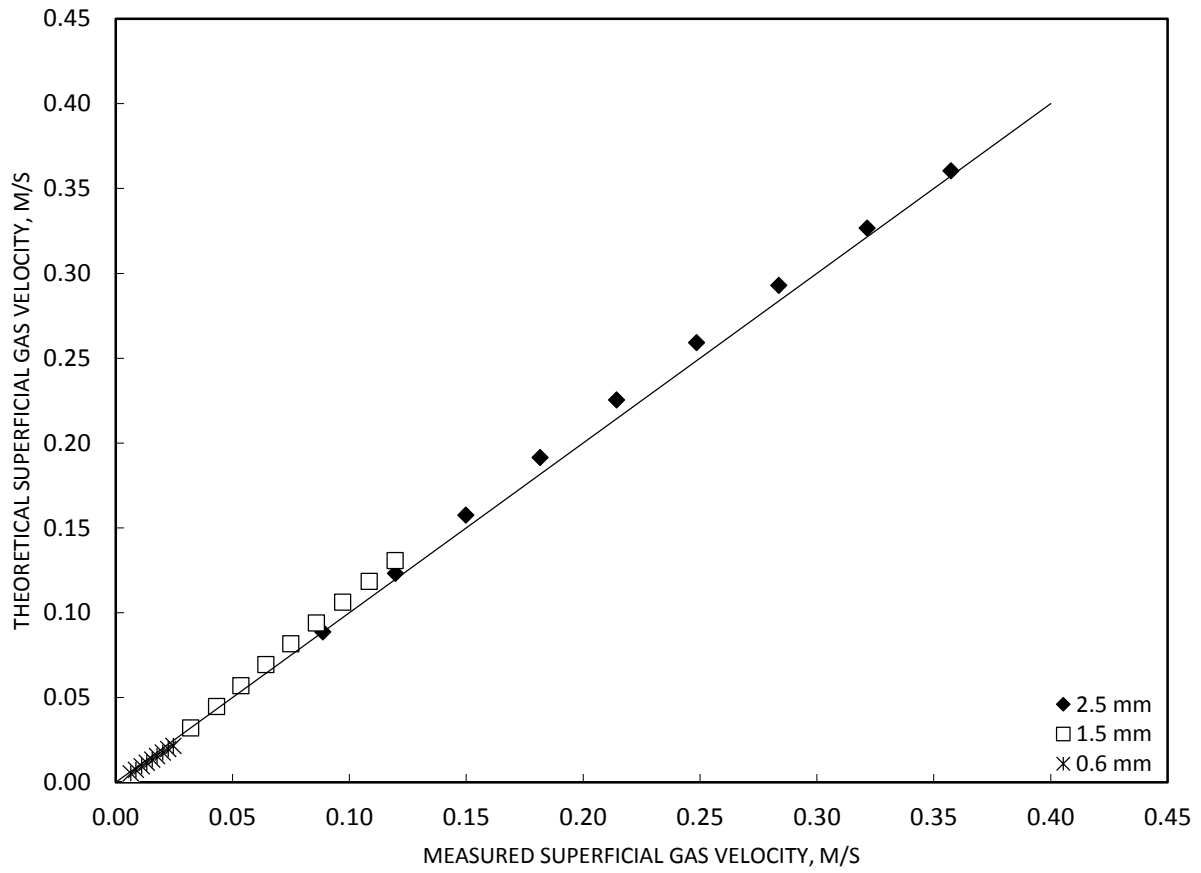
Figure A.4: Measured vs theoretical superficial gas velocity
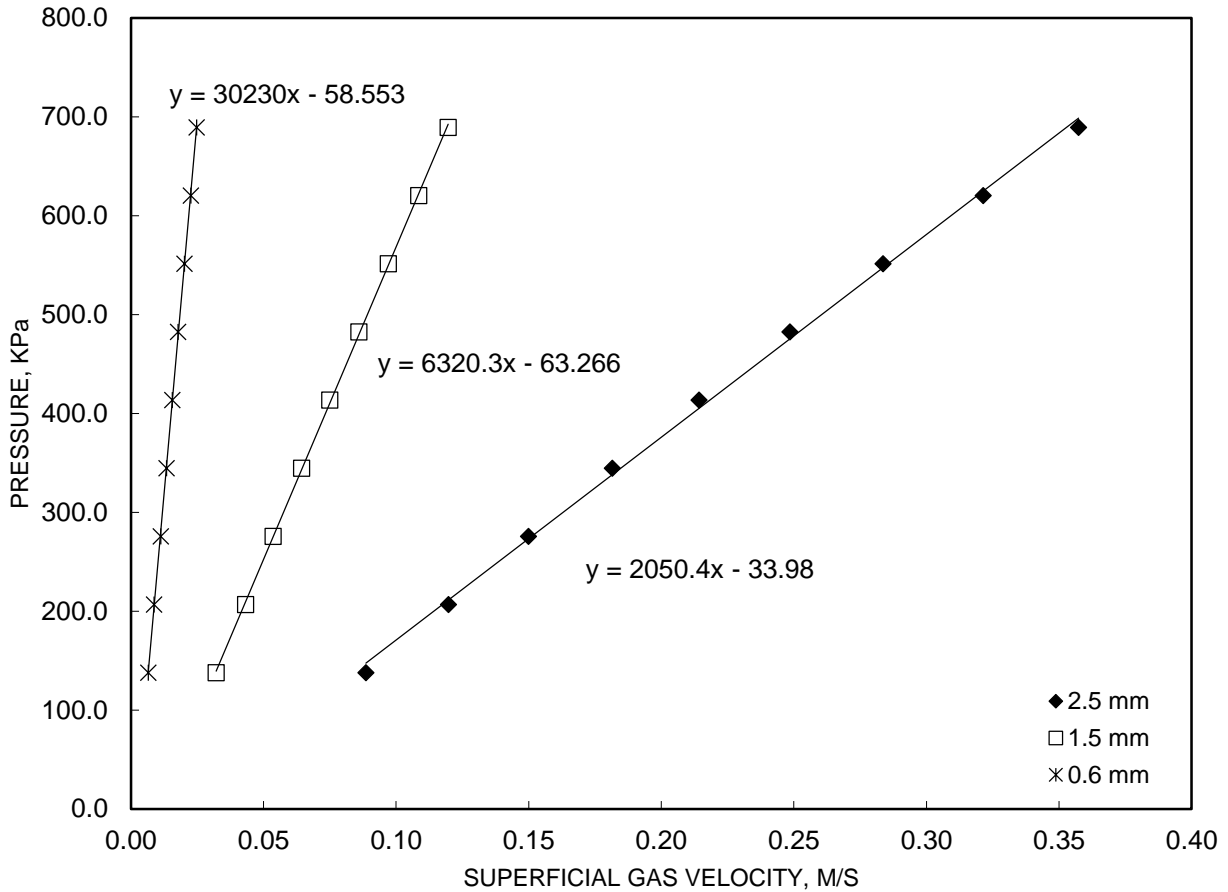
Figure A.5: Upstream pressure vs superficial gas velocity

Ideally, the data obtained from both the sonic nozzle and orifice plate calculations should be identical. If such was the case, the data from Figure A.3 would lie exactly on the '*y=x*' line shown. However, experimental errors (such as the parallax error encountered during the reading of pressure gauges) are responsible for the measured data's slight deviation from ideality when working in a pressure range between 138 to 189 kPa (20 to 100 psig). When working at pressures below 138 kPa, the error in the measured data is much greater.

Appendix B – Calibration of Pressure Transducers

The pressure transducers used in the column (OMEGA Type PX541-7.5GI and Type PX541- 45 15GI) were calibrated by filling the column with known heights of water and by noting the corresponding voltages using LabVIEW 8.0. The physical channels of each of the two transducers were added to LabVIEW thus allowing the acquisition of voltage data from the system. LabVIEW was configured to obtain 60 data points per second. The column was then filled with water to a height of 0.127 m and voltage data for the transducers was collected for about 15 seconds using LabVIEW 8. This step was repeated for water heights of 0.254, 0.381, 0.508, 0.635, 0.762, 0.889, 1.016, 1.143, 1.270, 1.397, 1.524, 1.651, 1.778, 1.905, 2.032 and 2.159 m. An average of the obtained voltage data for each, respective set was taken, and a plot of transducer voltage vs height of water was made. This plot can be seen in Figure B.1.
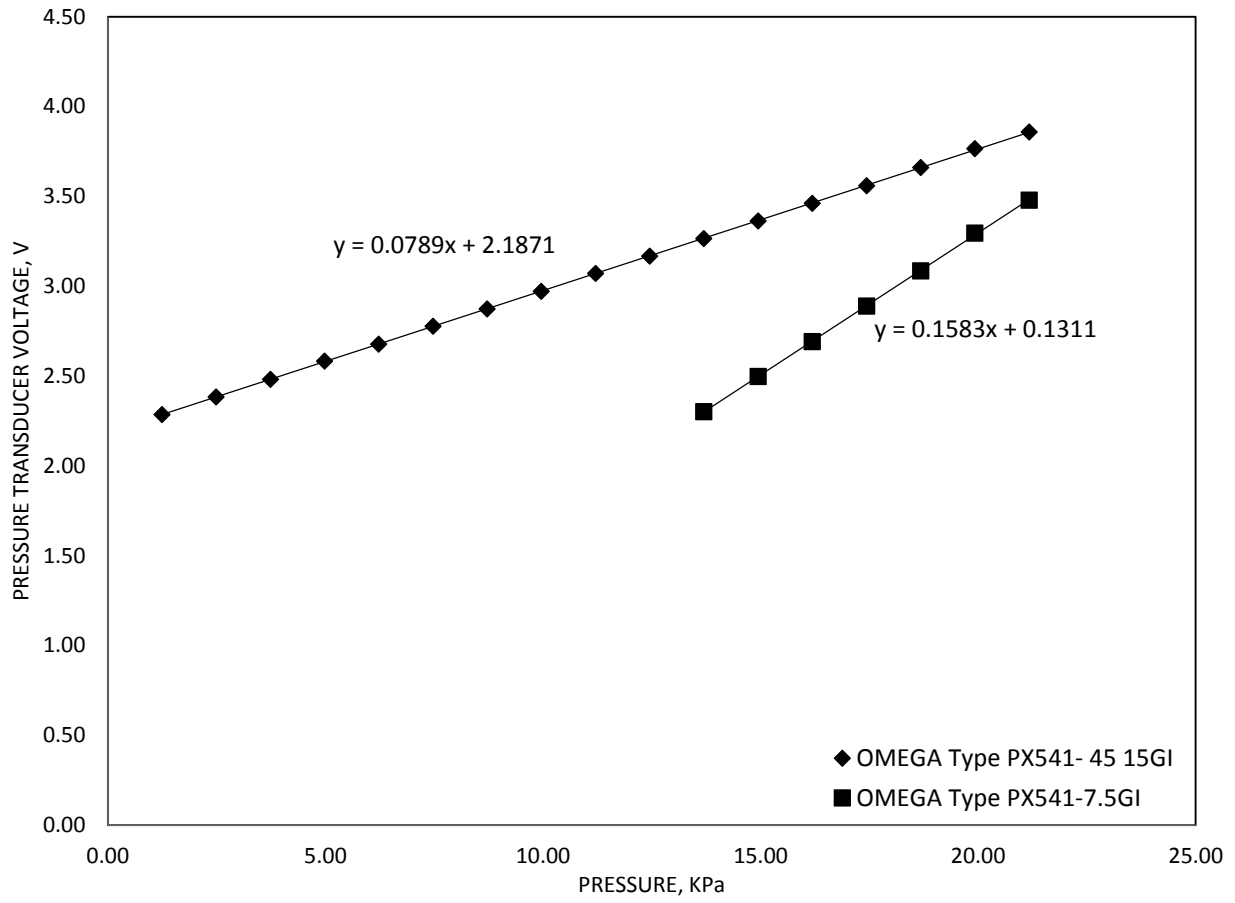
Figure B.1: Pressure transducer voltage vs hydrostatic pressure

Appendix C – Neutrally Buoyant Particle Design

Plastic jewellery beads (assorted diameters) were purchased along with silicone gel, fluorescing neon green spray paint and sandpaper. Two different types of beads were purchased – black and pastels. Table C.1 summarizes the properties of the materials purchased and used. Beads with diameters ranging from about 5.5 to 10.5 mm were selected, and the ends of the hollow found in those beads were sealed off with silicon. Silicone was applied to the beads using a pipette tip which was secured to the end of the silicone containing tube. The beads were left to dry for at least three hours and were dropped in water to determine how close their densities were to that of water. Beads that sank too quickly in water were discarded while beads that rose fairly rapidly in water were preserved for potential use provided that additional silicone was added to their hollows. Beads that were found to sink or rise slowly in water were collected for measurement. Any pastel coloured near-neutrally buoyant beads were spray painted neon green to enhance their visibility when placed in a running bubble column. To do so, the layer of paint lining the bead was removed using sand paper. The beads were then given a light coating of green paint and allowed to dry overnight. To ensure that the spray painted beads remain as neutrally buoyant as possible, this procedure was only performed on near-neutrally buoyant, pastel beads that were slightly less dense than water. In addition to this precaution, the beads were only given a single coat of paint.

Upon examination, the beads were observed to be spherical in appearance with slightly flattened ends, thus allowing them to be appropriately modelled as bi-truncated spheres. A representation of this model may be seen in Figure C.1 below. The minimum number of bead measurements taken can also be seen in Figure C.1. Additional $2r_i$ measurements were taken if the maximum difference between $2r_1$ and $2r_2$ exceeded 0.02mm. In general, five different radius measurements were taken

for each bead. The volume of the beads were estimated by doubling that obtained from the standard

mathematical proceedure for determining the volume of a truncated hemisphere, with inputs of h

and average of r_i. The sphericity of the beads was estimated by comparing the surface area of a

perfect sphere of equivalent volume with the theoretical surface area of its respective, bitruncated

sphere. As stated earlier, the volumes and surface areas of these shapes were obtained from

standard mathematical equations. The new mass of the beads was taken with a balance with

presision of 4 decimal places, and the density of the beads was found by dividing that mass by the

previously estimated volume. Table C.2 summarises the properties of the modified, near-nutrally

buoyant beads (particles).

The settling velocity of the beads, the last characterizing property measured for the near-nutrally

buoyant beads, can also be found in Table C.2 below. To obtain this property, the beads were

allowed to fall a known distance in water under timed conditions. The settling velocity was

calculated by dividing the distance travelled by a bead by the time taken to do so. To ensure

accuracy, the respective beads were allowed to fall a short distance before timing to make certain

that steady state is achieved and thus, all forces acting on individual beads are balanced.

Table C.1: Summary of materials used in near-neutrally buoyant particle construction

Materials	Properties
Jewellery Beads	Black: Estimated Density - 928.9 kg/m^3 Pastel: Estimated Density - 842.3 kg/m^3
GE Premium Waterproof White Silicone Kitchen/Bath/Plumbing Caulk	Density - 1283.38 kg/m^3
Norton Blue-Bak Waterproof T414 Paper (Sandpaper)	Grit Range 320
RONA Fluorescing Spray Paint, Turf Green	Mass - 312 g, VOC - 677 g/L

Table C.2: Complete summary of near-neutrally buoyant particle properties

Particle	Diameter, mm		Volume, m^3	Mass, kg	Density, kg/m^3	Sphericity	Settling Velocity, m/s
	h	$2r_{avg}$					
Particle 1	9.29	9.64	4.62×10^{-07}	0.467	996.4	0.999	− 0.69
Particle 2	4.08	5.52	7.97×10^{-08}	0.083	1046.2	0.850	0.89
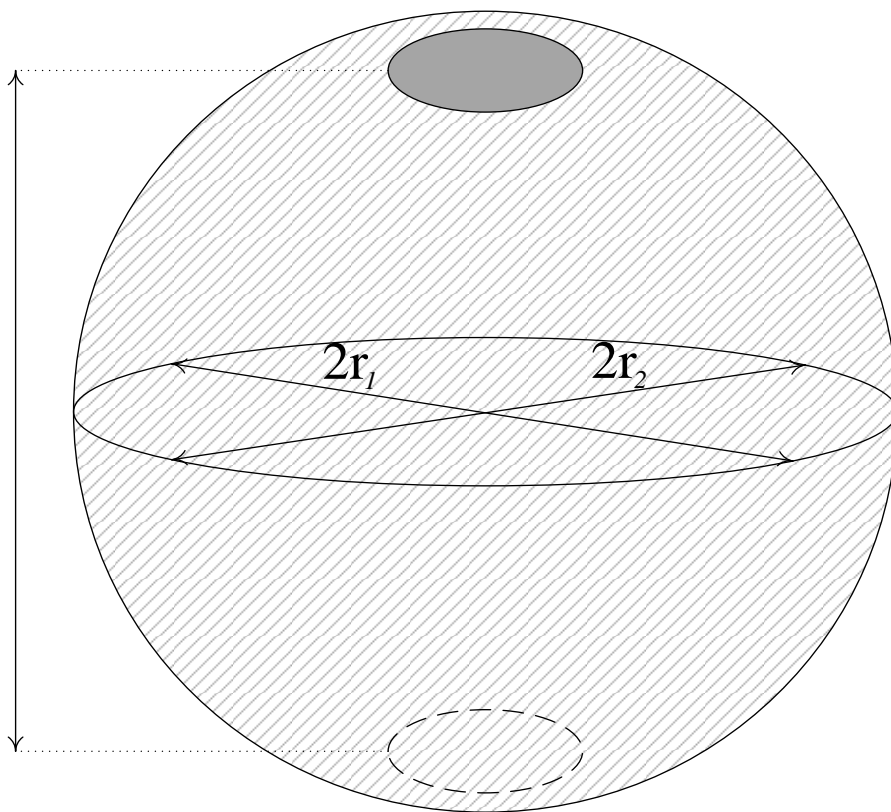
Figure C.1: Schematic of particle model

Appendix D – Calibration of Pump

The pump used in the tracer injection system described in Appendix E (VWR Variable-Flow Chemical Transfer Pump) was calibrated by measuring the time taken for the pump to transfer 0.0002 m^3 of water into a measuring cylinder for high and low pump voltage settings. The measurements at each setting were carried out twice. The volumetric flow rate at a given dial setting was determined by dividing the volume of water transferred by the average of the times taken to complete the transfer. A plot of the obtained results is presented in Figure D.1.

Figure D.1: Pump flow rate vs voltage

Appendix E – Injection System Design

Figure E.1: Schematic of tracer injection system

The tracer injection system was originally designed for the 15 s injection of 5% hydrochloric acid into the bubble column system using quarter inch steel tubes. This system contains two sections. The first section, the open loop, refers to the path which allows for the addition of acid to the column and can be considered to be the complete injection system. The closed loop (which 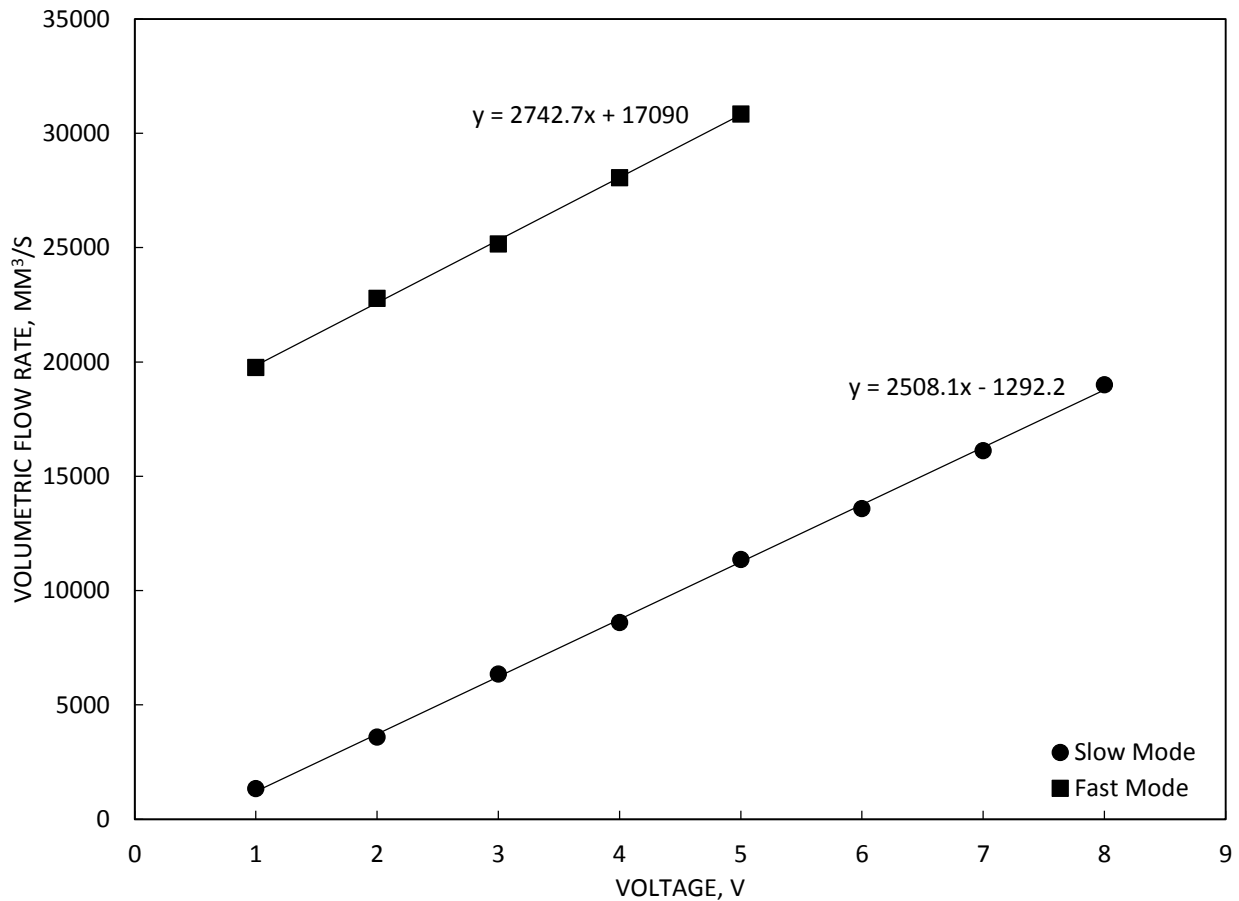refers to the path which returns pumped acid to the supply) is a supporting precaution that has been added to ensure that a certain degree of steady flow has been achieved by having the acid circulate within the closed loop for a substantial amount of time before transfer into the open loop. All calculations were made based on the stated worst case scenario with respect to acid injection: the addition of acid to a bubble column reactor that has been filled to the desired dynamic height of 2.1336 m, but has not been exposed to air flow. This was regarded as the worst case scenario because this case would require the largest volume of acid (and thus, the longest amount of time) to bring the column to the desired final pH of 3.

The total volume of acid required was determined by back-calculating the amount of acid required to change the final pH of the column to the desired value stated earlier. From this data, the volumetric flow required for the complete deposition of this critical acid volume within 15 s was calculated. Based on this value, quarter inch steel tubes were thought to be reasonable for the application. From then onwards, calculations estimating the required pump head were carried out for the near-worst case scenario with respect to pump positioning: pump positioned below the reactor with moderate supply head. This was thought to be a reasonable worst case as in this position, the pump would be required to provide near maximum head and would be exposed to maximum, frictional major loss.

The losses for the open and closed loop cases were both calculated, the worst of which used in determining the maximum required pump head. For each case, the required pump head was obtained using the standard Bernoulli's equation that had been extended to account for pump energy inputs as well as various energy losses (elevation, major and minor losses, sparger pressure drop losses). The major losses (losses due to friction along the length of pipe) and the minor losses (losses due to geometric variation within the loop) were obtained through elementary fluid mechanics. The major equations used are shown below.

$$\frac{P_1}{\rho g} + \frac{v_1^2}{2g} + z_1 + h_{pump} = \frac{P_2}{\rho g} + \frac{v_2^2}{2g} + z_2 + h_L \qquad \text{E.1}$$

$$h_L = \left(\sum f\frac{L}{D} + \sum K_L\right)\frac{v^2}{2g} + \frac{\Delta P_{dist}}{\rho g} \qquad \text{E.2}$$

The pressure drop across the sparger was obtained through the following correlations (McCabe 2001, Denn, 1980):

$$D_o \leq 0.7\frac{D_p}{\sqrt{N_o}} \qquad \text{E.3}$$

$$\Delta P_{dist} = \frac{Q_{go}^2 \times \rho_g \times \left[1 - \left(\frac{D_o}{D_p}\right)^4\right]}{2C_o^2 \times A_o^2 Y^2} \qquad \text{E.4}$$

The required, near-worst case scenario pump head was determined by summing the various losses existing within both the open and closed loop cases and by selecting the larger of the two values.

130

A pump capable of providing the maximum head was selected for the system. A schematic of the

system can be seen in Figure E.1.

References

Albright L. Albright's Chemical Engineering Handbook. Boston: CRC Press (2008).

Alvaré J, Al-Dahhan MH. Liquid phase mixing in trayed bubble column reactors. Chemical Engineering Science (2006), 61: 1819-1835.

Baker RC. Flow Measurement Handbook: Industrial Designs, Operating Principles, Performance, and Applications. USA: Cambridge University Press (2005).

Bando Y, Hayakawa H, Nishimura M. Effect of equipment dimensions on liquid mixing time of bubble column with draft tube. Journal of Chemical Engineering of Japan (1998), 31(5): 765-770.

Bhatia B, Nigama KDP, Aubanb D, Hebrard G. Effect of a new high porosity packing on hydrodynamics and mass transfer in bubble columns. Chemical Engineering and Processing (2004), 43: 1371-1380.

Bouaifi M, Hebrard G, Bastoul D, Roustan M. A comparative study of gas holdup, bubble size, interfacial area and mass transfer coefficients in stirred gas–liquid reactors and bubble columns. Chemical Engineering and Processing (2001), 40: 97-111.

Briens C. Procedure #6 – Design and Calibration of Sonic Flow Nozzle Meter. E.S.496 Class Notes, The University of Western Ontario, London, ON, Canada (1993)

Bukur DB, Petrovic D, Daly JG. Flow regime transitions in a bubble column with a paraffin wax as the liquid medium. Industrial and Engineering Chemistry Research (1987), 26(6): 1087-92.

Chen J, Li F, Degaleesan S, Gupta P, Al-Dahhan MH, Dudukovic, MP, Toseland BA. Fluid dynamic parameters in bubble columns with internals. Chemical Engineering Science (1999), 54: 2187-2197.

Camacho Rubio F, Sánchez Mirón A, Cerón García MC, García Camacho F, Molina Grima E, Chisti Y. Mixing in bubble columns: a new approach for characterizing dispersion coefficients. Chemical Engineering Science (2004), 59: 4369-4376.

Daly JG, Patel SA, Bukur DB. Measurement of gas holdups and sauter mean bubble diameters in bubble column reactor by dynamic gas disengagement method. Chemical Engineering Science (1992), 47: 3647-3654.

Davis ME, Davis JR. Fundamentals of Chemical Reaction Engineering (1st Edition). New York: MGraw-Hill Companies (2003).

Deckwer WD, Schumpe A. Improved tools for bubble column reactor design and scale-up. Chemical Engineering Science (1993), 48: 889-911.

Deckwer WD. Bubble Column Reactors. Great Britain: Wiley (1992).

Deckwer WD, Louisi Y, Zaidi A, Ralek M. Hydrodynamic properties of the Fisher–Tropsch slurry process. Industrial and Engineering Chemistry Process Design and Development (1980), 19: 699-708.

Deckwer WD, Burckhart R, Zoll G. Mixing and mass transfer in tall bubble columns. Chemical Engineering Science (1974), 29: 2177-2188.

Degaleesan S, Dudukovic M, Pan Y. Experimental study of gas–induced liquid–flow structures in bubble columns. American Institute of Chemical Engineer Journal (2001), 47: 1913-31.

Degaleesan S, Dudukovik MP. Liquid backmixing in bubble columns and the axial dispersion coefficient. American Institute of Chemical Engineer Journal (1998), 44(11) 2369-2378.

Denn, MM. Process Fluid Mechanics. Englewood Cliffs, NJ: Prentice-Hall, (1980).

Doshi YK, Pandit AB. Effect of internals and sparger design on mixing behavior in sectionalized bubble column. Chemical Engineering Journal (2005), 112: 117-129.

Dreher AJ, Krishna R. Liquid-phase backmixing in bubble columns, structured by introduction of partition plates. Catalysis Today (2001), 69: 165-170.

Duduković MP, Larachi F, Mills PL. Multiphase catalytic reactors: a perspective on current knowledge and future trends. Catalysis Reviews (2002), 44: 123-246.

Duduković M, Devanathan N. Bubble column reactors: some recent developments. Nato ASI Series E Applied Sciences (1992), 225: 353-377.

Fan LS. Gas–liquid–solid fluidization engineering. Boston: Butterworths (1989).

Fogler HS. Elements of Chemical Reaction Engineering (4th Edition). New Jersey: Prentice Hall (2006).

Gandhi BC. Hydrodynamic studies in a slurry bubble column. Ph.D. Thesis, The University of Western Ontario, London, ON, Canada (1997).

Gupta P, Al-Dahhan M, Dudukovic MP, Toseland B. Comparison of single– and two bubble class gas–liquid recirculation models – application to pilot–plant radioactive tracer studies during methanol synthesis. Chemical Engineering Science (2001), 56: 1117-1125.

Hills JH. Radial non-uniformity of velocity and voidage in a bubble column. Industrial and Engineering Chemistry Process Design and Development (1974), 20: 540-5.

Hyndman CL, Larachi F, Guy C. Understanding gas-phase hydrodynamics in bubble columns: a convective model based on kinetic theory. Chemical Engineering Science (1997), 52: 63-77.

Jamialahmadi M, Muller-Steinhagen H, Sarrafi A, Smith JM. Studies of gas holdup in bubble column reactors. Chemical Engineering and Technology (2000), 23(10): 919-921.

Jhawar AK. Effects of internals configurations on heat transfer and hydrodynamics in bubble columns – with and without solid particles. Ph.D. Thesis, The University of Western Ontario, London, ON, Canada (2011).

Kadic E, Heindel TJ. An Introduction to Bioreactor Hydrodynamics and Gas-Liquid Mass Transfer. New Jersey: John Wiley and Sons (2014).

Kantarci N, Borak F, Ulgen KO. Bubble column reactors. Process Biochemistry (2005), 40: 2263-2283.

Kara S, Kelkar BG, Shah YT, Carr NL. Hydrodynamics and axial mixing in a three-phase bubble column. Industrial and Engineering Chemistry Process Design and Development (1982), 21: 584-94.

Koide K, Takazawa A, Komura M, Matsunga H. Gas holdup and volumetric liquid phase mass transfer coefficient in solid-suspended bubble column. Journal of Chemical Engineering of Japan (1984), 17: 459-66.

Krishna R, Van Baten JM. Scaling up Bubble Column Reactors with the Aid of CFD. Chemical Engineering Research and Design (2001), 79(3): 283-309.

Krishna R, De Stewart JWA, Ellenberger J, Martina GB, Maretto C. Gas holdup in slurry bubble columns: effect of column diameter and slurry concentrations. American Institute of Chemical Engineer Journal (1997), 43: 311-6.

Krishna R, De Stewart JWA, Hennephof DD, Ellenberger J, Hoefsloot HCJ. Influence of increased gas density on hydrodynamics of bubble column reactors. American Institute of Chemical Engineer Journal (1994), 40: 112-9.

Krishna R, Wilkinson PM, Van Dierendonck LL. A model for gas holdup in bubble columns incorporating the influence of gas density on flow regime transitions. Chemical Engineering Science (1991), 46(10): 2491-2496.

Larachi F, Desvigne D, Donnat, L, Schweich D. Simulating the effects of liquid circulation in bubble columns with internals. Chemical Engineering Science (2006), 61: 4195-4206.

Levenspiel O. Chemical Reaction Engineering (3rd Edition). United States of America: Wiley (1998).

Li H, Prakash A, Margaritis A, Bergougnou MA. Effects of micron-sized particles on hydrodynamics and local heat transfer in a slurry bubble column. Powder Technology (2003), 133: 171-184.

Li H, Prakash A. Heat transfer and hydrodynamics in a three-phase slurry bubble column. Industrial and Engineering Chemistry Research (1997), 36: 4688-94.

Li H, Prakash A. Influence of slurry concentrations on bubble population and their rise velocities in a three-phase slurry bubble column. Powder Technology (2000), 113: 158-167.

Lin TJ, Tsuchiya K, Fan LS. On the measurements of regime transition in high-pressure bubble columns. Canadian Journal of Chemical Engineering (1999), 77(2): 370-374.

Lockett MJ, Kirkpatrick RD. Ideal bubbly flow and actual flow in bubble columns. Transactions of the Institution of Chemical Engineers (1975), 53: 267-73.

Luo X, Lee DJ, Lau R, Yang G, Fan L. Maximum stable bubble size and gas holdup in high-pressure slurry bubble columns. American Institute of Chemical Engineer Journal (1999), 45: 665-85.

McCabe WL, Smith JC and Harriott P. Unit Operations of Chemical Engineering, 6th Ed. USA: McGraw-Hill (2001).

Mena PC, Ruzicka MC, Rocha FA, Teixeira JA, Drahos J. Effect of solids on homogeneous-heterogeneous flow regime transition in bubble columns. Chemical Engineering Science (2005), 60(22): 6013-6026.

Merchuk JC, Ben-Zvi S, Niranjan K. Why use bubble-column bioreactors? Trends in Biotechnology (1994), 12: 501-511.

Miller DN. Gas holdup and pressure drop in bubble column reactors. Industrial and Engineering Chemistry Process Design and Development (1980), 19: 371-7.

Moustiri S, Hebrard G, Thakre SS, Roustan M. A unified correlation for predicting liquid axial dispersion coefficient in bubble columns. Chemical Engineering Science (2001), 56: 1041-1047.

Muhsin HAA, Abid MF. Experimental study of liquid dispersion in bubble column. Diyala Journal of Engineering Sciences (2008), 1(1): 56-85.

Ohki Y, Inoue H. Longitudinal mixing of the liquid phase in bubble columns. Chemical Engineering Science (1970), 25: 1-16.

Olmos E, Gentric C, Poncin S, Midoux N. Description of flow regime transitions in bubble columns via laser Doppler anemometry signals processing. Chemical Engineering Science (2003), 58: 1731-1742.

Pandit AB, Joshi JB. Mixing in mechanically agitated gas-liquid contactors, bubble columns and modified bubble columns. Chemical Engineering Science (1982), 38(8): 1189-1215, 1983.

Prakash A, Margaritis A, Saunders RC, Vijayan S. Ammonia removal at high concentrations by the cyanobacterium plectonema boryanum in a photobioreactor system. Canadian Journal of Chemical Engineering (1999), 77: 99-106.

Ruzicka MC, Drahos J, Fialova M, Thomas NH. Effect of bubble column dimensions on flow regime transition. Chemical Engineering Science (2001), 56(21-22): 6117-6124.

Sanchez Miron A, Contrerea Gomez A, Garcia Camacho F, Molina Grima E, Chisti Y. Bubble column and airlift photobioreactors for algal culture. American Institute of Chemical Engineer Journal (2000), 46: 1872-1887.

Sanchez Miron A, Contrerea Gomez A, Garcia Camacho F, Molina Grime E, Chisti Y. Comparative evaluation of photobioreactors for large-scale monoculture of microalgae. Journal of Biotechnology (1999), 70: 249-270.

Sarrafi A, Jamialahmadi M, Muller-Steinhagen H, Smith JM. Gas holdup in homogeneous and heterogeneous gas-liquid bubble column reactors. Canadian Journal of Chemical Engineering (1999), 77(1): 11-21.

Saxena SC, Rao NS, Saxena AC. Heat transfer and gas holdup studies in a bubble column: air-water-sand system. The Canadian Journal of Chemical Engineering (1992), 70: 33-41.

Saxena SC, Rao NS, Saxena AC. Heat-transfer and gas-holdup studies in a bubble column: air–water–glass bead system. Chemical Engineering Communications (1990), 96: 31–55.

Schlüter, S., Steiff, A., Weinspach, P.M., 1995. Heat transfer in two- and three-phase bubble column reactors with internals. Chemical Engineering and Processing 34, 157-172.

Schumpe A, Grund G. The gas disengagement technique for studying gas holdup structure in bubble columns. The Canadian Journal of Chemical Engineering (1986), 64: 891-6.

Shah YT, Godbole SP, Deckwer WD. Design parameters estimations for bubble column reactors. American Institute of Chemical Engineer Journal (1982), 28: 353-79.

Shah YT, Kelkar BG, Godbole SP, Deckwer WD. Design parameters estimations for bubble column reactors. American Institute of Chemical Engineer Journal (1982), 28: 353-379.

Shah YT, Stiegel GJ, Sharma MM. Backmixing in gas-liquid reactors. AlChE Journal (1978), 24(3): 369-400.

Shaikh A, Al-Dahhan MH. A review on flow regime transition in bubble columns. International Journal of Chemical Reactor Engineering (2007), 5: R1.

Shaikh A, Al-Dahhan M. Hydrodynamics of slurry bubble column reactors. CREL Internal Report (2006).

Shiea M, Mostoufi N, Sotudeh-Gharebagh R. Comprehensive study of regime transition throughout a bubble column using resistivity probe. Chemical Engineering Science (2013), 100: 15-22.

Thorat BN, Joshi JB. Regime transition in bubble columns: experimental and predictions. Experimental Thermal and Fluid Science (2004), 28(5): 423-430.

Urseanu M. Scaling up bubble column reactors. Ph.D. Thesis, University of Amsterdam, Amsterdam, the Netherlands (2000).

Van Baten JM, Krishna R. Scale up studies on partitioned bubble column reactors with the aid of CFD simulations. Catalysis Today (2003), 79-80: 219-227.

Vandu CO, Koop K, Krishna R. Large bubble sizes and rise velocities in a bubble column slurry reactor. Chemical Engineering and Technology (2004), 27(11): 1195-1199.

Wilkinson, PM, Spek AP, Van Dierendonck LL. Design parameters estimation for scale-up of high-pressure bubble columns. American Institute of Chemical Engineer Journal (1992), 38(4): 544-54.

Wilkinson PM. Physical aspects and scale-up of high pressure bubble columns, Ph.D. Thesis, University of Groningen, Groningen, the Netherlands (1991).

Yang S. Bioprocessing for Value-Added Products from Renewable Resources: New Technologies and Application (Revised). The Netherlands: Elsevier (2011).

Yamashita F. Effect of shape of baffle plates and mesh and cross sectional area of wire gauze on gas holdup and pressure drop in a bubble column. Journal of Chemical Engineering of Japan (1987), 20(2): 201-204.

Yamashita F. Effect of liquid depth, column inclination, and baffle plates on gas holdup in bubble columns. Journal of Chemical Engineering of Japan (1985), 18(4): 349-353.

Youssef AA. Fluid dynamics and scale-up of bubble columns with internals. Ph.D. Thesis, Washington University in St. Louis, St. Louis, MO, USA (2010).

Youssef AA, Al-Dahhan MH. Impact of Internals on the Gas Holdup and Bubble Properties of a Bubble Column. Industrial and Engineering Chemistry Research (2009), 48: 8007-8013.

Curriculum Vitae

Name	Keller Joshell Hadassah George

Post-Secondary Education and Degrees

The University of Western Ontario
London ON, Canada
MESc in Chemical Engineering
2013 – 2015

Illinois Institute of Technology
Chicago IL, USA
BSc in Chemical Engineering
2010 – 2013

Related Work Experience

Research Assistantship
The University of Western Ontario
London ON, Canada
2013 – 2015

Teaching Assistantship
The University of Western Ontario
London ON, Canada
2014 – 2015